DEVELOPMENT OF A TORQUE-CONTROLLABLE UPPER LIMB EXOSKELETON FOR INDUSTRIAL APPLICATIONS

A Thesis

by

Sinan Coruk

Submitted to the
Graduate School of Sciences and Engineering

In Partial Fulfillment of the Requirements for

the Degree of

Master of Science

in the

Department of Mechanical Engineering

Özyeğin University

December 2021

DEVELOPMENT OF A TORQUE-CONTROLLABLE UPPER LIMB EXOSKELETON FOR INDUSTRIAL APPLICATIONS

Approved by:

Asst. Professor R. Barkan Uğurlu
Advisor,
Department Mechanical Engineering
Özyeğin University

Asst. Professor Özkan Bebek
Department Mechanical Engineering
Özyeğin University

Professor Dr. Duygun Erol Barkana,
Department of Electrical and Electronics Engineering
Yeditepe University

To Badem and Vanya

ABSTRACT

Chronic upper body pain and injuries are undesirable physical disorders that result from regular exposure to external forces that strain the musculoskeletal system. These symptoms reduce both the quality of life and employability of the person. Although these disorders are mostly seen in people working in heavy industry and factory workers, they can also be seen in anyone who works physically. The use of upper limb exoskeletons has been seen as a practical solution to prevent the aforementioned ailments. These systems have two basic approaches to prevent chronic upper body pain, depending on the nature of the physical work done. The first of these is to prevent the factory worker from being forced ergonomically while working; the second is to reduce external forces on the musculoskeletal system by providing strength support to the factory worker who lifts heavy loads. In this context, companies operating in many industrial areas, have provided different types of upper limb exoskeletons for their employees to use. Although these developed exoskeletons achieve their intended purpose, they have not been highly accepted by their users. While there are many different and individual reasons for this unacceptance, the most cited reasons are potential users' safety concerns and other types of difficulties in the expense of the system's promised conveniences, such as reduced mobility and increased time to get the work done.

The main purpose of this thesis is to develop an upper limb exoskeleton with a robust actuator structure and innovative human-robot interface, which is intended to have high user acceptance, while supporting factory workers against the external forces they are exposed to in their work environment. During the thesis, a 4 degrees of freedom left arm exoskeleton was developed; an innovative sensor structure with a high weight/data

input ratio has been developed for the aforementioned exoskeleton, which can read and process the limb force response from 16 different points in real time and thus perform intention estimation. The aforementioned exoskeleton is equipped with the developed sensor structure and driven by enhanced Series Elastic Actuators (SEA) for high-fidelity torque control.

ÖZETÇE

Kronik üst vücut ağrı ve sakatlıkları, kişinin düzenli olarak kas-iskelet sistemini zorlayan dış kuvvetlere maruz kalması sonucu ortaya çıkan istenmeyen fiziksel rahatsızlıklardır. Bu semptomlar hem kişinin yaşam kalitesini hem de istihdam edilebilirliğini düşürmektedir. Bu rahatsızlıklar en çok ağır sanayide çalışan kişilerde ve fabrika işçilerinde (endüstri çalışanları) görülmekle birlikte, fiziksel olarak iş yapan herkeste görülebilmektedir. Bahsi geçen rahatsızlıkların önüne geçilmesi için üst vücut dış iskeletlerinin kullanımı pratik bir çözüm olarak görülmüştür. Bu sistemlerin kronik üst vücut ağrılarını engellemeye yönelik, yapılan fiziksel işin doğasına göre, iki temel yaklaşımı mevcuttur. Bunlardan ilki endüstri çalışanının iş yaparken ergonomik olarak zorlanmasını önleme; ikincisi ise ağır yük kaldıran endüstri çalışanına kuvvet desteği sağlayarak kas iskelet sistemine olan dış kuvvetleri azaltma şeklindedir. Bu bağlamda birçok endüstriyel alanda faaliyet gösteren şirket, çalışanlarının kullanması adına farklı tiplerde üst vücut dış iskeletleri temin etmişlerdir. Geliştirilen bu dış iskeletler hedefledikleri amacı gerçekleştirmek ile birlikte kullanıcıları tarafından yüksek oranda kabul görmemişlerdir. Bunun için pek çok farklı ve kişiye özel sebep olmakla beraber, en çok belirtilen sebepler potansiyel kullanıcıların güvenlik endişeleri ve sistemin vaat ettiği kolaylıkları sağlarken düşen hareket kabiliyeti ve işin yapılma süresini uzatması gibi başka tip zorluklar ortaya çıkarması şeklindedir.

Bu tezin temel amacı endüstri çalışanlarının iş ortamlarında maruz kaldıkları dış kuvvetlere karşı destek olmakla birlikte, gürbüz eyleyici yapısı ve yenilikçi insan-makine ara yüzü barındıran, kullanıcı kabulü yüksek olması amaçlanan bir üst uzuv dış iskeleti geliştirmektir. Tez süresince 4 serbestlikli bir sol kol dış iskeleti geliştirilmiş; ilgili dış

iskelet için 16 farklı noktadan uzuv kuvvet tepkisini gerçek zamanlı olarak okuyabilen ve işleyebilen ve bu sayede niyet kestirimi gerçekleştirebilen yenilikçi ve ağırlık/veri giriş oranı yüksek bir sensör yapısı ile donatılmış; ve de yüksek bağlılıklı tork kontrolü için geliştirilmiş Seri Elastik Eyleyiciler (SEE) ile tahriklenmiş. Geliştirilen SEE modüllerinin ilk versiyonları bu tez çalışmasının öncesinde gerçeklenmiş olup, bu tez kapsamında geliştirilen modüller önceki versiyonlardan tork/ağırlık oranının arttırılması, tahriklenme halindeyken ortaya çıkan mekanik aksaklıklar giderilmesi ve dönel kodlayıcılardan veri alımının mekanik olarak istikrarlı hale getirilmesi gibi iyileştirmeler gerçeklenmiştir.

ACKNOWLEDGMENTS

First and foremost, I would like to express my sincere gratitude to my thesis supervisor, Asst. Prof. Barkan Ugurlu for his invaluable assitance during my M.Sc. study.

I wish to thank my fellow labmates in Ozyegin University; Sinan Emre, Erim Can Ozcinar, Baris Balcı, Ulas Yildirim, Mert Karacı, Mustafa Derman, Omid Khosrowshahi, Oguzhan Dalgıc and Barıs Baysal; with a special thanks to Burak Ozkaynak, Deniz Ugur, Alihan Kuru, Ahmed Fahmy Soliman, Ammar Alkhaled and Mehmet Can Yildirim.

Finally, I would like to thank to my parents and rest of my family, my friends and Irem Naz Yildiz who supported and motivated me throughout my thesis study.

TABLE OF CONTENTS

LIST OF TABLES

LIST OF FIGURES

SEA	Series Elastic Actuators
OMID	Occupational Muscle Injuries and Disorders
HRS	Human Robot System
ADL	Activities of Daily Living
EMG	Electromyography
FSR	Force Sensitive Resistor
DOF	Degrees of Freedom
AFS	Activities of Factory Setting
DAQ	Data Acquisition System
RMSE	Root Mean Square Error
$\mathbf{R^2}$	Coefficient of Determination
CoEx	Compliant Exoskeleton
DC	Direct Control
HD	Harmonic Drive
TBMs	Torquer Brushless Motor Series
ST	Spring Thickness
FT	Feder Thickness
FEA	Finite Element Analysis
H-H	Humeral Head
IMU	Inertial Measurement Unit
SAA	Shoulder Abduction-Adduction
EFE	Elbow Flexion-Extension
SFE	Shoulder Flexion-Extension
EE	End Effector
MCU	Microcontroller Unit
SSI	Synchronous Serial Interface
ISO	International Organization for Standardization

DOB Disturbance Observer

CHAPTER I

INTRODUCTION

1.1 Motivation

Occupational muscle injuries and disorders (OMIDs) can be described as problems that occur in a work setting, due to experiencing external loads that strain the musculoskeletal structure of a person [1,2]. These problems are most common in people who make their livings doing physical labor due to the nature of their work [3,4]. In time, these musculoskeletal strains result in chronic pains or injuries lowers the afflicted factory worker’s quality of life and employability. As of today, an estimate of 60% of the European population are suffering from OMIDs [5], and a majority of these individuals are workers in factories, agriculture, and municipalities [6]. The most common types of OMIDs are seen in the upper body of individuals, as it is subject to external loading in object manipulation [5-11]. Due to repetitive strain-inducing and tendon overloading work, complications such as carpal tunnel syndrome, tendinitis, and lateral epicondylitis occur in hands, tennis elbow and bursitis occur in the elbow, rotator cuff tears are observed in the shoulder, and various types of hernia are experienced at the back of individuals. Such conditions take a long time to recover [12].

The high risk of experiencing such severe health problems is also disadvantageous for the employers as these health and safety risks both increase the wage of factory workers. Furthermore, the company may have to compensate workers financially during the recovery process [6]. The apparent solution to elevate the problem could be full automation, yet this is not always financially feasible.

Thus, employers are adopting different strategies to reduce the risk of OMIDs in their work environment. Decreasing the amount of strain exposure by introducing more breaks, shortening shifts, and utilizing task rotation among factory workers for strain-inducing tasks are possible non-costly solutions that are being implemented [5]. Although these solutions are successful to some degree, they may not be effective in fully dispersing the risk of OMIDs [6].

A slightly more costly option that is available in the factory setting is to provide assistive equipment to factory workers. Industrial exoskeletons, a type of wearable assistive equipment, are especially promising, as they are shown to provide the necessary assistance to their users while conducting strain-inducing tasks in the laboratory environment, especially lifting high payloads [13], tool holding [14,15], stabilizing posture to conserve energy and conducting predetermined tasks.

1.2 Literature Review

This study focuses on three main areas: i) developing a safer, more efficient, and more accurate sensor-based interfaces for human-robot systems, ii) development of an upper-limb exoskeleton for industrial applications and iii) implementing the sensor interfaces and the SEA structure that was previously developed to the upper body exoskeleton by adding some upgrades.

In this section, the literature regarding these areas is reviewed separately. In Section 1.2.1. the state-of-the-art wearable sensor designs and their utilizations for wearable systems is presented. In section 1.2.2 the state-of-the-art industrial upper-body exoskeletons are provided.

1.2.1. Human-Robot Interfacing: State of the Art

Wearable sensor interfaces are proven to be useful, if not crucial, for a more efficient interaction in human-robot systems (HRS) [14]. Such sensors are commonly utilized in teleoperation applications, in which a robot mimics the movements of a remote individual wearing these sensors. In order to realize this, the sensors observe the variance in torque and position trajectories and output a correlated response. This output is then interpreted in a processing unit as the proper physical quantity and provided to the robot [16].

While actuated exoskeletons are structurally different than conventional teleoperated robots as they are wearable systems, they still need to receive torque or position trajectory inputs in order to function. Some exoskeletons are designed to carry out a specific function. These include upper body systems which assist individuals to recover and to conduct Activities of Daily Living (ADL), lower body exoskeletons which aim to conserve metabolic energy during walking and non-self-balancing lower-body exoskeletons that stabilize their users via utilizing upper body strength, i.e. using crutches. For these types of exoskeletons, trajectory can be supplied to the system in terms of predefined trajectory sets. Furthermore, the torque assistance could be supplied and regulated via torque controllable actuators in order to ensure the safety of users.

However, these types of exoskeletons may not be as beneficial in factory settings. The workers may not require assistance from the exoskeleton to carry out only a specific task but instead, they might need to use an exoskeleton in various tasks, such as lifting a payload from any random location and carry it to any other random location. These tasks would typically be carried out in less structured, more diverse and random environments. In such applications, establishing predetermined trajectory sets may not be feasible.

Therefore, a human-machine system that enables the exoskeleton to interpret the intention of its user is more appropriate for factory workers.

The actuators of a torque-controllable system may be used to collect torque data as the system operates in terms of change in applied load. They could interpret this data and respond to it accordingly for power augmentation. However, the information on the time and direction of the response are still supplied to such systems in terms of predetermined trajectories [17] or via trajectory triggered mechanisms [18].

While this approach could be satisfactory due to its simplicity and straightforward nature for systems with a set of pre-engineered functions such as lower-body exoskeletons or rehabilitation systems, this methodology is often impractical as the number of possible trajectories increases. The use of exoskeletons with specific tasks ultimately results in lower user acceptance by factory workers as they require a system designed to carry out a variety of tasks with different trajectories or to carry out same tasks with varying trajectories due to subject-dependent user preference [19].

To overcome this challenge, a multitude of researchers have been focusing on sensory-based control techniques. One of the prominent techniques that is used to acquire data is surface EMG (Electromyography) sensors. These sensors can detect the presence of a muscle response or electrical activity in response to a nerve’s stimulation of the muscle when they are moved. Thus, they offer the user a way to communicate their intentions with the exoskeleton [19].

With that being said, the utilization of EMG sensors may also introduce the need for day-to-day calibration. The sensors produce small electrical signals and require a certain threshold to be surpassed for their engagement. Conventionally, this threshold is achieved by calibrating the sensors on the user, then making the user flex and stretch the attached muscles with certain trajectories and finally establishing the lowest reading as the activation input [20]. While this approach may be accurate for short sessions of use for a single individual, it could be counter-intuitive and time-consuming for a group of factory workers. The electrical signals collected via EMGs depend on various factors, such as the users' biological determinants which show subject-dependent changes and may be even different for the same individual at different times of the day [19]. Therefore, the exoskeleton would require day-to-day or even task-to-task calibration for each factory worker.

Another disadvantage of the utilization of EMG sensors in a factory setting is that the EMG sensors only relay the information regarding the presence of muscle activity. This introduces the necessity for a rather complex interpretation algorithm which should take into account of all the variables discussed above in order to convert muscle activity of the individual into trajectory inputs for the exoskeleton [21].

A further concern for the use of EMG sensors in a factory setting stems from their fixation method. For EMG sensors to get a reading from the muscles, they need to be attached to the skin of the user. This could introduce difficulties in attaching these sensors, as most of them are required to wear long-sleeved jumpsuits in accordance with the factory regulations for safety reasons. Even though this obstacle may be overcome; there are only a limited number of effective ways of attachment for the sensor reading to be realized such as using a sticky layered sensor and pasting it onto the skin or fastening the sensors with a tight armband to ensure the contact. However, neither way is maintainable since in a factory setting, the worker would presumably sweat and thus the sticky layer would dislodge, and the armband would slip [19].

Another explored avenue of acquiring data from the user is through the use of load cells. These sensors are capable of converting the axial tension and compression forces into a corresponding electrical signal. One advantage of utilizing these types of sensors over EMG sensors is that they are independent of users' biological factors. Furthermore, these sensors can be used to measure the interaction forces between the user and the exoskeleton with only an initial calibration for each sensor. However, this convenience at the measurement would be at the expense of additional weight and complexities in placement of the sensor on the exoskeleton. The complexities in placement could result in improper data collection.

An alternative approach could be the utilization of force sensitive resistors (FSRs). These structures' internal resistance changes in the presence of an applied force and as a result they output a corresponding voltage. They are thinner and lighter, thus easier to place in comparison to the conventional load sensors. With that being said, their outputs are nonlinear and they need to be placed on a rigid surface for them to function properly. [22]. This thesis aims to provide a viable method of placement for FSRs and the linearization of their outputs. The methodology will be further explained in the upcoming chapters.

1.2.2 Upper-Body Industrial Exoskeletons: State of the Art

Upper-body exoskeletons are proven to be useful systems in preventing or diminishing the cases of OMIDs in factory workers [23,24]. The state-of-the-art exoskeletons with higher adaption rates are generally passive systems designed to assist their users with a specific task or relieve the stress experienced by a specific section of the body (i.e. back or arm) [25-29]. These systems function by storing the energy in one direction and releasing it in the opposite. Although the energy they utilize is not generated actively by the exoskeleton, but instead by the user, such systems are effective for the niche tasks that they are designed for. VT-Lowe's passive lifting exoskeleton by Alemi et. al [30] and Back-X by Suit-X [25] are examples of exoskeletons with niche application of assisting their users in torsal lifting while H-Vex by Hyun et. al [31] and EksoVest by EksoWorks [32] are examples of exoskeletons with niche application of overhead arm manipulation assistance. Even though these exoskeletons are proven to be effective in the tasks that they are specifically designed for, they evidently cannot be used for other tasks while maintaining their benefits.

Correspondingly, the second school of thought is to provide factory workers an interface that is compatible with a variety of tasks that they could benefit in factory settings. Due to this multitude of functions, the most effective strategy in achieving this interface is via the utilization of actively powered joints.

The state-of-the-art exoskeletons in this field are generally dual-arm exoskeletons with three active DOFs (Degrees of Freedom) per arm [33-38]. Two of them are A/A joint and F/E joint along the shoulder and the remaining one is the elbow F/E joint [35]. However, exoskeletons that contains only one DOF [37] or two active DOFs per arm are also present. The designs containing a fourth one along the spine to assist in bending of the torso [38] are also present in the literature.

The increase of the number of active DOFs evidently increases the usability of an industrial upper-body exoskeleton in various tasks, yet this is at the expense of increasing the weight of the system in general. Consequently, increasing the number of active DOFs is not a viable method for industrial upper body exoskeletons given that the weight of the exoskeleton is carried by their users. These exoskeletons are not full-body exoskeletons that transmit the carried load to the ground directly but instead towards their user's base support area (generally this would be the back or the hip section). Due to this fact, their load-carrying capacity cannot exceed the load carrying capacity of these areas without harming the worker or without generating risk of OMIDs in the support area.

A possible way to bypass this limitation could be turning the upper body exoskeleton into a full-body exoskeleton that transmits the load to the ground; yet this would be at the expense of increased complexity in design, added weight, and cost. While this approach may theoretically solve the issue, such systems have low acceptance rate [39]. Thus, most of the state-of-the-art active systems abide by these limitations and offer partial support for the workers.

Although exoskeletons are being developed for industrial applications at an increasing rate with the aforementioned intentions for almost three decades, a widespread adoption is evidently lacking as the OMID cases are not diminishing [5,6,39]. The most prevalent reason for this is the high user rejection rate for utilizing exoskeletons. While there are various specific reasons for a person to reject to use an exoskeleton, the most common engineering-related rejection causes can be put into five categories. These are as follows; i) perceived unsafety, ii) difficulty of operating, iii) non-task-compatibility, iv) lack of durability and v) lack of reliability [39]. Due to these experienced shortcomings by the factory workers, most of the developed exoskeletons are left unused after an initial testing period. Thus, in order to achieve the continuous use of an exoskeleton by factory workers, these five concerns should be addressed.

1.3 Methodology

The literature highlights the necessity for improvement concerning the current powered industrial upper-body exoskeletons, regarding their application to factory settings as well as the challenges that stem from this application.

Addressing the reasons for rejection of exoskeletons that were categorized above and proposing an abiding design would be a step in the right direction in improving the applicability and increasing the adoption of the powered industrial upper-body exoskeletons in factory settings. In that regard, the challenges to be addressed are i) perceived unsafety of the system, ii) difficulty of operating (or difficulty of learning to operate), iii) non-task compatibility, iv) lack of durability and v) lack of reliability. [39].

The literature also points out existing tools and methods from a variety of fields that could offer solutions to these problems. Perceived unsafety of the system by potential users could be ameliorated by introducing an anthropomorphic and non-intrusive design, in addition to utilizing several layers of safety layers to the system [40,41]. Issues regarding to the difficulty of operating (and/or difficulty of learning to operate) could be addressed by robust intention estimation capabilities [42,43]. Both these implementations could increase the compliance of the exoskeleton to its user. As a consequence, the exoskeleton would be transparent.

Lack of compatibility of a system with a given task could be bypassed by actively supporting the required joints and equipping the system with utilities for activities of factory setting (AFS) [42]. This may result in the generation of sufficient torque, which could not only offer partial support to its user, but it may also enable its user to conduct a given task without partitioning the torque requirement with the exoskeleton.

Lack of durability is an unfavorable consequence of an upper-body exoskeleton that transmits its load not to the ground but onto the back or hip of users. Due to the load-carrying capacity of the individual, the exoskeleton could be manufactured as a lighter structure. However, this may adversely affect the durability of the system. [44,45]. As discussed in Section 1.2.2, this issue can be bypassed by enabling the exoskeleton to transmit its load to the ground [46].

Lack of reliability may stem from various parameters that become relevant during the installation, operation, and maintenance phases of a robot. For an exoskeleton robot to be considered reliable in the installation phase, the system should be easily transportable within the given facility and be able to have short and device-on (don) and device-off (doff) procedures for different individuals [42]. The ease in transportation can be achieved by either making the system light enough to be carried around easily, which on the other hand, contradicts with the reliability criteria, or by making the system mobile. The short and straightforward don/doff procedures could be achieved by rendering system size adjustable and utilizing a strap-on strap-off procedure [41]. Regarding the reliability in the operation phase, the system needs to be responsive to its user with accuracy. This could be achieved by torque controllable actuator with high fidelity torque control. In case of any failure during the operation, the system should shut itself down instead of conducting erratic trajectories on its own, which can be achieved by utilizing mechanical, electrical and software-based safety protocols [47]. For a system to be reliable during the maintenance phase, any minor issue in the robot should be able to be fixed in under 8 hours, and for any major issue, acquisition of spare parts should be possible [41].

In the light of these challenges, development of a size adjustable upper-left arm exoskeleton with 4 active DOFs actuated via custom-made Series Elastic Actuators

(SEAs) is considered. Equipping this exoskeleton with custom-made intention estimating sensors and placing it on a mobile stage is viewed as a viable option. The design process of the system initiated with the development of the Intention Estimating Brace, a dynamic wearable force-sensing arm pad for intention estimation (see Chapter 2). In addition, for the actuation of the system, the SEAs that were previously developed by Yildirim et. al [48] were considered due to their robust torque sensing and control capabilities. Along with the duration of the thesis, design of the SEAs is altered to improve the encoder measurement accuracy and converted into a modular design to render its maintenance easier to conduct (see Chapter 3). Following that the design of the upper limb exoskeleton, the mobile stage, and the multipurpose modular end-effector were accomplished in accordance with the design of the actuator, human parameters, requirements of the factory setting, and ease of use (see Chapter 3). Finally, controller synthesis, kinematic and dynamic structure of the exoskeleton and the torque control experiments were conducted (see Chapter 4).

CHAPTER II

HUMAN-ROBOT INTERFACE

In order to achieve a robust interface between the human and the exoskeleton, a brace structure for the utilized load sensors to be placed is designed. The finalized brace design is a result of a long-term iterative development process. The timeline for the iterative brace design procedure can be seen in Figure 1.

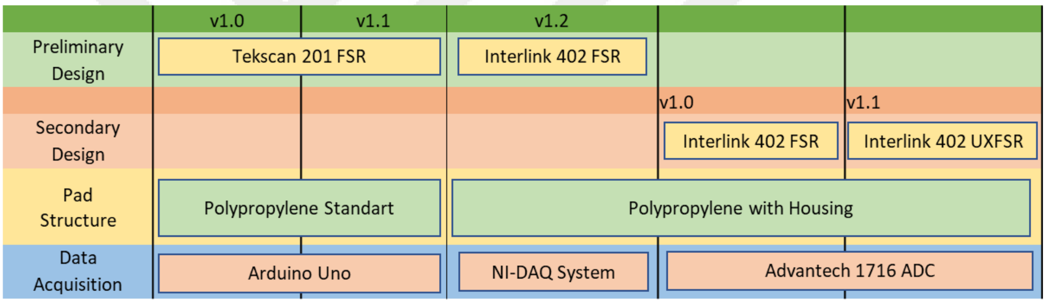

Figure 1: *Brace design timeline*

This Chapter aims to explain the development of a novel human-robot interface design (named as smart brace) for industrial upper limb exoskeleton. In Sections 2.1 to 2.3 of this chapter; design methodology of the brace for force sensitive resistor-based sensor (FSR) structure, the initial design, secondary design and comprehensive final design of the brace will be covered. The design and the manufacturing of the brace housing on the pad is given in Section 2.4. The data acquisition circuit designed for the brace is presented in Section 2.5, and finally the calibration experiments and the trajectory tracking performance of the brace is demonstrated in Section 2.6.

2.1 Design Methodology

The setback in the conventional load sensors comes with scalability, both in terms of cost and the bulky nature as well as the weight it introduces to a wearable system. Since these sensors can measure the tension and compression in a singular direction, for an exoskeleton with an "*N*" degrees of revolute freedom for a distinct axis, a total of 2*N sensors would need to be placed per connection pad between the user and the exoskeleton.??? However, due to aforementioned constraints, many studies on intention estimation were able to place 1 or 2 load sensors in their systems at the critical locations to compensate for the weight and abide geometrical features that the design allows [49]. This trade-off, however, is favorable neither for the scalability, as the bulky load sensors would still cause discomfort, nor for the accuracy as the needed 2*N amount of sensors would not be present.

An alternative solution to eliminate this trade-off is to utilize FSR sensors. These sensors are lightweight and owing to their paper like form, they are non-intrusive. However, in order for them to function, they need to be placed on a rigid surface. If placed on elsewhere, they would not be able to acquire any reliable data [50].

On the other hand, the connection members (pads) between the human and the exoskeleton need to be elastic, in other words non-rigid, both for the ergonomics of the user and for pads to be size adjustable as they are intended to be used by different individuals.

Due to this necessity, FSR sensors cannot be placed on such connection elements. Thus, they are commonly used in end effectors of rigid robotic arms to acquire tactile information during the robots' operation [51-55] instead of an agent of human-robot interface. Albeit there are some studies in the literature that utilizes FSR sensors in biomechanical characterization efforts and exoskeleton applications by using localized rigid surfaces on the pad structure.

These rigid structures also introduce a higher combined modulus of elasticity in the placed sections of the pad based on the combined elasticity, as shown in Equation 1.

$$\boldsymbol{E_c = E_F V_F + E_M V_M} \tag{1}$$

This assembly results with the pad losing its elasticity in the respective region, thus, losing its size adjustable nature at the placement section. To preserve the overall ergonomics and size adjustability of the pad, these regions are commonly required to be distributed further away from each other. Therefore, a maximum amount of 2-3 regions can comfortably be fitted on a size adjustable pad without sacrificing the integrity of the data to be acquired [56-58].

Additionally, it could be argued that in these studies, a material scientist point of view is not considered. In accordance with their operational principles, the pads need to undergo cyclic deformation and relaxation cycles during don doff. In this process, the elastic pad experiences a cyclic strain and stress flow. Permanent alteration of these pads via adding high rigidity sections would likely render these cycles to be non-uniform. As a result, over extended usage of the pad likely to cause loss of functionality due to localized plastic deformations at the best and tearing and cracks due to creeping at the worst case scenario [59,60]. In light of the points discussed above, using pads with localized rigid structures are satisfactory for single DOF systems for short periods. However, as the amount of distinct DOFs and the desired lifetime of a system increases, a higher number of sensors placed on a pad with uniform modulus of elasticity would be needed.

Throughout my literature survey, two distinct strategies were encountered, to utilize higher number of on-body sensors. The initial strategy is to use rigid braces which are custom designed for a specific individual. This way the required number of FSR sensors can be placed along the inner curved surface of the pad and due to the rigid material of the pad, these sensors could get accurate data from the user [61].

The second strategy is to place the FSR sensors in the inner curvature of an elastic band and to place the elastic band to a proximate but different axial plane than the pad coverage for a given limb. Although no accurate force data is acquired by this configuration, by utilizing this method, the FSR sensors would be able to pick up the muscle contraction and activate due to their placement location and use them as triggers similarly to EMG sensors [62-65].

Both discussed alternatives have inherent problems that would not make them suitable for the factory setting. The first strategy would be hard and costly to apply for the intention estimation interface for an industrial upper limb exoskeleton, which is targeted to be used by more than one specific individual. The second strategy reintroduces all the limitations of the EMG sensors in a factory setting, in addition to decreasing the quality of the acquired data.

Because of these various trade-offs between the accuracy versus the comfort of the patient and the accuracy versus mass-scale applicability, the available commercial and experimental sensorized pads have certain disadvantages; meaning that a good compromise is yet to be implemented.

In order to overcome this obstacle and hence make use of FSR sensors on the pads without making these sacrifices, a brace design was developed to act as an intermediary rigid element between the human's respective limb and the elastic size adjustable pad. The secondary design version 1.1. of the brace can be seen in Figure 2.

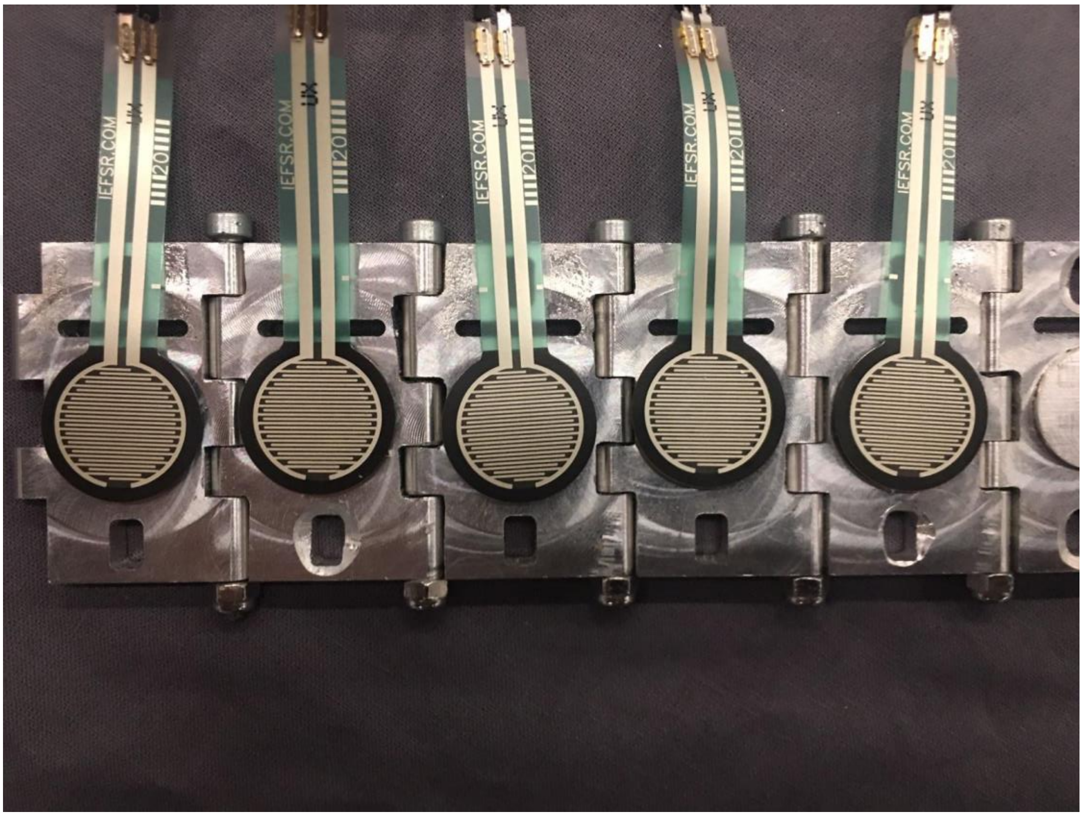

Figure 2: *Secondary design version 1.1 of the brace.*

2.2 Preliminary Design

There are two main aspects to be taken into consideration when designing the brace. First, it should have a curved shape to be placed around forearm or upper arm. Second, it should abide by the operational limitations of the FSR sensor.

Figure 3: *Huawei metallic wrist watch*

In inspiration of metallic watch wrist straps and magnetic bracelets as demonstrated in Figure 3; the brace design both adopts a curved structure while being rigid in order to ensure that FSR sensors abide to its operational limitations.

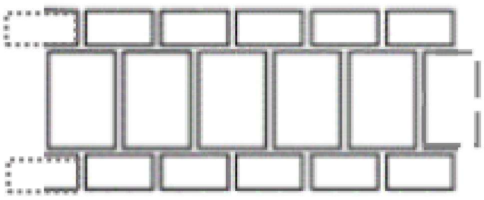

Figure 4: *The pattern used for the design*

The design consists of two primary types of pieces: namely the FSR house (shown as piece A in Figure 5) and the house connector (shown as piece B in Figure 5). As displayed in Figure 5, house connectors are connected above and below of the FSR houses in order to form the assembly of the brace. The connection of the two pieces are enabled via cylindrical shafts.

The metallic strap will be formed by repeating the pattern on Figure 5 until the desired circumference length is reached, which would be rotatable to different curved shapes depending on the forearm or upper arm diameters.

Figure 5: *The locations of FSR houses (A) and house connectors (B) on the pattern used for the design*

2.2.1 Design of the FSR House and House Connector

2.2.1.1 Design of the FSR House

For the design of the FSR house, the ratio of the length of the individual metallic piece to the metallic watch strap is calculated. The circumference of the wrist is then extrapolated to an average arm circumference while maintaining the aforementioned ratio, thus an average height and length for the brace house is attained. Correspondingly, the dimensions of the FSR house are calculated as follows:

- Height: 40 mm
- Length: 20 mm
- Width: 4 mm

CAD model of the FSR house can be seen in Figure below.

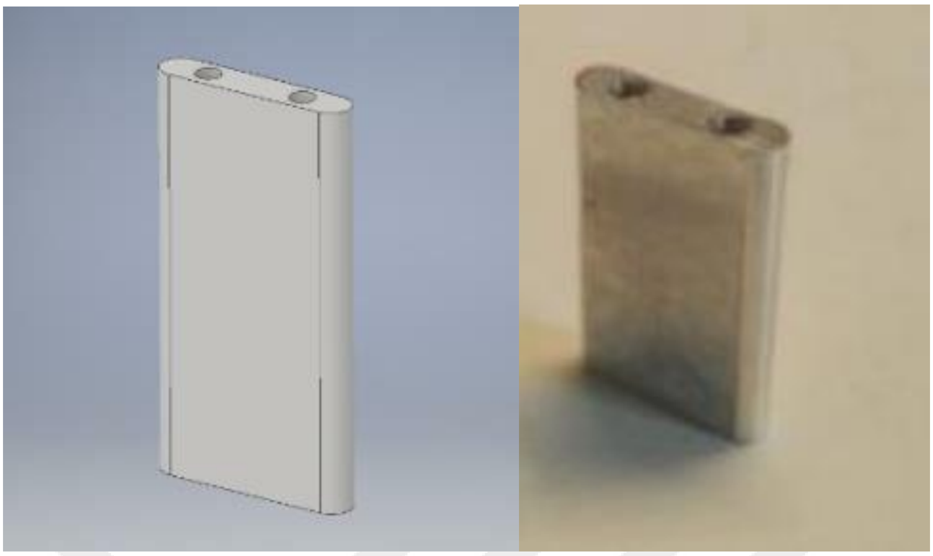

Figure 6 : *CAD model of the FSR house (left)*

and the manufactured FSR house (right)

Nonetheless, this initial design was insufficient as there was no clearing in the brace house design to ensure the contact between the FSR sensor's reading surface and the limb that the brace is placed on. Thus, it was not adequate for healthy data acquisition. In order to remedy this impediment, a punched-out surface was added to the design as demonstrated in Figure 7.

Figure 7: *FSR house design with punched-out surface*

2.2.1.2 Design of the House Connector

The house connector was designed with respect to the FSR house to cover the latter half section of the n^{th} FSR house and the initial half section of the $(n+1)^{th}$ FSR house to form a continuous chain. Consequently, the length of the house connector became the half of the length of the house. The dimensions of the house connector are calculated as follows:

- Height: 10 mm
- Length: 20 mm
- Width: 4 mm

CAD model of the house connector can be seen in Figure 8.

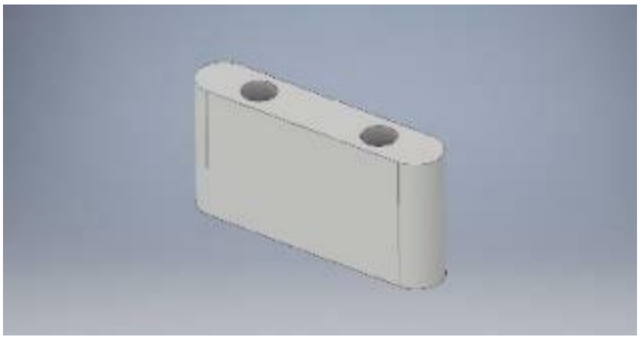

Figure 8: *CAD model of the house connector*

2.2.2 CAD Assembly of the Initial Prototype

After the design of the individual pieces are completed; an assembly was formed in CAD model to analyze the final chain formation of the metallic strap. The relative free motion of the pieces and the overall motion of the chain structure along the cylindrical coordinate frame is ensured as no interference between the pieces was observed. The CAD model of the assembly can be seen in Figure 9. The assembly configuration on the manufactured parts can be seen in Figure 10.

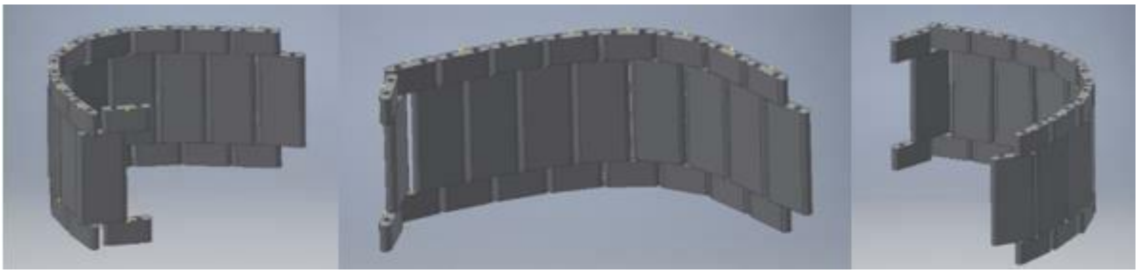

Figure 9: *CAD model of the brace assembly*

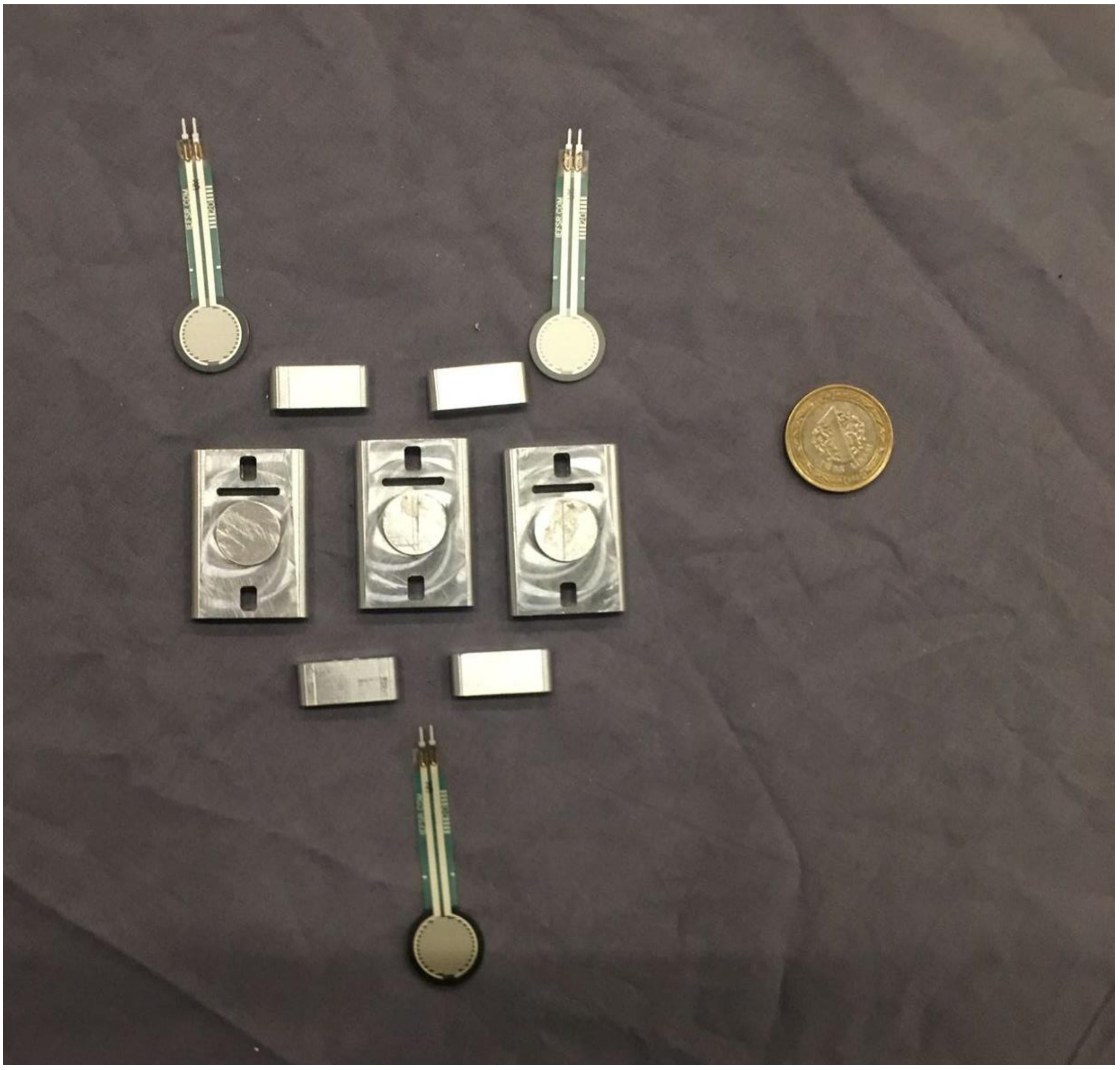

Figure 10: *The assembly configuration of the manufactured parts*

Figure 11: *Assembled v1.1 of the prototype on a healthy subject*

2.3 Secondary Design

After the initial prototype design, several improvements were conducted with following goals in mind:

- Easing the manufacturing process
- Reducing the manufacturing cost
- Devising an optimal method to attach the brace structure to the orthotic pad
- Reducing the physical assembly effort to form the brace structure

In order to achieve these goals the number of different elements in assembly pattern, that was detailed in the previous section, was diminished. To this end, two components of the design were merged into a singular unit. Additionally in order to allow the FSR sensors tips to be secured, slots were added to the component. Finally, to secure the brace to the pad two screw passages were added. The resulting product can be seen in Figure 12.

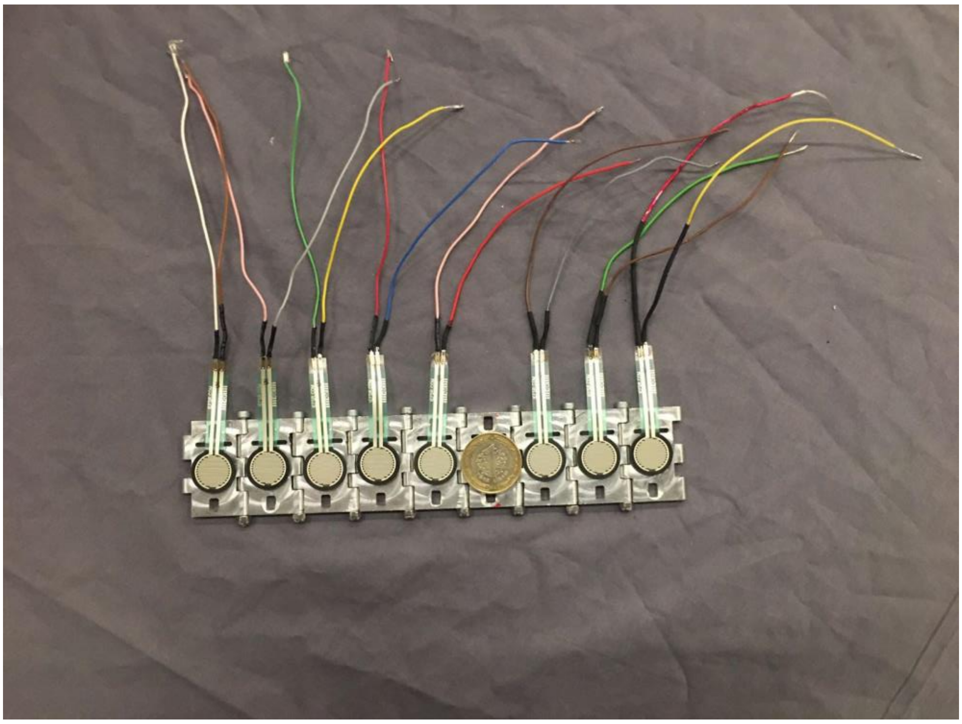

Figure 12: *V1.2 of the intention estimating brace*

2.4 Pad Design

2.4.1 Pad Material Selection

A critical factor for the successful operation of an exoskeleton is the alignment between the mechanical limb and the user's limb. This could be achieved by attaching the exoskeleton and the actual limbs with orthosis limbs while preserving the DOF relation in between them [40]. Given that the users of the exoskeleton are to manipulate heavy payloads, it is essential to ensure the security of the connection between the exoskeleton and the user with a high grip. The literature reveals that many exoskeleton designs, indeed attend to these issues [31-35,37,38].

Predominantly, materials such as polyethylene, polypropylene and polycarbonate are used in the making of orthosis molds. Nevertheless, the use of lighter materials, such as aluminum, is also possible. The reason why plastic and its derivatives are the most preferred materials for exoskeleton is their flexibility. The type of plastic material to be used varies, depending on its appliance. The summary of the plastic types and their corresponding appliance can be found in Table 1.

Table 1: *Different types of plastic materials and their corresponding appliance*

	Polyethylene	Polypropylene	Polycarbonate
Stiffness	Soft	Soft	Rigid
Shape Adjustability	Yes	Yes	Non
Durability	Low	Average	High
Manufacturing Type	Firing	Firing	Vacuum drying
Density	Low	High	High

As demonstrated in Table 1, the orthosis made of polyethylene and polypropylene (heat-treated members) have less rigidity comparing to the ones made of polycarbonate (vacuumed members); henceforth making them more elastic and size-adjustable for different limb sizes. Even though vacuumed members are considered to be more durable comparing to heat-treated members, they cannot be used by different individuals as they are designed for one individual with specific dimensions. Given that lighter molds decrease the required torque output from the actuators; they are convenient to be utilized in such an endeavor. In the light of all the issues discussed above, using polypropylene orthosis attachments is the most preferable approach.

2.4.2 Polypropylene Mold Forming

In order to shape the polypropylene into a pad structure, the most convenient method to be used is sheet vacuum forming, which is a subtype of thermoforming. In this procedure, a solid polypropylene sheet with the desired thickness is placed inside a vacuumed tray. The material of the tray can be anything, as long as the tray's material has a melting point that is higher than the polypropylene. Following that, the tray is placed in a high temperature industrial grade oven and heated to a temperature range of 160-180 ^{o}C. Once the molten state is achieved, the tray is removed from the oven. The molten polypropylene is then removed from the tray and shaped using a mold. Plaster cast of the specific body part is used as a mold for the specific application of forming the wearable pad. After the shaping process, the molten polypropylene sheet is stretched around the plaster and left for cooling. Followingly the belt buckles and the straps are bolted on to the pad's sides for adjusting the structure for different sizes. Finally, in order to establish an ergonomic contact between the pad and the human, a neoprene fabric was placed as an intermediary layer.

2.4.3 Pad Housing Design & Manufacturing

After the selection of the most convenient material for the pads to be utilized in the exoskeleton and the intention estimating brace structure it is equipped with, the optimal placing options for the brace along the pad structure should be considered. The pad's undeformed form is assumed to be a uniform cylindrical shell with a constant radius and a height for this reason. The midsection of the pad with respect to its height is considered as a placement region, as it offers the most secure fastening area between the user's limb and the pad. This placement, independent of the location, prevents the entirety of the brace to engage with the user’s arm due to this additional thickness. As a result, the preservation of the DOF between the user and the pad is jeopardized. This also diminishes the grasping performance of the pad.

While the grasping performance of the pad in this state may be enhanced by a tighter strapping, this would also increase the discomfort of the user. In order to minimize this effect and render the brace to be as non-intrusive as possible, the form of the pad and sink the brace inside the pad were altered, up until the punched-out surface. The punched-out surface is not intended to be not sunk, in order to ensure that the FSR sensor it houses contacts the user’s arm. As a result, a uniform housing section with 4 mm depth and 60 mm height is settled on.

In order to manufacture the pads with the desired housing, the initial design of the brace is used as an emboss. This version is placed on the desired region of the forearm plaster and covered with a vacuumed film to prevent any undesired weld forming between the molten polypropylene and the emboss. The molten material is then placed onto the plaster, stretched and left for cooling. The resulting product can be seen in Figure 13.

Figure 13: *Pad with the brace housing*

After the solid structure is attained, the same procedure is repeated for the upper arm as well. The CAD model of the assembled brace chain on this pad can be seen in Figure 14.

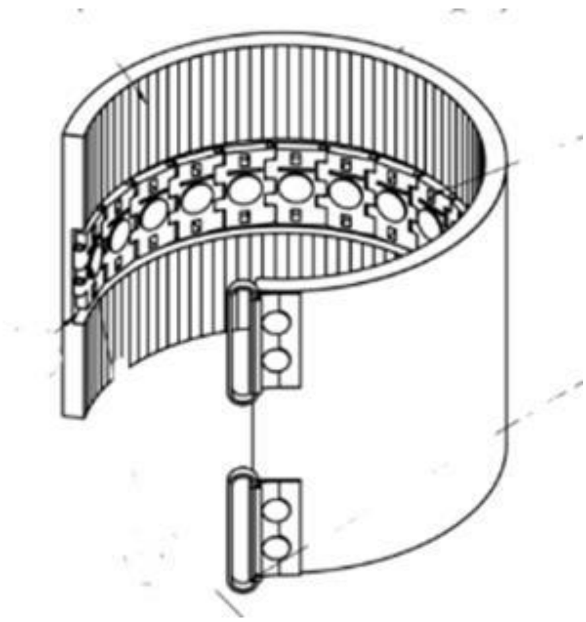

Figure 14: *CAD model of the assembled brace chain*

2.5 Electronics Design

In order to amplify the aforementioned range and preserve the linear output relation while doing this, an inverted operating amplifier circuit is developed for each brace and a voltage range between 0 to 10V is achieved. The circuit's operation flow and DIP trace model can be seen in Figure 15 and Figure 16 respectively.

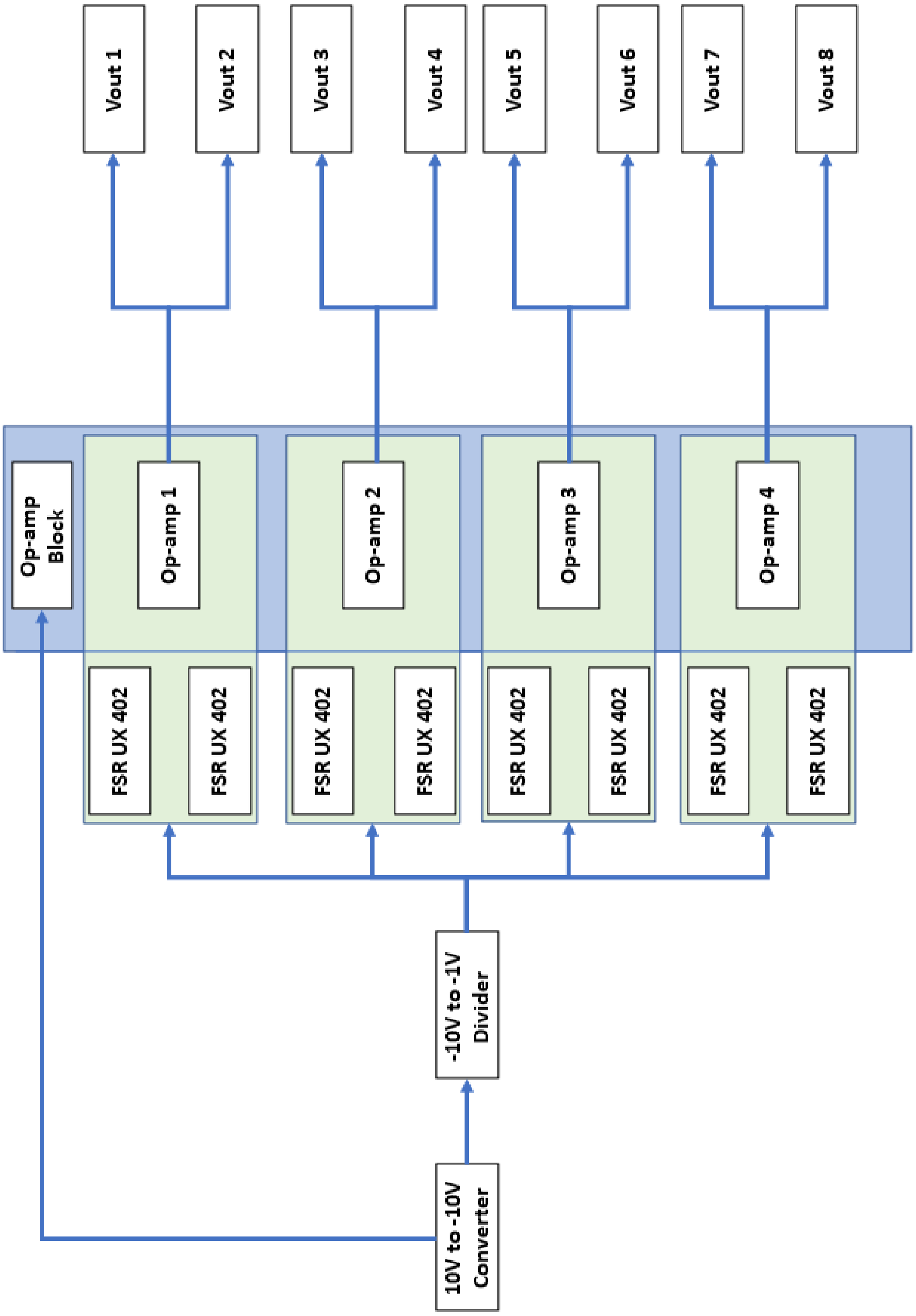

Figure 15: *Operation flow of the PCB*

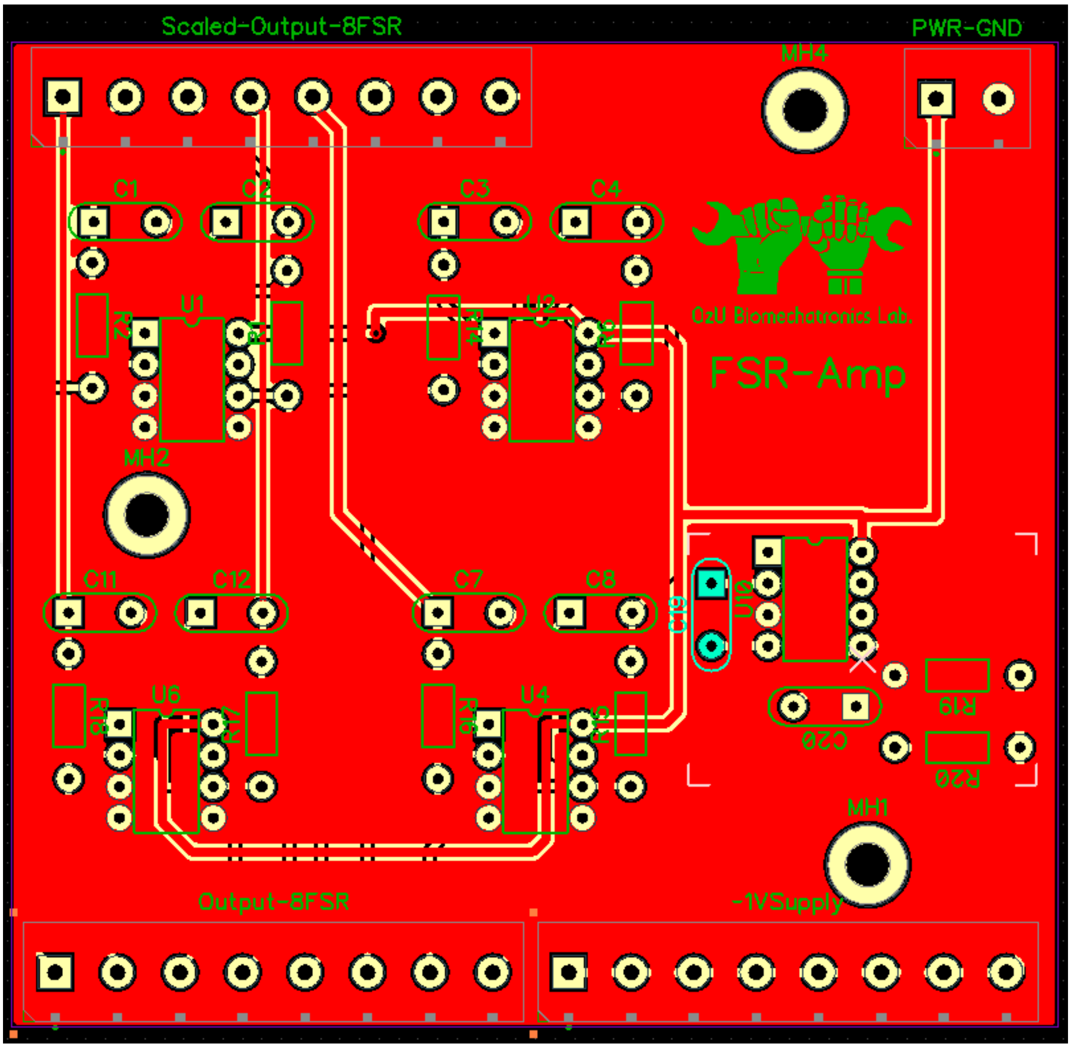

Figure 16: *Dip trace model of the PCB*

Each PCB can operate 8 different FSRs. In the circuit, Op-Amp's are fed symmetrically via -10 V. In order to achieve that 10V supply was converted to -10V using a voltage converter. Also, FSR's are fed with -1V which is divided by -10V. According to the intended circuit design, PCB is printed; which can be seen in Figure 17.

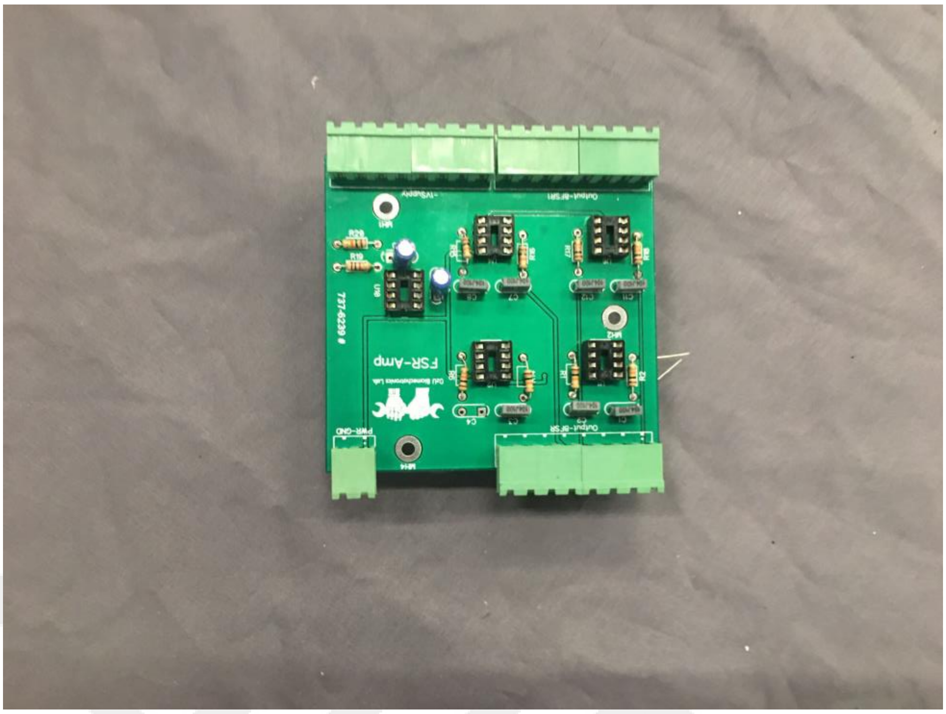

Figure 17: *Manufactured PCB*

2.6 Calibration & Experiments

2.6.1 Calibration

For the calibration of the FSR sensors, various objects with varying masses were used. In order to calibrate the output voltage and convert them into actual force values, combined static and dynamic calibration approach was utilized. This methodology was selected as it takes into account possible non-linearity and the hysteresis of the sensors as well as other environmental factors.

In order to realize this calibration the FSR sensor, it was placed on a 6 axis force sensor (Optoforce 6-Axis Force Sensor), which was connected to a NI-DAQ System. The FSR sensor was initially exposed to a static load to get an output from the FSR for the static load. Followingly, varying forces with random intervals were applied to the mass on top of the FSR sensor in order to create a dynamic state. The force values obtained from Optoforce sensor. In addition to that, the output from the FSR sensors were recorded.

Approximately 80000 samples have been collected from the system by using a DAQ (with a rate of 500 samples per second recorded for approximately 160 seconds). The voltage data obtained from the FSR testing,which was collected by DAQ is fitted to the reference force (which was obtained from Optoforce sensor). The results of different degree of curve fitting of voltage to the reference force is shown in Figure 18.

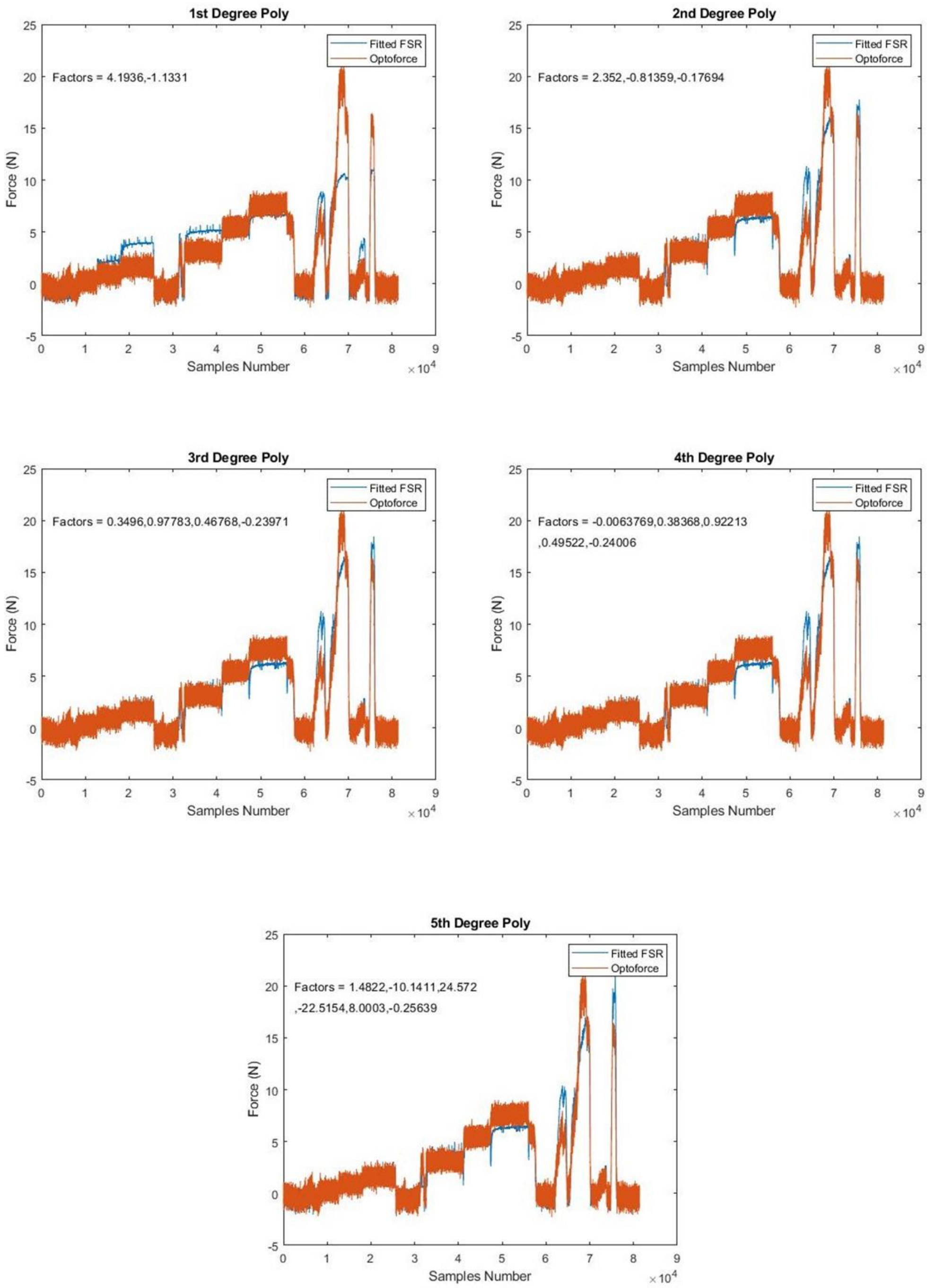

Figure 18: *The Results of the calibration*

To assess the performance of the fitting, the root mean square errors (RMSE) and R^2 factors where obtained for all the five fittings. The RMSE, R^2, the fitting improvement percentage with respect to the previous polynomial level and the coefficients of the polynomials can be seen in Table 2.

Table 2: *RMSE, R^2, fitting improvement percentage and polynomial coefficients*

	RMSE	R^2	Fitting Improvement Percentage Over the Previous Fitting	Polynomial Coefficients
1st Degree Fitting	1.9781	0.3112	100%	[4.194, -1.133]
2nd Degree Fitting	1.2758	0.1095	64.81%	[2.352, -0.814, -0.177]
3rd Degree Fitting	1.2661	0.1077	1.64%	[0.350, 0.978, 0.468, -0.240]
4th Degree Fitting	1.2661	0.1077	0%	[-0.00638, 0.384, 0.922, 0.495, -0.240]
5th Degree Fitting	1.2303	0.1011	6.13%	[1.482, -10.141, 24.572, -22.515, 8.000340, -0.256]

Based on the acquired RMSE and R^2 values the fitting improves as the order of the polynomial increases. The only exception to this trend is the 4^{th} order polynomial which gives the identical tracking performance as the 3^{rd} order polynomial. It can be said that the fitting is bound to increase as the order of polynomial increases, however based on the data at hand this increase in fitting performance would not justify the computational cost that a higher order of polynomial would bring forth.

To validate this assumption fitting attempts with 6^{th} order, 10^{th} order, and 13^{th} order polynomials were conducted. The level of polynomials were chosen arbitrarily. RMSE, R^2, the fitting improvement percentage with respect to the previous polynomial level and the coefficients of the polynomials can be seen in Table 3.

Table 3: *RMSE, R^2 and fitting improvement percentage for higher order polynomials*

	RMSE	R^2	Fitting Improvement Percentage Over the Previous Fitting
3rd Degree Fitting	1.2661	0.1077	1.64%
5th Degree Fitting	1.2303	0.1011	6.13%
6th Degree Fitting	1.2202	0.0993	0.82%
10th Degree Fitting	0.8819	0.0495	27.72%
13th Degree Fitting	0.8704	0.0482	1.3%

To increase the accuracy R^2 of the fitting by roughly 6% the polynomial level would need to be increased by a level of ten. This increase would improve the performance of the sensors at the cost of increased computation time. This increase would contribute to the inherent lag of the sensors measured in 10s of milliseconds [66]. This would result with the sensor readings to delay and would prove counter beneficial for tracking efforts. Thus, a trade-off between the tracking accuracy and the polynomial order needs to be established. Based on the acquired RMSE and R^2, and due to having a relatively lower polynomial 3rd order polynomial fitting is selected. The equation of this fitting can be seen in Equation 2.

$$F = 3.76V^3 - 11.21V^2 + 10.88V - 0.1642 \qquad (2)$$

2.6.2 Data Collection Experiments

For the demonstration, the lower leg swinging motion has been chosen as a sample motion and the data collection from NI-DAQ system was made for a 10 second duration. The force readings throughout the experiment can be seen in Figure 19.

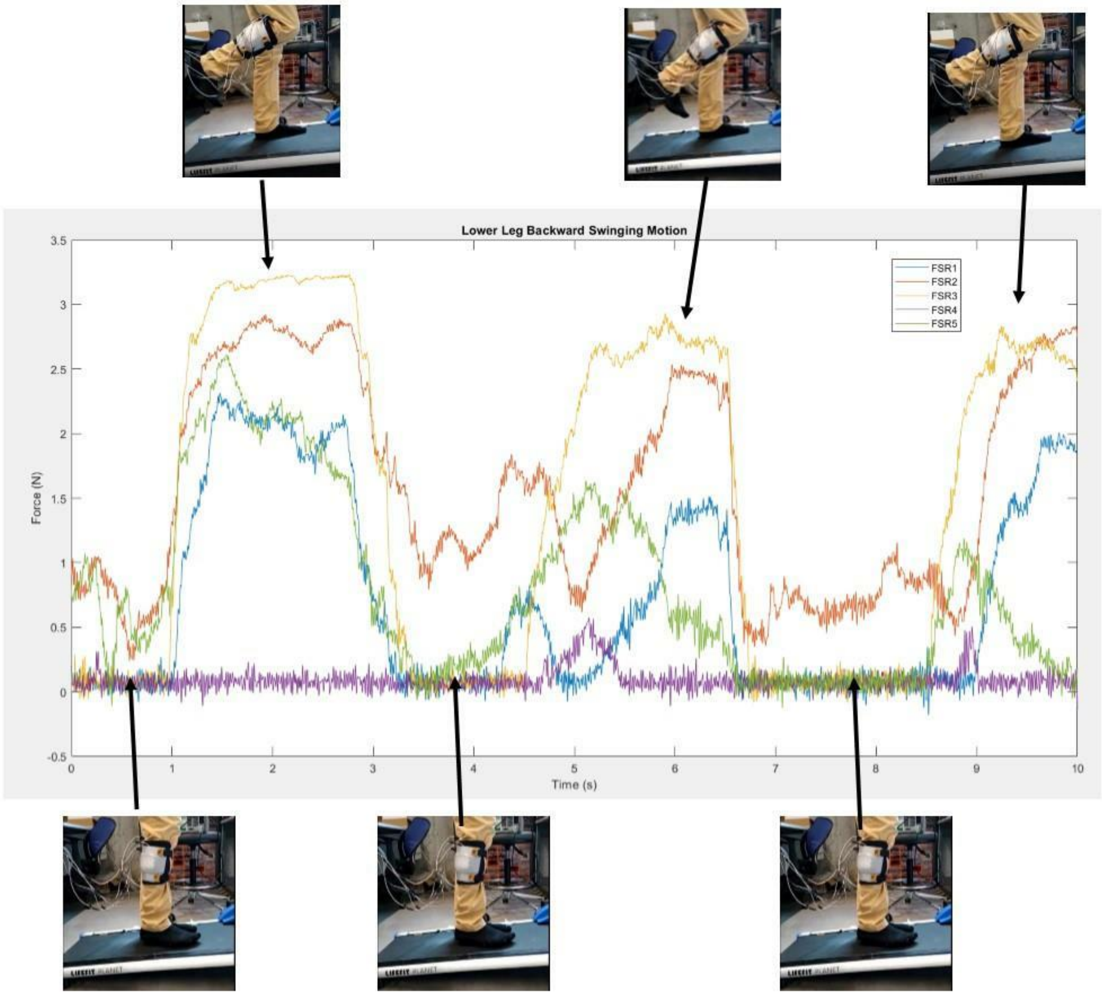

Figure 19: *The results of the demonstration*

As illustrated in Figure 19, the peaks of the motion show how the force goes higher as the pressure from the shank muscles is acting more on the brace within the swinging motion. Also, the FSR#4 of the brace, which is in the side of the thigh, is outputting very slight negligible force values as they are not affected by the swinging motion.

Finally, the swinging motion shows a close approximation of the system output behavior illustrated from the data shown in Figure 20. The final data obtained from the demonstration can be seen as well in Figure 20.

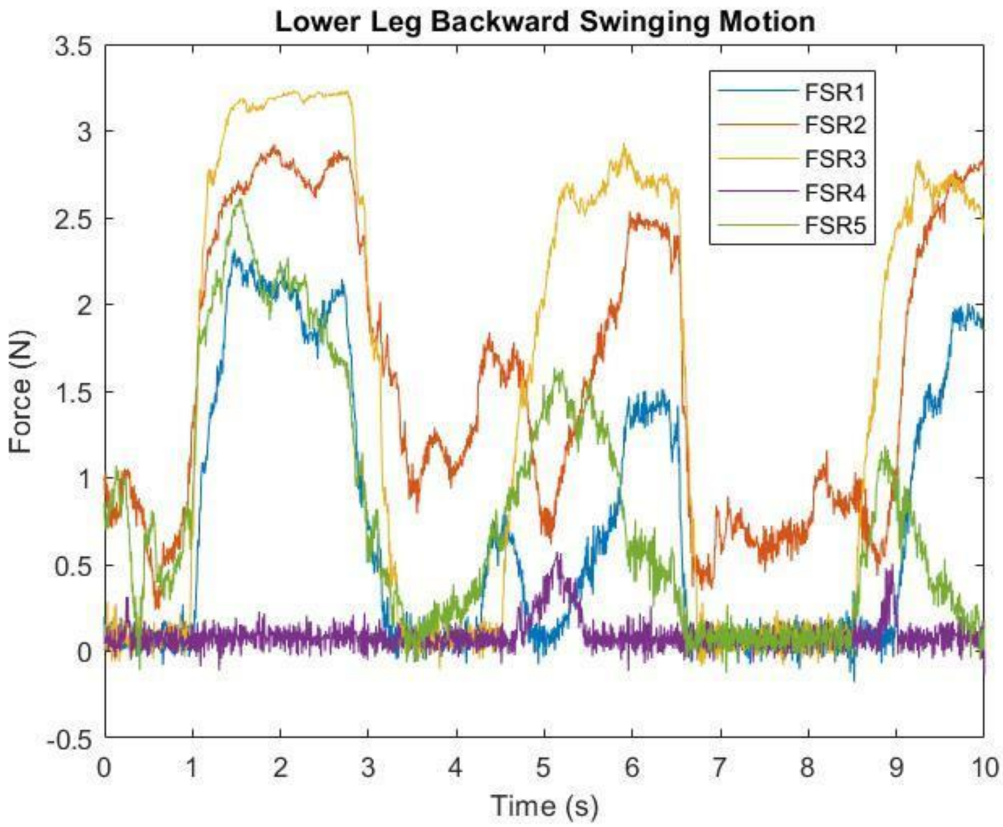

Figure 20: *Data obtained from lower leg backward swinging motion*

CHAPTER III

UPPER LIMB EXOSKELETON MECHATRONICS HARDWARE DESIGN

The upper limb exoskeleton was initial designed to be a testbed for the initial versions of the SEA that were being developed. In that regard, the aforementioned exoskeleton was initially designed as a fixed system that can carry high payloads, similar to an industrial robot arm like the models developed by companies like KUKA or Franka [67,68]. Followingly, the second and final iteration of the exoskeleton is initiated. This version is redesigned for it to be utilizable in factory settings based on the considerations discussed in Chapter 1.

3.1 Actuator Design and Improvements

3.1.1 Preliminary Design

Prior to this thesis two distinct types of SEAs were developed by Yildirim et. al. [48]. These actuators are named as "Compliant Exoskeleton-SEA A & B (CoEx-SEA). Each of these SEA modules consists of three sublayers, namely: i) a brushless frameless DC (BFDC) motor (Kollmorgen TBMs-7615 & 7631 respectively), ii) a strain wave gear (Harmonic Drive (HD) CSG-25, 1:100 transformation ratio) and iii) a torsional spring that acts as a torque sensor. The timeline of their development process can be seen in Figure 21.

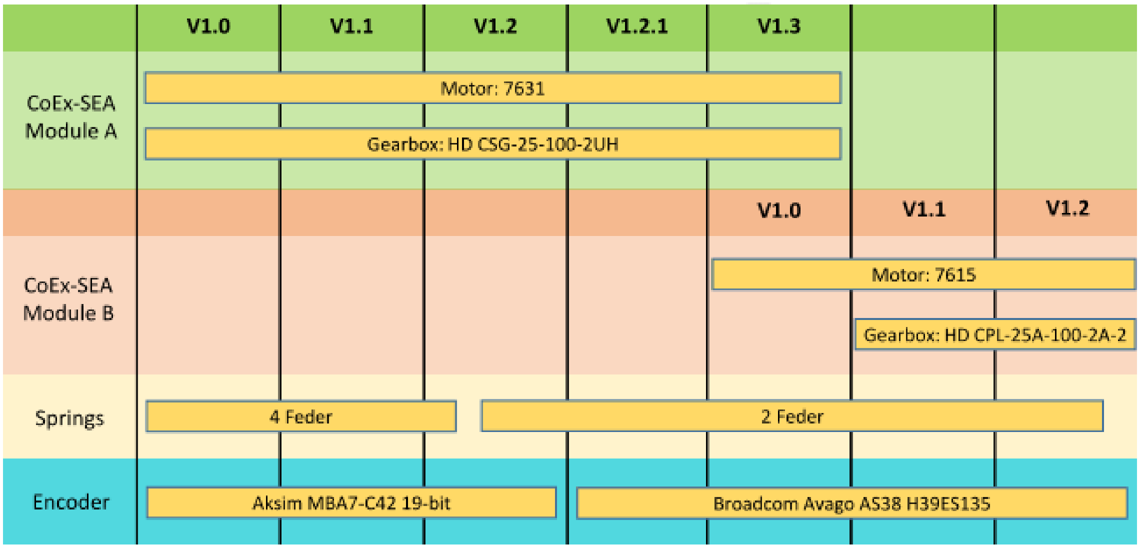

Figure 21: *The timeline for the initial versions of the SEA's development*

In Figure 22; the CAD model of Co-Ex-SEA module A v1.3 and Co-Ex SEA module B v1.2 can be found.

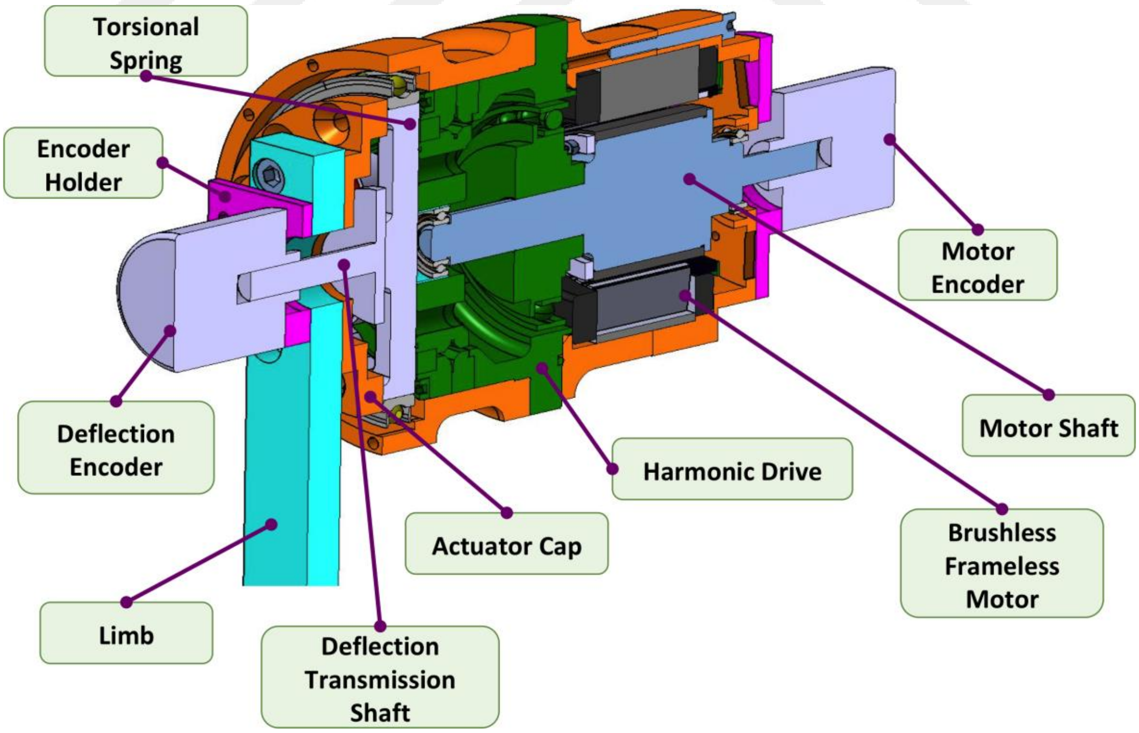

Figure 22: *The CAD model of Co-Ex SEA Module A v1.3 and Co-Ex SEA Module B v1.2*

The assembly of the SEAs are initiated from the motor side. The respective frameless motor's stator is placed in a Al 6061 frame. The magnetic stator is then placed onto a shaft. This shaft-rotor assembly is fixed to the bearing at the frame's cap. This assembly is then inserted into the stator-frame assembly and secured via bolts. Followingly the Harmonic Drive (HD) is placed inside a frame. The remainder of the shaft is inserted inside the HD's input and the two frames are connected via bolts. The output of the HD is attached to the torsional spring at the HD's center. The input of the spring and the output cap of the unit are attached to the outer circle of the spring. One of the 23-Bit (Broadcom Avago AS38 H39ES135) encoders is connected to the measured motor angle, whereas the other one is connected to the torsional deflection. In the literature, it has been contended that encoder-based torque sensing is more favorable when compared to load-cell based torque sensing [69]. The actual Co-Ex SEA A&B units can be seen in Figure 23.

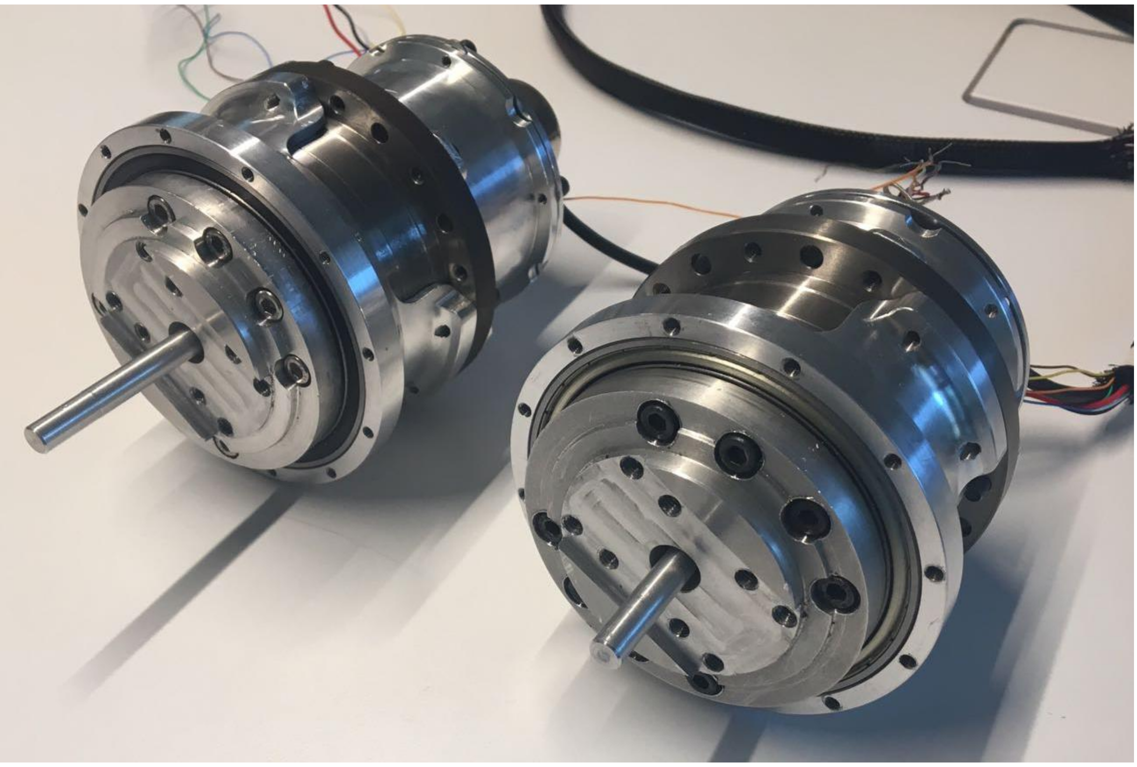

Figure 23: *The actual Co-Ex SEA A &B units*

Table 4: *Co-Ex SEA A & B specifications*

Specification	Unit	*CoEx-SEA (A)*	*CoEx-SEA (B)*
Max. Angular Velocity	rpm	26.33	26.33
Max. Continuous Torque	Nm	164	96
Mass	kg	3.09	2.87
Stiffness	Nm/deg	91	91
Torque Resolution	mNm	3.90	3.90
Max. Continuous Torque/Weight	Nm/kg	53.07	33.45

The final topology of the torsional spring was a product of iterative design, analysis and experimentation process that takes stress distribution life cycle and fatigue of the spring into account [48,70]. The finalized spring model is a two-feder spring with a diameter of 80 mm, an overall thickness of 10 mm, a spring thickness (ST) of 8 mm and a feder thickness (FT) of 9 mm. The corresponding locations of the ST and FT dimensions can be seen in Figure 24.

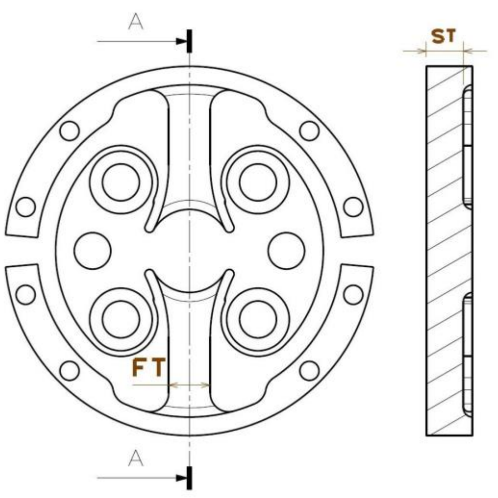

Figure 24: *FT and ST measurements*

The spring can deform elastically within a range of +/-1.8º. It has a torsional stiffness of 91 Nm/deg within this range, which was achieved via the utilization of the specific ST and FT variables. The relation that was derived by using Finite Element

Analysis (FEA) and further verified empirically, shows the relationship between these two variables and the resulting stiffness. This relation can be seen in Equation 3.

$$\begin{aligned} k_{EMP} &= -8.5 - 0.34ST^2 + 0.52FT^2 + 3.42ST \\ &- 4.34FT + 1.03STFT \end{aligned} \quad (3)$$

3.1.2 Improvements on the SEA Design

While these SEAs are fully operational, during the initial control experiments and long duration testing, some problems that needed to be tackled were observed by Yildirim et. al.:

- Single unit design is hard to assemble and disassemble. When an inspection or maintenance needed, this block design causes problems.
- Unpredicted lateral forces may affect the spring structure thus the spring stiffness.
- The lack of internal mechanical fastening strength in the selected encoder's design causes the deflection encoder to record less than optimal torque measurements.
- For the unit CoEx-SEA-B, mass-to-torque ratio cannot be improved with the previously selected gearbox.
- Increase in the length of the rotor shaft increases the possible assembly problems.

Some of the main points were evaluated and a set of improvements were conducted on the design by Yildirim et. al. prior to this thesis:

- Motor side was redesigned as a single unit.
- Rotor shaft is made shorter.
- HD unit is changed with a newer and a lighter frameless version (Harmonic Drive (HD) CPL-25, 1:100 transformation ratio).

- Spring is supported with an additional bearing.

Along the duration of this thesis, these initial improvements were further cemented with complimentary design adaptations. A lighter and smaller spring was designed with respect to the empirical modeling in order to improve the torque to weight ratio of the actuators (Section 3.1.2.1), the spring housing section was consequently redesigned to accommodate the new design (Section 3.1.2.2). The harmonic drive side and the spring box were separated and were redesigned as single units, similarly to the motor side (Section 3.1.2.2). An encoder stabilizer module was derived in order to compensate for the lack of fastening strength of the selected encoders (Section 3.1.2.3).

3.1.2.1 Spring Design

The spring's size-related boundary conditions were established based on the version 1.2.1 of the Co-Ex-SEA A, which has the HD CSG-25 with 1:100 transformation ratio, and the Kollmorgen 7631A BFDC motor. Later on, these components were replaced with HD CPL-25 with 1:100 transformation ratio and the Kollmorgen 7615A BFDC motor, yet the spring structure was not altered.

The unaltered spring is perfectly functional with these new components. However, as the maximum continuous output torque of the SEA is decreased from 164 Nm to 96 Nm with the change in the BFDC, a more optimal stiffness value could be utilized. Furthermore, the spring was designed to fit the strain gear's output section, which was at the center, and was supported by a bearing whose outer diameter was secured via the outer extremity of the output section. Thus, its radius and thickness were dependent on the inner and outer diameter sizes and the thickness of the aforementioned bearing. However, as the strain gear is altered in the later iterations, this dependency was no longer valid and a new dependency could be established based on the current strain gear dimensions. The fact that the current strain gear has a smaller diameter output section allowed me to alter the spring size and increase the torque to weight ratio further due to reduction of weight that this will result in.

In light of these new dependencies, the diameter was shrunk from 80 mm to 55 mm and overall thickness was shrunk from 10 mm to 9 mm to better fit with the new strain gear model. Additionally, the spring stiffness was aimed to be scaled down from 91 Nm/deg to approximately 55 Nm/deg using the empirical formula while applying these alterations in size.

Using the empirically established formula, the ST and FT values are calculated as 8 mm and 6.5 mm respectively. Consequently, a spring was modeled with the aforementioned dimensions in CAD environment.

In order to further verify the accuracy of the empirically derived formula, FEA and Fatigue analysis were conducted on the design, which can be seen in Figures 25-28 and Table 5.

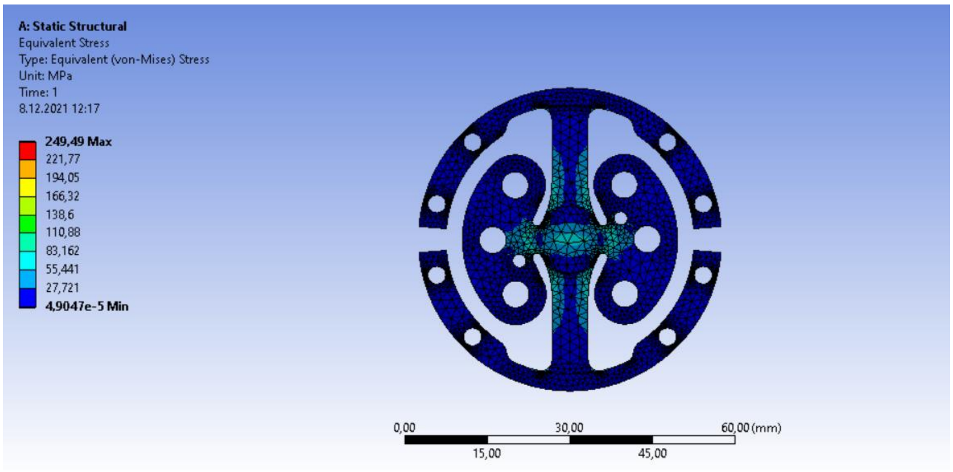

Figure 25: *Stress distribution Von Misses*

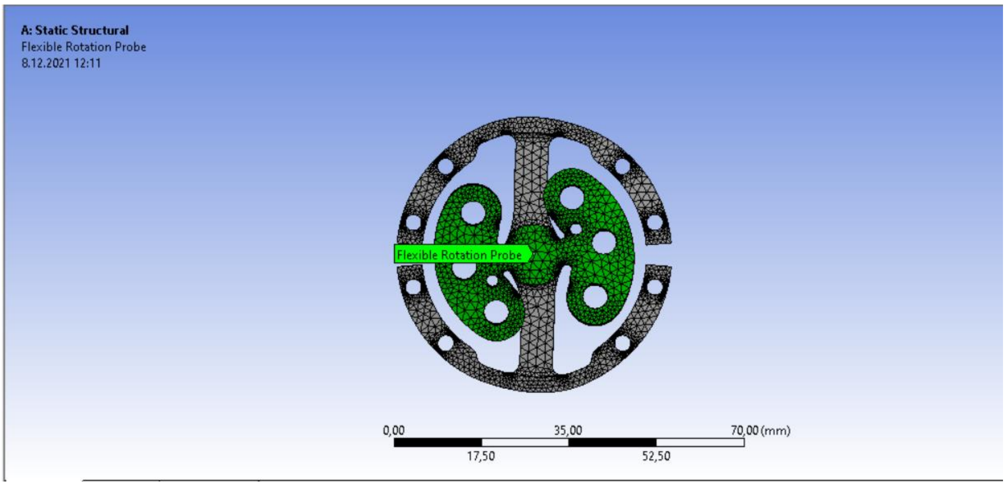

Figure 26: *Deflection of the spring*

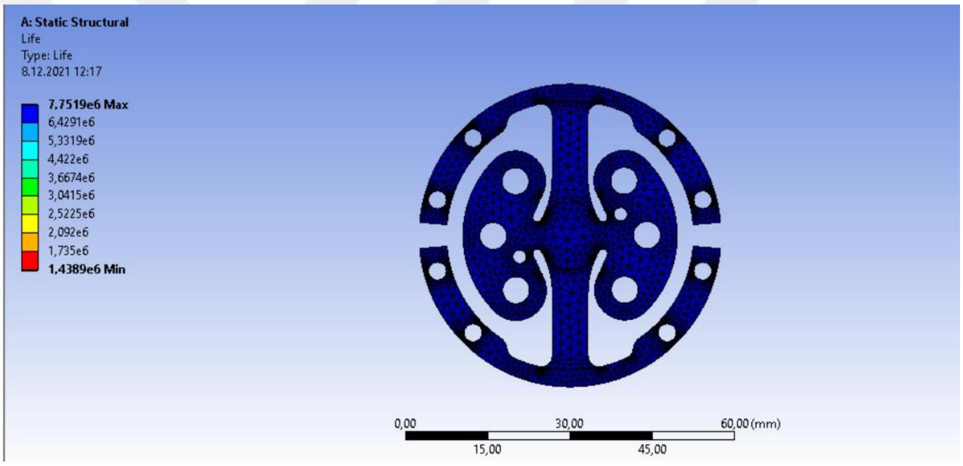

Figure 27: *Life factor of the spring*

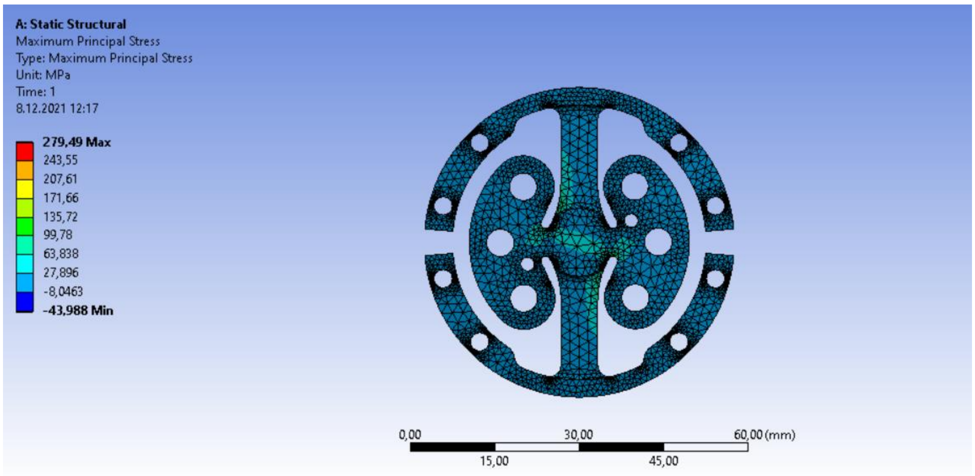

Figure 28: *Principal stress of the spring*

Table 5: *Details of mesh*

Element Order	Quadratic
Element Size	3,9079 mm
Defeature Size	1,954e-002 mm
Curvature Min Size	3,9079e-002 mm
Curvature Normal Angle	60º
Proximity Min Size	3,9079e-002 mm
Num Cells Across Gap	3
Proximity Size Function Sources	Faces and Edges
Bounding Box Diagonal	78,158 mm
Average Surface Area	117,11 mm^2
Minimum Edge Length	0,12457 mm
Nodes	450790
Elements	298071

During the simulation the spring experienced a 1.9º deflection under given inputs. Based on the life analysis the spring's operational life was calculated to be 453 days.

3.1.2.2 Modular Spring Box Design

After the design of the new smaller spring a spring box component was designed for housing the spring. In the previous versions the spring and the HD were a single cohesive structure. In order to work on either one, a disassembly of the entire unit was required, which in turn increased the maintenance effort. In light of the strategy of converting the design into a modular assembly, which was previously conducted for the motor side, to ease any possible maintenance effort, the spring box was designed as a modular component and was separated from the HD. This separation consequently achieved modularity in the HD side as well. In Figure 29 full assembly of the spring box can be seen.

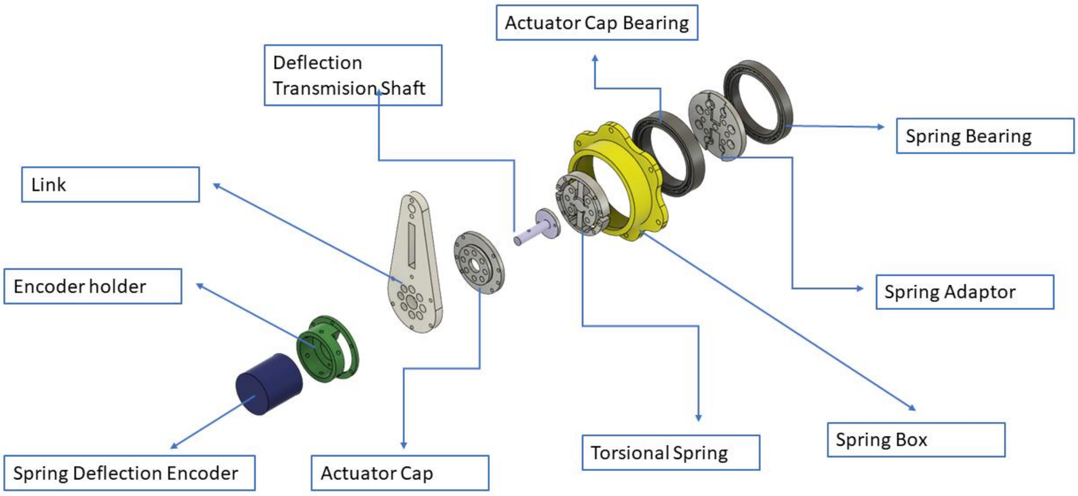

Figure 29: *Full assembly of the spring box*

A further advantage that this modular structure introduces to the overall Co-Ex SEA structure is that with the possible addition of offsetting elements, which can be in the form of simple cylindrical structures with varying heights that act as adaptors between two of the connected parts along the shaft axis of the SEA, the modular SEA module can be attached to any given geometry from either the end of the motor side, harmonic side or spring side.

3.1.2.3 Encoder Stabilizer

In versions after 1.2.1 of the Co-Ex SEA module A, Broadcom Avago AS38 H39ES135 model encoders are used for both the measurement of the motor angle as well as the spring deflection. The mechanical operation of these encoders on the motor side were achieved via fixing the base of the encoder to an adaptor by using two 160º apart M3 bolts. In accordance with the design limitations, the adaptor is designed attached to the motor frame by using four rectangularly situated M4 bolts, whereas the rotary cap of the encoder is connected to the shaft of the motor by using two 90º apart M3 setscrews. For the case of the deflection encoder, the base of the encoder is fixed to the respective link of the exoskeleton and the rotary cap is fixed by using the same fastening arrangement, to an extension shaft that is based on the center of the spring.

Throughout the testing of the versions between Co-Ex SEA module A 1.2.1 and Co-Ex SEA module B 1.2, no apparent misreading was observed on the motor side of encoder that would jeopardize the integrity of the data collection. However, as the exoskeleton operates, shifting torque characteristics were expected to be encountered by the exoskeleton. These variances were directly observed by the link side (i.e the spring encoder) and they have caused slight dislodges in the encoder cap connection due to the poignant fastening.

Additionally, any design is bound to have manufacturing errors within some acceptable tolerance. However, in heavily integrated assemblies like the SEAs at hand, these tolerable errors on various parts could form a positive feedback loop upon a disturbance, like the shift in torque characteristics, and further amplify the disturbances' effect. As a result, the aforementioned dislodging may be further amplified. Although, this has not been actively observed, it remains as a possibility and further proves the requirement for a more intact fastening.

Having a much lower angular displacement range in comparison to motor side encoder, means that any such momentary dislodging would result in a serious safety hazard. To clarify, if the encoder were to slightly dislodge and hence cause misreading about 0.1 degrees, this would correlate as roughly 4.7 Nm in terms of torque measurement. This would delay any operation at best and cause a certain injury to the user at worst.

Considering that any alteration on the mechanical aspects of the encoder is not possible, this problem was remedied by designing a new encoder adaptor. The encoder is tightly fitted inside the cylindrical housing on the new adaptor. The mechanical fastening between the adaptor and the encoder is achieved using the same configuration (two 160º apart M3 bolts). Instead of the previous rectangular arrangement with four M4 bolts, a circular configuration of eight M4 bolts is adopted to better distribute the effect of the disturbance moment. Furthermore, in order prevent any relative motion between the connector and the region of the link, semicircular bolt head slots were designed for them to be attached. To further cement the fixation of the encoder inside the adaptor's cylindrical housing, a circular pattern of eight setscrew is used.

Throughout the utilization of this design, no slippage was observed and torque measurements of the exoskeleton appeared to have improved. In order to demonstrate this improvement, a comparative experiment for the initial and the final design was carried out. In the experiment, a link connected to the Co-Ex SEA-A underwent a sinusoidal trajectory with a 5 degrees amplitude and 1 Hz frequency while carrying a load of 15 kg. The experiment was conducted twice; once with the initial design and once with the final design. The given position reference and the actuator's response can be seen in Figure 30.

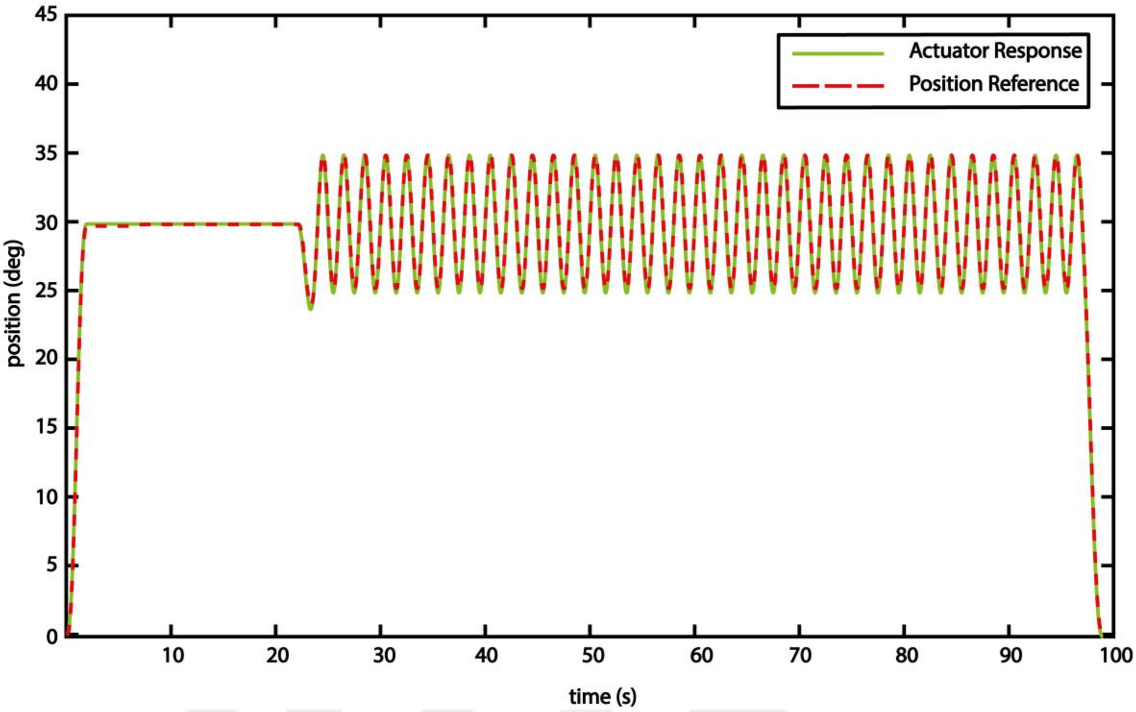

Figure 30: *Position tracking of the system*

Each trial was divided into four phases. In the initial phase, the actuator is rotated from its home position (which is about 164º with respect to the ground's norm axis) to the experiment position. In the second phase, the actuator waited in this orientation for 20 seconds for the 15 kg load, prior to be connected to the link. This load consists of three 5 kg dumbbells and it is connected to the link via stiff cable. In the third phase, the sine wave trajectory is given to the actuator and the torque response is measured. In the final phase, the actuator momentarily stopped for the removal of the payload and then returned to its home position.

In the initial phase to torque reading was expected as the payload had not been inserted. In the second phase after the insertion of the load a stable reading of 10.3 Nm was expected to be observed. This value was calculated with respect to torque equation shown in Equation 4.

$$\vec{\tau} = \vec{F} x \vec{r} \qquad \vec{r} = 0.068204\ m$$

$$\vec{F} = 147.15\ N \tag{4}$$

Based on these parameters the torque in this state was calculated as shown in Equation 5.

$$\vec{\tau} = 10.03\ Nm \tag{5}$$

For the third phase due to an angular displacement of +/-5º is applied to the motor with respect to its home position. Since the load was attached via a stiff cable, the load would oscillate and a comprehensive theoretical peak-to-peak torque value could not be attained. However, due to these oscillations a gradual vertical shift it is expected to be observed.

For the final phase, the torque output of the system is expected to reach 0 Nm as the load is removed. The torque response acquired from these two trials can be seen in Figure 31.

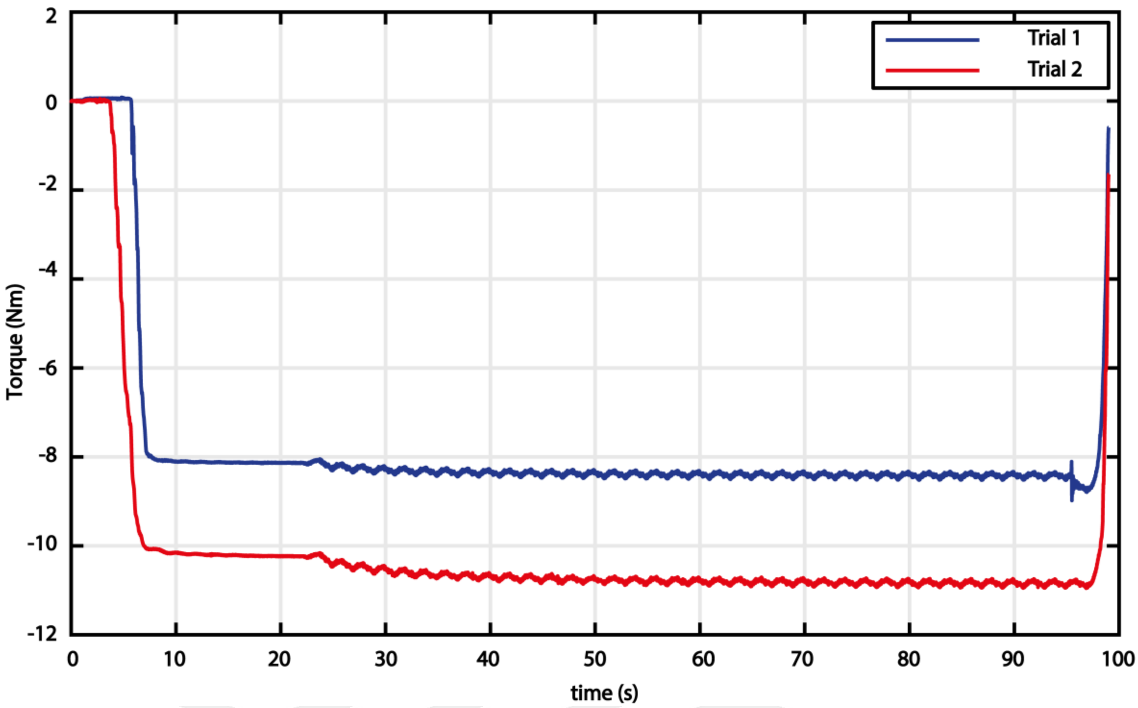

Figure 31: *Torque response of the initial and final designs*

As can be seen from the Figure the tracking performance of the final design almost matched the expected torque value in the second phase (10.02 Nm). For the third phase the expected gradual shift is more apparent in the final design in comparison to the initial one. In the final phase, just before the load was removed, a shift in torque reading was observed in the initial design. In the final design such a shift is not observed. Based on these results it can be said that the final design is able to acquire healthier torque data than the initial one.

3.1.2.4 Discussion

Several improvements have been done on the system as discussed. The resulting product can be seen in Figure 32.

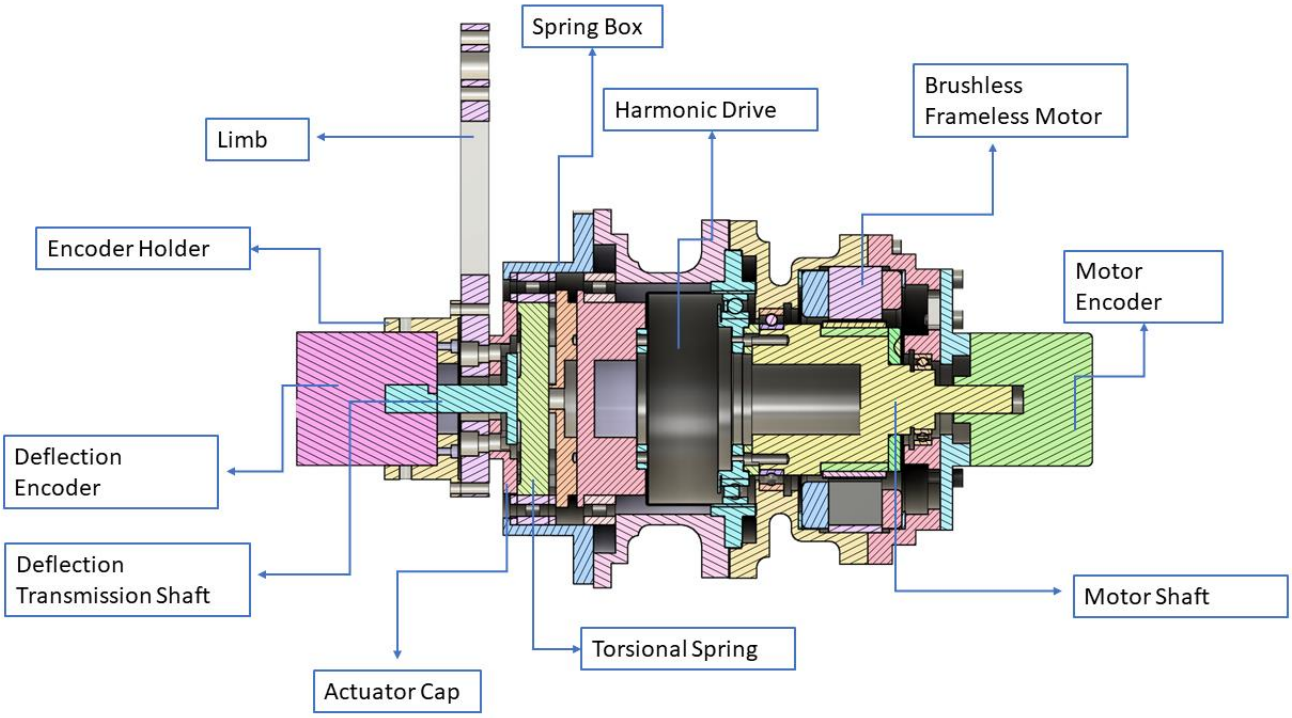

Figure 32: *CAD model of the final Co-Ex SEA B*

3.1.3 Prismatic Joint Design

In addition to the aforementioned SEA structure, the exoskeleton also consists of a prismatic joint. This joint was added onto the design to compensate for the Humeral Head (H-H) elevation of the shoulder as the user moves. The prismatic actuation unit could be integrated with an IMU to control the required H-H elevation for a given configuration based on the data acquired in [71].

Additionally, this joint can be used for adjusting the height of the exoskeleton for a specific user. The details on the height adjustability will be further explored in the following section.

In order to realize the prismatic joint, a brushed DC motor (Femsan 5M.06.06) was coupled with a reductor (Neugart PLPE 090 with a conversion ratio of 1:25). The motor is equipped with an emergency brake (YBF 02) and an incremental encoder (FNC 40HFS 8S1630V-R2). This assembly is then fitted on top of a linear stage (DKZM15) with a stroke length of 500 mm. The specifications of this assembly can be seen in Table 6 and the CAD model of the system can be seen in Figure 33.

Table 6: *Prismatic joint specifications*

Specification	**Unit**	**HH Joint**
Voltage	V	48
Max. Continuous Torque	Nm	72.5
Max. Angular Speed	rpm	80
Joint Reach	mm	500

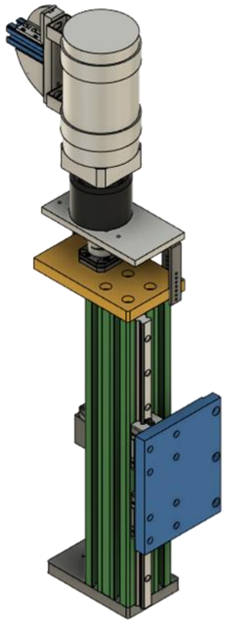

Figure 33: *CAD Model of the prismatic joint*

3.1.4 Actuator Placement

In the upper limb exoskeleton, a total of four actuators were used to realize four active DOFs. The configuration of the actuators can be seen in Figure 34.

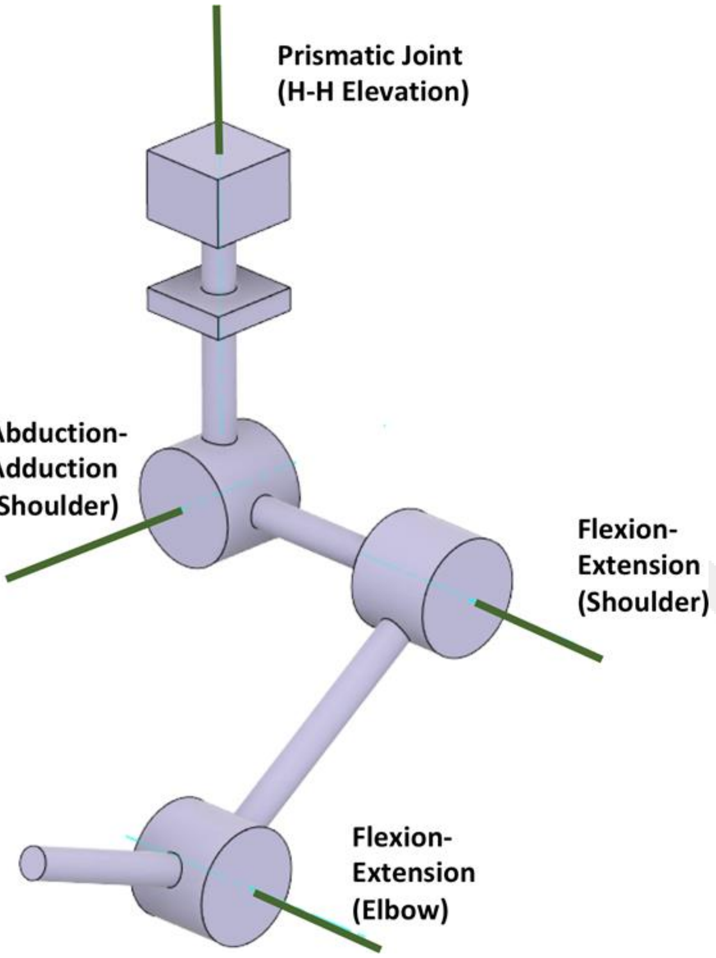

Figure 34: *Actuator layout*

This configuration could be sufficient enough to enable the user to conduct the majority of the tasks within factory settings [72]. The initial joint is the aforementioned prismatic joint that consists of a motor-reductor-linear stage assembly. The remaining joints of the system are SEAs. However, the improved designs of the system are incorporated to a different exoskeleton and this current exoskeleton consists of older versions namely two Co-Ex SEA B v1.0 and one Co-Ex SEA A v1.2.1.

For the shoulder abduction-adduction joint (SAA joint) and the elbow flexion-extension joint (EFE joint), Co-Ex SEA B models are used. For the remaining shoulder flexion extension joint, Co-Ex SEA A was used. These torque encoder caps of the older units were upgraded to the current design in order to get healthy torque data.

3.2 Exoskeleton Design

3.2.1 Identification of Design Requirements

Designing an exoskeleton is a complex engineering problem. As mentioned in Chapter I, safety is a main concern, as the system is intended to be worn by human subjects. In order to ensure the safety of such wearable systems, various measures and exoskeleton design strategies have been studied in the literature for a long time [31-35]. Various exoskeletons with varying design methodologies proposedly achieved the intended safety requirements.

A consideration that is evidently under explored in the literature is the effect of carrying an upper limb exoskeleton. Almost all of the upper limb exoskeletons that enable lower body mobility, transmit the load to either the back or hip section of their users. This inherently limits the load carrying capacity of these devices to what the load transmitted areas can safely carry. Additionally, although the arm section of the user is relieved from the effects of the load, the load and the weight of the exoskeleton are directed to the transmitted section of the body which then adversely affects this section instead of the arm. Thus, a critical design consideration for the exoskeleton is to transmit the load to the ground, without turning it to a full body exoskeleton, to render the system fit for heavy load manipulation.

A solution for this issue presented in the literature is the full body exoskeletons with upper limb focus. These systems allow the loads to be transmitted to the ground, however they

Followingly, as stated in the Literature survey, the state of the art commercially available industrial exoskeletons are generally passive systems that aim to assist their users in certain tasks such as lifting a load up or stabilizing the arms during a hard-to-maintain posture. Such systems achieve these features by storing energy during easier-to-conduct activities and releasing during harder-to-conduct ones. In other words, passive systems do not generate energy like actuated systems but repurpose the priorly generated ones.

With that being said, the utilization of this repurposed energy has to be task specific. For instance, a passive exoskeleton that is designed to hold a tool cannot assist its user to conduct overhead tasks, or an overhead task focused exoskeleton cannot assist its user to manipulate heavy loads. There are of course several passive exoskeletons that have more than one operation function, but they still need to be adjusted for that specific mode, which can be time consuming.

While the high preference of using passive systems in comparison to the active systems in applications with heavy load manipulation could appear counter intuitive, the passive systems have significant advantages over the active ones in a factory setting:

- Firstly, passive systems are lighter as they do not require power sources. Also spring systems that are used in the passive systems are lighter in comparison to actuators which are used in the active systems. This enables its user to wear the system which is similar to a backpack and move around with it easier. Undoubtedly, this is beneficial for the workers as tasks in factory settings are time dependent and the user needs to move around to achieve their tasks [72].

- Secondly, passive systems have a lower cost in comparison to the active systems due to lacking more expensive components such as the aforementioned actuators or power source. This is evidently more favorable for the employers.
- Thirdly, due to their lighter and less bulky nature; passive systems, on average, have a shorter don doff time.
- Fourthly, passive systems are sleeker; hence making them more comfortable to be used by the workers.

While this is the case for the industrial exoskeletons, the active upper limb exoskeletons appear to be more prevalent in medical and rehabilitative applications. The reasons for this preference can be summarized as:

- Firstly, the patients are unable to comfortably operate an energy input requiring system, due to their injury.
- Secondly, as there is no need for lower body mobility during the rehabilitation process of the upper body, the system can be an immobile system, which transmits the system's weight and the weight of the user's arm to the ground.
- Thirdly, the patient is in need of assistance during every stage while the exoskeleton is being worn. Thus, unidirectional assistance that the conventional passive systems offer is not beneficial.

Even with the specific advantages that the active and passive systems provide to the areas they are being predominantly developed for, there are also advantages of using passive systems for rehabilitation purposes or active systems for industrial purposes. A properly designed passive upper body system may assist patients, whose injuries do not prohibit them to operate the system, to undergo rehabilitation while they conduct ADL; whereas an active system with higher torque generation capacity allows its user to manipulate heavier loads comfortably than a passive system can support. Furthermore, in my opinion, active systems are more flexible for improvements. The hinderances that such systems would bring to the overall product can be either bypassed or diminished with comparatively simple alterations. Unlike the passive systems, these alterations would not result with the requirement to adjust the working principle of the system. The only inflexible aspect of the active systems is their cost. Although the cost cannot be reduced to a comparable level to a passive system without jeopardizing the functionality of the system, a more comprehensive and beneficial final product can be achieved. Hence, in my opinion, the benefits of utilizing an active system over a passive system would overweigh this cost.

Thus, for the design of the upper limb exoskeleton an active system which tolerates heavy loads and gives its user the liberty of choosing the assistance they require without using a different exoskeleton for different tasks was chosen, as would be the case in a task specific passive exoskeleton. Also, based on the considerations suggested by Elprama et. al. [34] the aforementioned hindrances of the active systems were attempted to be minimized.

In order to remedy the don-doff time, the exoskeleton is designed as a single arm structure with two strapped size adjustable connection pads; one for the forearm and the other for the upper arm of the user. In order to render the exoskeleton usable by different individuals the limbs were designed as sliders. These adaptations and the considerations behind them are detailed in Section 3.2.2.

As high torque outputting actuators are used in the system, the load carrying capacity of a typical active dual-arm exoskeleton can be transferred to this single arm. With that being said the limbs of the exoskeleton is also required to remain mechanically intact during such operations. The mechanical design and the validation of this design is further explored in Section 3.2.3.

In order to ensure that the exoskeleton is viable to be used in a factory setting a modular end effector design is derived. During this derivation the considerations for the limbs were taken into account in addition to nature of various common AFS. Respective design is further explored in Section 3.3.

In order to bypass the limitation on the load carrying capacity introduced by the human muscoskeletal structure, the weight of the system is required to be projected to the ground. In order to achieve this without sacrificing the mobility of the system, a wheeled frame is designed to house the exoskeleton. The specifics of this frame is detailed in section 3.4. Finally the electronic components and communication design is explored in Section 3.5.

3.2.2 Exoskeleton Limbs Design Methodology

3.2.2.1 Adjustability

The developed exoskeleton is of the anthropomorphic type, therefore the length of limb segments and the joints of the human should overlap on the plane of motion for effectively assisting the user and eliminating any discomfort due to misalignment. Henceforth, segment limb of the exoskeleton should be the same as the user’s limb size. Introducing this nature to the exoskeleton would be a straightforward process, as it would be achieved by measuring the individual’s arm segment lengths, arm segment radii, and the person’s height. However, this would only be the case where the exoskeleton is being designed for a specific individual, which is not applicable for the exoskeleton at hand.

In the following subsections, the methodology and design selections for achieving a size adjustable exoskeleton considering these parameters will be explored.

3.2.2.2 Height Adjustability

For rendering the system usable by individuals with different heights, the exoskeleton is equipped with a prismatic joint to adjust the elevation of the exoskeleton arm. The range of this prismatic motion is selected to be 500 mm. This selection aims to achieve two objectives, namely; i) to accommodate the 95% distribution of the world’s population, which has a height between 155-195 cm [73] and ii) to accommodate for the shoulder’s Humeral Head elevation joint that displaces approximately +/-5 mm from anatomical home position during a full swing of the arm.

3.2.2.3 Segment Length Adjustability

Since the current exoskeleton is intended to be used in factories by different individuals, it should be designed in a way to accommodate different individuals with different arm lengths and heights. An easy and straightforward method of achieving this could be coming up with a design that has a high range of adjustability that covers more than the range from the shortest to the longest possible arm length. However, this would be counter intuitive to the design methodology of the exoskeleton, as this range would be much larger than it needs to be. This would result in the exoskeleton having additional unnecessary weight, which would diminish the payload carrying capabilities of the exoskeleton itself. Thus, the range of the adjustability should be as minimal as possible while continuing to accommodate the majority of the people within the height range of 155-195 cm.

The maximum and minimum limits of this intended adjustability are, however, significant challenges; as the literature did not offer many comprehensive studies regarding to these extremities for the human upper limb. The available sources in this stage were mostly related to estimating the average biomechanical properties of the human arm segments and did not offer me a meaningful range. In order to proceed, two calculated assumptions were made:

- Male individuals have, on average, longer arm span than female individuals with the same height.
- The upper extremity length is directly proportional with the individual's height.

The later assumption allowed me to expand my literature survey to include research that focus on the relationship between the arm length and the person's height. With this information, I was able to deduce a mean value of arm length for a given height. Nevertheless, it should be underlined that the participants which were utilized as datasets on these research were not very diverse regarding to correlation between the height and the arm span [74,75]. Thus, while using the data, a +/-10% error margin for the upper and lower limit values of the range was applied.

In order to devise the individual lengths of the subsegments of the arm (namely upper arm, forearm and the upper hand), the data presented in de Leva et al.'s work was utilized [76], in which the mean percentile ratios of the arm segments with respect to the entirety of the arm is presented for male and female individuals in a test group.

In pursuance of achieving the size adjustability of the anthropomorphic exoskeleton, the exoskeleton limb segments similar to the structure presented by Wang et al [33] were designed. Each limb consists of three parts: i) one male, ii) one female and iii) the motor holder at the end of the male limb. Male and female sub-parts for the limbs are connected via slider-like structure. The male part is directly attached to the motor's actuator cap that is carried by the motor holder of the previous limb and fastened by bolts. The male part is fitted inside the slider rail depending on the intended limb size on the male part and then fixed to that location via bolts. The motor holder that was used to actuate the next limb was then fastened to the other end of the female part. This assembly can be seen in Figure 35.

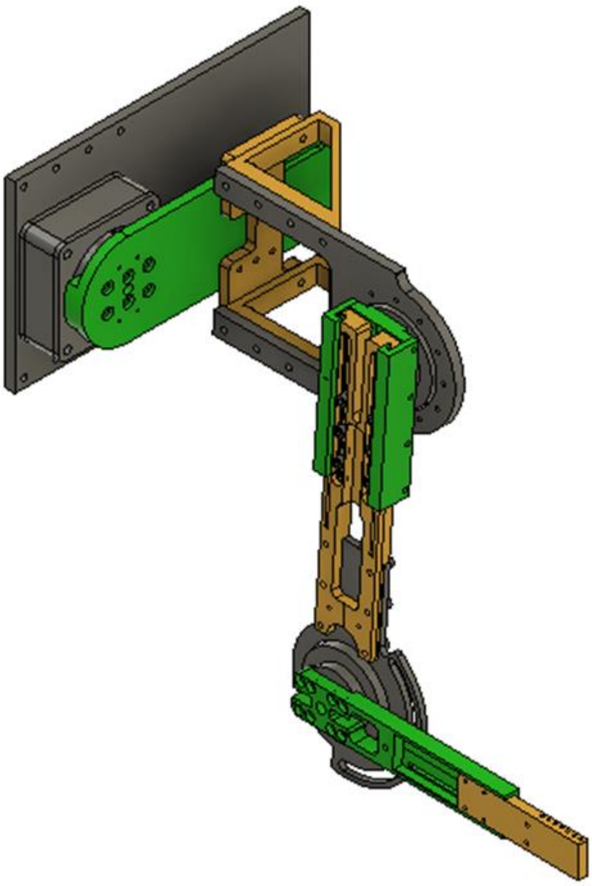

Figure 35: *Exoskeleton limb assembly*

3.2.2.4 Segment Radii Adjustability

Similarly, the different users of the exoskeleton are bound to have different arm thicknesses. In order to accommodate for these variations between possible users, the exoskeleton's connection pads are also made adjustable. The range for this adjustability is acquired from de Leva's work [76], in which he provides the percentile radii of gyration for the longitudinal axis of the body segments in accordance with their lengths for males and females.

In light of this data and previously established maximum and minimum possible sub segment lengths, the upper and the lower limits for the pad structure were deduced. These limits and the range of the exoskeleton limbs can be seen in Table 7

Table 7: *Upper and lower limits for the pad and the limbs*

	Upper Range for the Limb	**Lower Range for the Limb**	**Upper Range for the Limb Circumference**	**Lower Range for the Limb Circumference**
Upper Hand	105 mm	45 mm	-	-
Forearm	305 mm	195 mm	210 mm	370 mm
Upper Arm	340 mm	245 mm	260 mm	510 mm
Shoulder	280 mm	210 mm	-	-

3.2.3 Mechanical Design of the Limbs

3.2.3.1 Mechanical Design Methodology

I had to reach a certain point on a trade-off curve between safety and the weight, in order to realize the mechanical design of the limbs. Safety, as previously mentioned on numerous occasions, is a crucial aspect of the design of a wearable system. However, the design should also be as light as possible, in order to maximize the load carrying capacity of the system.

In order to ensure that the system is both safe and as light as possible, an iterative design procedure was utilized. In the first phase the limbs and the motor holders were designed in an over safe and bulky form, while staying loyal to the guidelines that I have established for size adjustability. For the material, Aluminum 6061 that has T6 grade tempering was chosen (Yield Strength 240 MPa) due to its high yield strength-to-weight ratio.

For the second phase, individual free-body diagrams for the individual limb parts were derived. While deriving these diagrams, several factors were taken into account, including the length of the limb, the mass, the center of mass, the amount, and the distance of the bolt connections for the parts. The free-body diagrams were constructed from the final limb (male forearm) to the initial one (female roll limb of the shoulder). Although each free body diagram is unique, only two distinct types could be generated throughout the system.

The initial one is named as the limb case. The distinction of this case is that the effective moments around the supporting bolts of the limbs are cumulative. This means that, when calculating the moment around a supporting section, all the previous forces should be taken into account. Therefore, the primary and the secondary shear forces at the supporting bolts also influence the effective moment. The second case is named as the motor holder case. All of the motor holders are circular and the load carried by them are supported via evenly distributed bolts. In this case, the moment of the previous forces is not cumulative. Instead, they are effectively acting on the center of the circle of the motor holder. The moment was calculated through the distance of the center from the supporting section of the link [77]. These forces were calculated based on Equation 6 and Equation 7.

$$F' = \frac{V}{N_{bolts}} \tag{6}$$

$$F'' = \frac{Mr_n}{\Sigma r_i^2} \tag{7}$$

In Equation 6, F’ is the primary shear, V is the total shear force exerted on the system and N bolts is the number of bolts that the limb is supported by. The primary shear is the same for all of the bolts and in the same direction as the resultant of the external forces. In Equation 7 F’’ is the secondary shear, M is the moment acting on the system, rn is the distance of the bolt to the center of rotation and Σr_i^2 is the sum of squares of the distance of the bolts to the center of rotation. F’ is the same for all of the bolts and in the same direction as the resultant of the external forces. F’’ is different for all of the bolts in magnitude, depending on the distance of the bolt to the center of rotation. It is in the same direction with the effecting moment.

In order to simulate the maximum possible stress that the system could undergo, an extreme case scenario was simulated. In this scenario, the exoskeleton is used by an individual who has a height of 195 cm (the upper height limit for the individual that can use the exoskeleton) and the longest arm configuration that the exoskeleton can be adjusted for. Followingly, the point where the application of the load is selected. This point was approximated about 0.2 meters away from the end effector module 1 along the central line of the male forearm link.

The described individual, who is wearing the system, tries to carry a load that is at the capacity of the actuators. To achieve this setting, a force input, that would match the SEA of the investigated limb’s maximum continuous torque capacity to effectively stall the motors was applied. In order to investigate the response of the system in this state; stress, safety, and displacement analyzes were conducted following the derivation of the free body diagrams for the parts in question. After this process, free body diagrams for these cases were constructed.

3.2.3.2 FEA for Mechanical Analysis

The exoskeleton limbs were analyzed concerning the stress, displacement, and the safety factors. During this analysis, the material's yield strength concerning the two types of limb components and end effectors were taken into account. The mechanical design at hand was reevaluated to diminish the over-safe parts by altering the topology of the examined parts. The topology of the examined parts were altered by machining these areas out. The result of the stress displacement can be found in Figure 36.

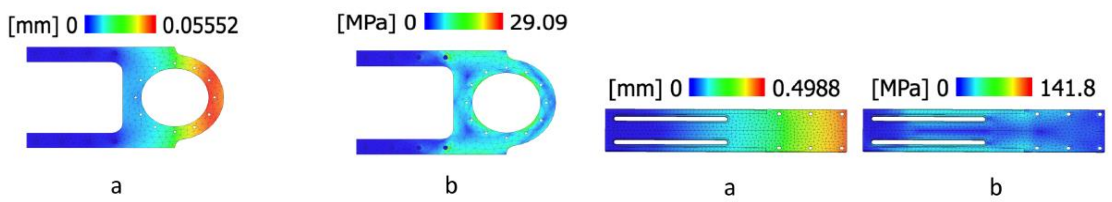

Figure 36: *The results of the stress and displacement*

In order to ensure the validity of the optimization, the redesigned parts were reanalyzed by considering the changes in the mass values. In addition to that, the structural integrity was validated by conducting this secondary analysis. The results of this secondary analysis in terms of stress displacement and safety factor as well as the CAD design of the newly acquired parts can be seen in Figure 37.

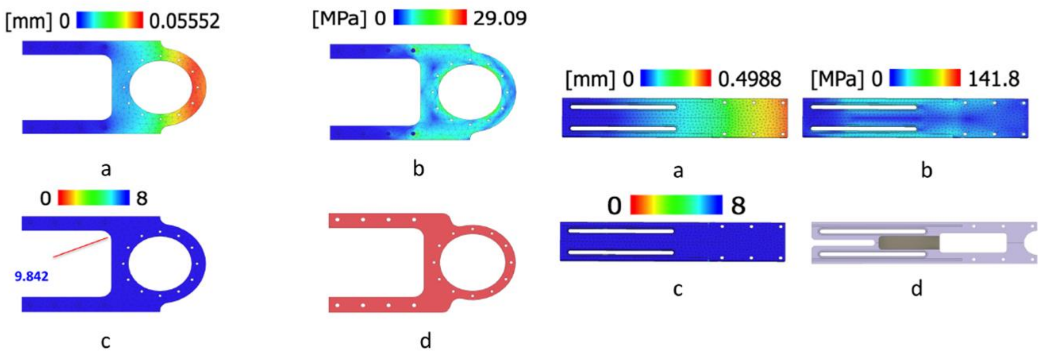

Figure 37: *The CAD design of the newly acquired parts*

3.3 End Effector Module Design

Throughout the duration of this thesis several end effector modules were designed. These designs have utilities to assist their user in the AFS that they would commonly encounter. In section 3.3.1 these AFS were categorized and the required utilities for the end effectors were obtained. In section 3.3.2 the resulting modular end effector design and its FEA analysis is given. In section 3.3.3 the second part of the modular end effector designs are relayed.

3.3.1 Categorization of AFS

In order to construct a comprehensive understanding of the common AFS, employer activities in various factories were taken into account based on [8,10].

In the literature, the consensus on leading factors of developing musculoskeletal disorders is the high repetition of AFS [8-10]. The most common tasks associated with such AFS can be categorized as follows:

- Experiencing high forces (i.e. conducting tasks such as lifting a heavy payload),

- Experiencing vibration (i.e. operating high vibration generating tools such as drills and cutters)
- Stretching and relaxing muscles frequently (i.e. conducting tasks including overhead object manipulation and using rotary tools like screwdrivers)

The proposed upper limb exoskeleton can potentially diminish the effects of the first and the last items for the arm of the user. However, the structure does not cover the wrist and the hand of the user. Therefore, this region remains susceptible to all of these factors. In order to extend the coverage of the exoskeleton to the wrist, an end effector that supports this area is required. Furthermore, the vibration from operating tools is initially experienced by the hand and is then transmitted to the body. Therefore, the end effector should also include a tool holding structure that transmits this vibration to the exoskeleton rather than to the user. In light of these concerns, a design of a modular end effector is proposed. The components of the end effector are named as End effector 1 (EE-1) and End effector 2 (EE-2). EE-1 is designed for securing the wrist during high payload manipulation and overhead object manipulation, whereas EE-2 is designed for securing power tools.

3.3.2 End Effector 1

EE-1 module is designed with the similar considerations that were applied to the upper body exoskeleton's limbs. These considerations are the size adjustability for a given individual's wrist and hand as well as the load carrying capacity of the system.

The size adjustability parameters (namely the width of the wrist and the wrist extend) for the module are attained from de Leva's work as stated in Section 3.2.1. Based on these parameters, EE-1 was designed to be size adjustable for the width of the wrist and the length of the wrist extend (the length from the end point of the upper arm to the mid-section of the palm).

In order to secure the wrist in an ergonomic manner, a cushioned holder that has variable stiffness was placed at the inner circumference of the module. This structure helps to transfer the torque load that the human wrist experiences to the exoskeleton properly while lifting an object [78,79].

Based on the exoskeleton’s targeted load capacity, the wrist was required to be designed to support the user with the longest limb dimensions to carry a payload of 20 kg. Nevertheless, as observed on the initial analysis, the yield strength of the Al 6061 T6, which was the material used in the rest of the limbs, was not sufficient. Thus, a hybrid design methodology with two different materials was utilized for EE-1. The material for the section where the back of the wrist is placed, as well as the size adjustable modules, are kept as Al 6061 T6. The adjacent section, which corresponds to the inner side of the wrist, was made of Aluminum 7075-T651, to be able to dissipate the stress of the carried load easily. Both of the aforementioned sections were coated with a variably stiff element to strengthen the grip of the user [80]. In order to validate their performance a FEA was conducted on this module and the integrity of the design is validated (Figure 38).

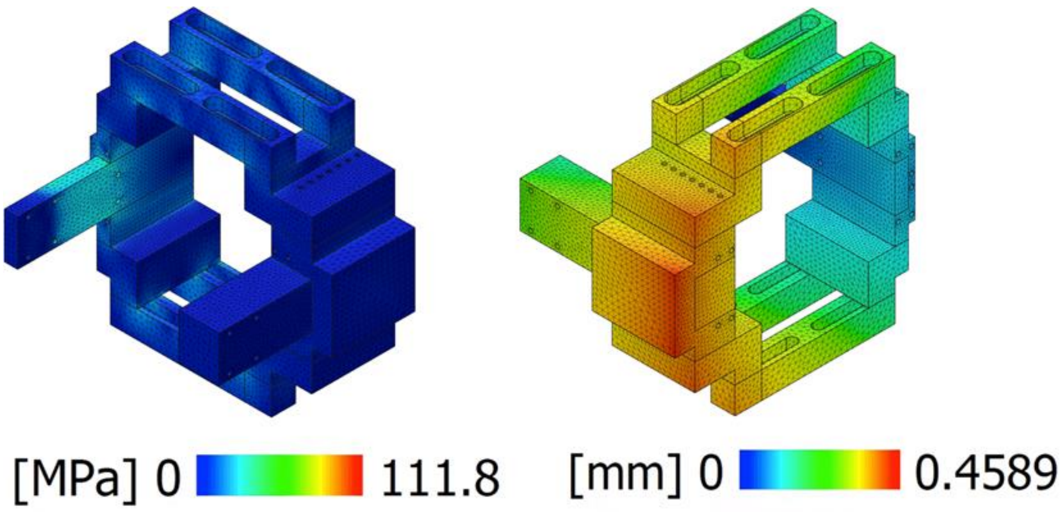

Figure 38: *Stress and displacement analysis for EE-1*

3.3.3 End Effector 2

This secondary module, EE-2, was designed to both secure a given power tool and to ensure that the load is to be carried by the exoskeleton instead of the user as well as to transfer the vibration of this tool to exoskeleton instead of the user during operation. A clamp form is selected, as it would be best suitable for this application. EE-2 is designed to be an add-on module to be used for holding a power tool. However, during heavy payload manipulation, it needs to be removed.

Similarly to EE-1, EE-2 is also designed to be size adjustable based on the length of the tool. However, the range for this adjustability was established arbitrarily contrary to the rest of the parts. This was due to the immense variety in power tools and varying grasping preferences of diverse users as well as differing positioning techniques of different power tools.

With that being said, based on the lower gravitational forces that this piece would experience, it is not needed to be a reinforced module. Thus, a light design can be utilized for it. Therefore, this arbitrary range is expected not to be detrimental to the load carrying capacity of the system.

In light of these considerations, several different EE-2 modules were designed, iteratively to best suit for a variety of tools. All of these modules have the same clamping principle. The initially designed mock-up version of EE-2 attached to EE-1 can be seen in Figure 39.

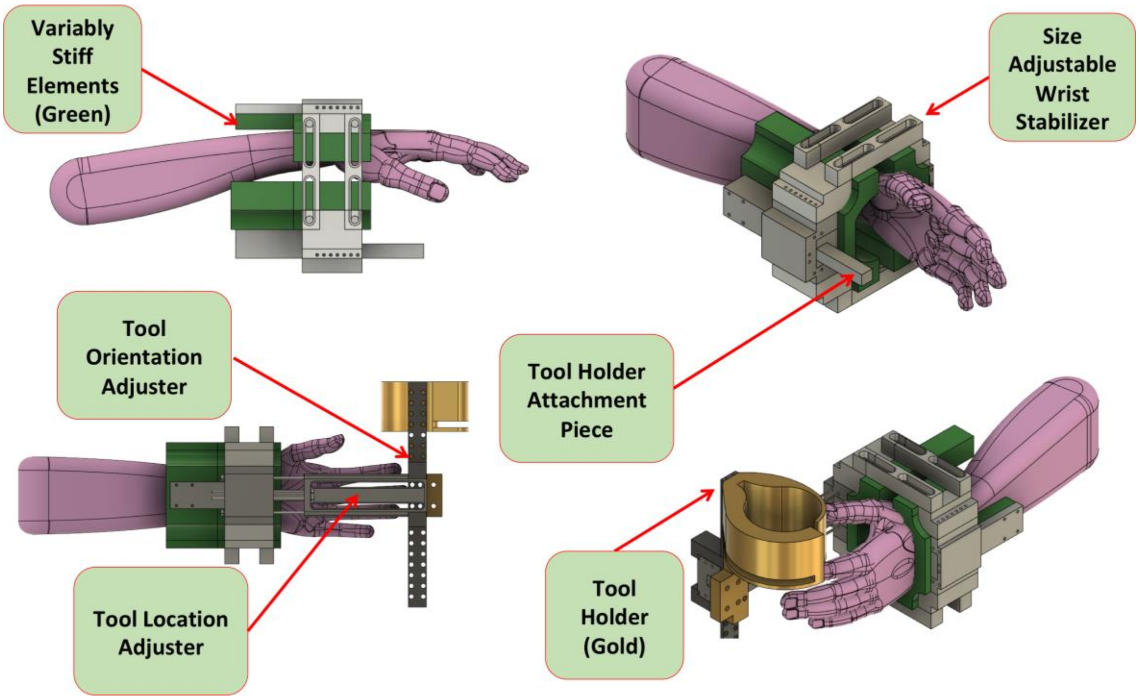

Figure 39: *The Initially designed Mock-up Version of EE-2 and EE-1*

3.3.3.1 End Effector 2 Universal Rotary Tool Form

This initial version of the end effector was designed specifically for securing rotary tools, in particular Dremel brand tools. It can safely secure Dremel 3000 and Dremel 4000 models.

The holder was made out of Al 6061 T6 and weighted 0.45 kg. The assembly of the Dremel tool is initiated from the middle clamp. The desired Dremel tool is inserted inside the clamp until it reached the midsection of the tool. Followingly, the back clamp is inserted to the back of the tool. After they are secured, the nut on the middle clamp is tightened to further constrict the tool. Subsequently, these clamps are fixed to the base plate. After this fixation, the tool tip of the Dremel is removed and it is inserted into the tool clamp. The extruding threaded surface of the Dremel is fastened via either the removed tool tip or a matching nut. Finally, the tool clamp is fixed to the base plate, which is then connected to the EE-1. In Figure 40 an exemplary assembly of Dremel EE-2 can be seen.

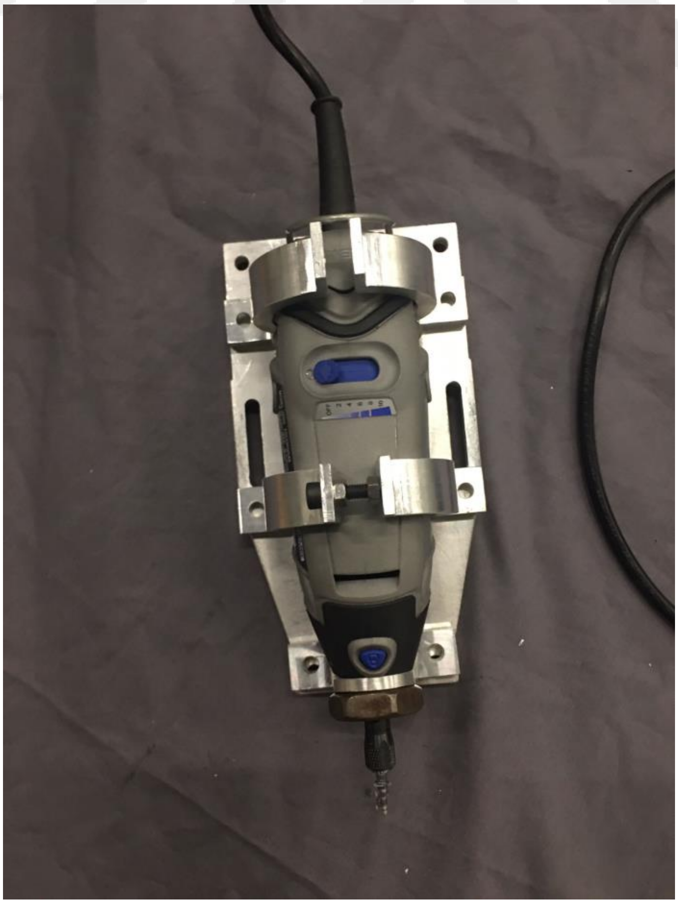

Figure 40: *The exemplary assembly of Dremel-EE-2*

3.3.3.2 End Effector 2 Opposable Thumb

Following this initial design, the form is altered for the module to be compatible with various tools such as drills, rotary saws and other common hand-held power tools. While coming up with a tool holder design, the majority of tools' grips are assumed to be designed to optimize the griping performance. Therefore, the best possible clamping option would be a tool holder in the shape of a hand. The grasping of any power tool is realized by contracting four fingers against the thumb. In this grasping motion, the thumb is relatively fixed and the finger phalanges are positioning themselves around the thumb to grasp the tool and secure it around the first interdigital space [81].

Based on these assumptions, a tool holder with a fixed thumb and rotatable index and middle finger was designed. The lengths of finger phalanges and the width of the first interdigital space are designed in accordance with an estimated average of human hand, based on the data presented by [82].

These fingers can be fixed at any given phalange to accommodate the tool that is being hold. The thumb extends to a fixed semicircular structure. This structure houses a slider that the finger assembly can be fitted based on the required diameter of the tool to be held. To be able to fit into this slider, the index finger is equipped with an additional phalange. The CAD design of this tool holder can be seen in Figure 41.

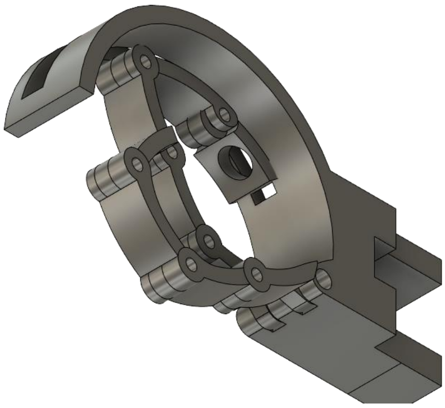

Figure 41: *The CAD design of EE-2 Opposable Thumb*

The initial prototype of this design is printed using Markforged 3D printer. Onyx polymer with a solid fill is used for these parts. The assembled version of this EE-2 was tested on several power tools.

Based on these trials it was concluded that the grasping performance of this tool holder was only suitable for power tools with a large diameter and the fixation method needed to be improved.

3.3.3.3 End Effector 2 Constricting Chain

Based on the conclusions derived from the previous EE-2 module, a secondary version was developed. This design utilized the same phalange structure, nonetheless the segment that would perform the task of the thumb was not fixed. The design consisted of an index and a thumb. These are placed on the upper left and lower right of a base frame. This frame acts as the first interdigital space between the finger and the thumb. The phalange structure of the finger and the thumb is repeated until they can surround the frame. The thumb and the finger digits are then fixed to obliquely placed shafts situated at the alternating sides of the base frame. These shafts can rotate and conduct a constrictive motion against each other. In order to secure the constriction, the shaft connected to the index finger is extended downwards to meet with the shaft of the thumb. In addition to that, a rigid connector rod is connected between these shafts to fix the constriction. Similarly to the previous module, this version was also tested on the same power tools.

Based on these trials, it was concluded that the grasping performance of this tool holder was suitable for all of the power tools that were tested. CAD model of the design and the actual design can be seen in Figure 42.

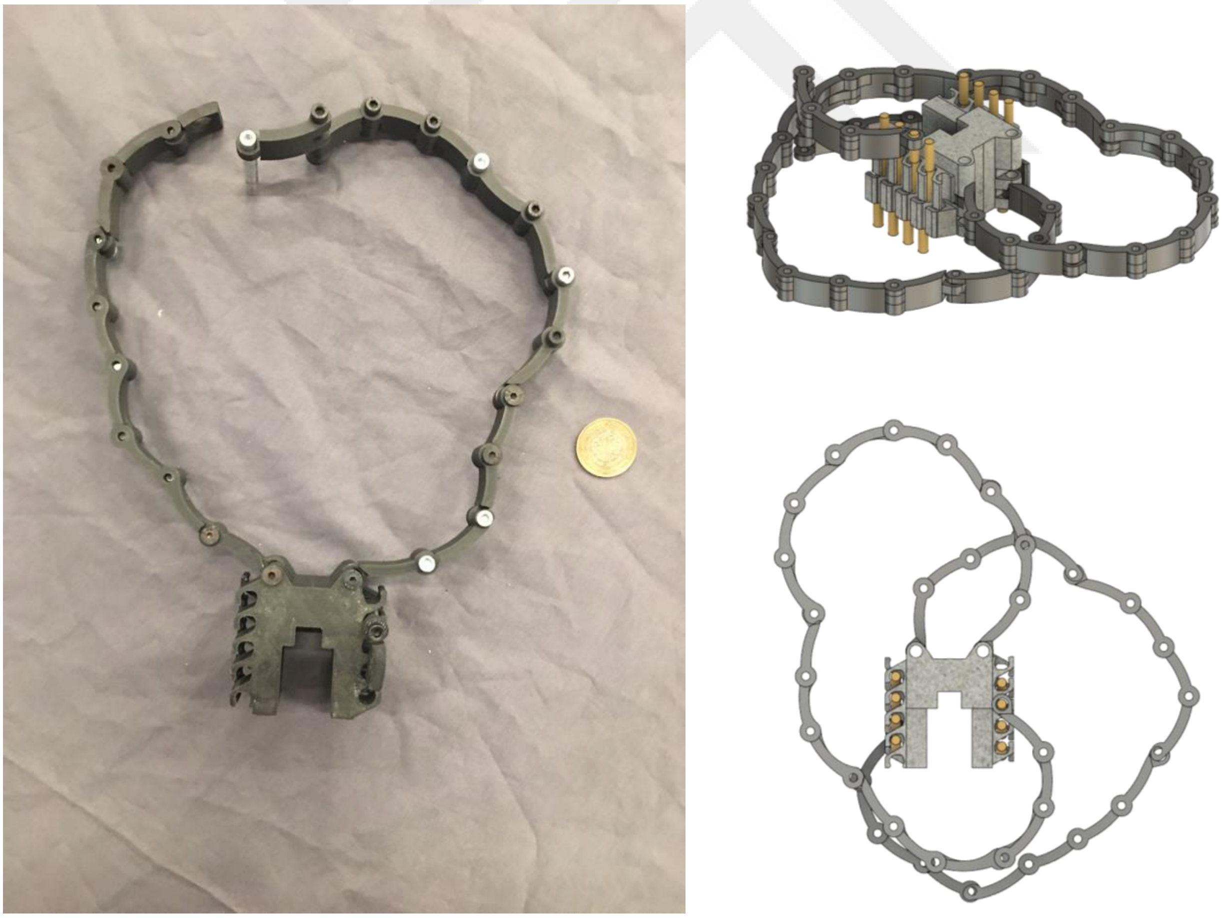

Figure 42: *The CAD assembly (right) and the manufactured prototype of the EE-2 Constricting Chain*

3.4 Platform Design

In order to achieve the transmission of the load to the ground without sacrificing the mobility of the system, the exoskeleton was mounted on a mobile frame. This frame consists of a 62 cm x 50 cm x 1.5 cm rectangular plate, which was kept small to transport the system easier as well as making it easier to work within confined spaces.

A central support column of 80x80 mm Al Sigma profile with a height of 1.1 m is used. The exoskeleton's stage is then connected to the support column via three 80x40 sigma profiles that are mounted perpendicularly to the support frame. This preference in the design was made in order to not restrict the range of motion of the exoskeleton.

A rectangular profile of 40x80 was cut on the mid length of the base plate to insert the support column. A rectangular arrangement of 40x80 sigma profiles are also connected to the bottom of the plate in a way that the righthand side of this configuration would touch the support column. The support column and the rectangular frame are then connected to each other via surface mount connectors.

The design is equipped with six legs. Each leg has a 12 cm diameter wheel with adjustable brakes on them. This number is selected to effectively support the weight of the support column on all sides. Four of the legs have a height of 68 cm and are distributed along the four corners of the rectangular configuration.

The front and the back legs on each side are connected to each other via additional sigma beams at an angle of 45^o for further support. The fifth leg, which has a length of 76 cm, is placed on the opposite side of the support frame. The last remaining leg is directly attached to the support frame at an angle to prevent the system from tipping due to the weight of the frame.

Even with this configuration, the exoskeleton is susceptible to tipping over, as the system is front-heavy, due to the moment created by the exoskeleton's weight. In order to stabilize the weight distribution, additional counterweights were placed at the back of the system.

A PC is then placed on the back of the plate. Two sigma profiles were added onto the plate, next to the support frame and in front of the PC to form an "U" shape. Then a plexiglass plate is inserted into this shape to house the circuitry, power sources and the motor controllers as well as separating the robot side from the computer side. The resulting arrangement can be seen in Figure 43.

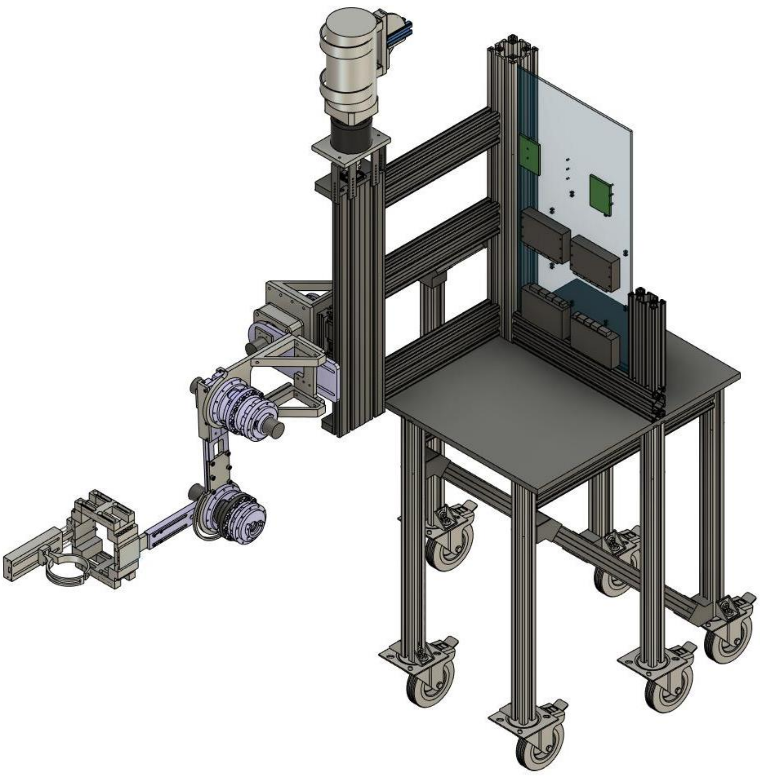

Figure 43: *The CAD assembly of the exoskeleton*

3.5 Electronics and Communication Design

The low-level electronic circuit consists of two Raspberry Pi 3B MCU (microcontroller unit), a DP83848 Ethernet module, a digital multiplexer integrated chip for reading multiple encoders and line drivers to convert differential signals of the SSI (Synchronous Serial Interface) into a singular signal. This configuration is capable of collecting the encoder position and velocity data simultaneously from the seven encoders in the system. The schematics of this chip can be seen in Figure 44.

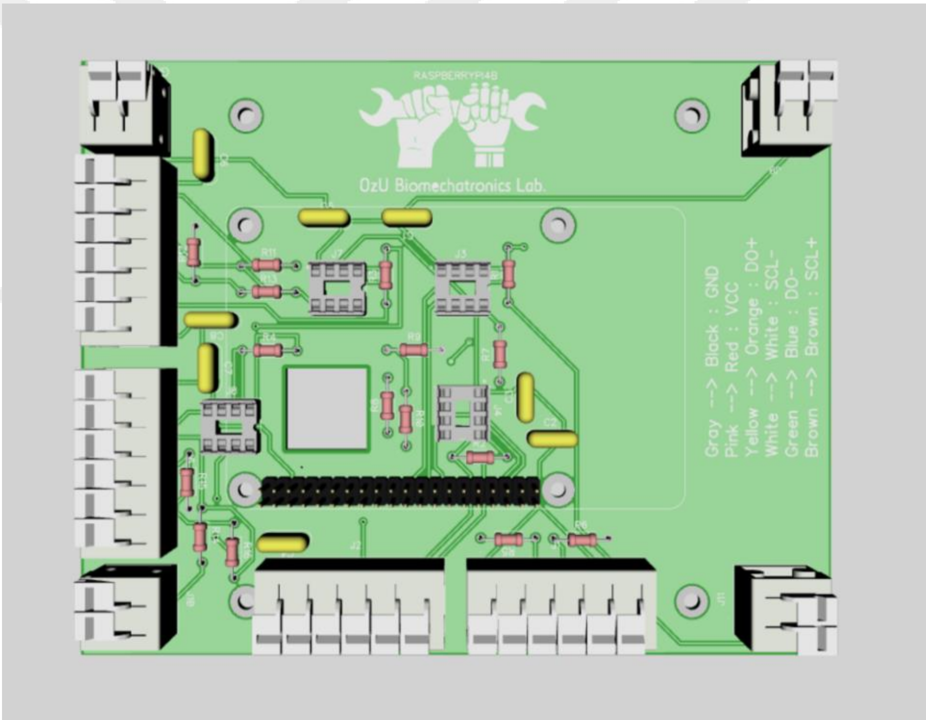

Figure 44: *Encoder data processing PCB*

The MCU runs FreeRTOS kernel to ensure real-time operations. The tasks that are handled by the MCU are collecting data from encoders and calculating the positional reading of each joint, as well as transmitting the data through the Ethernet port. The Ethernet speed was chosen as 100 Mbps for this application and the main loop for data collection was run in 1 kHz sampling frequency. The system also houses high resolution DAC (Advantech 1723) and ADC (Advantech 1716) cards to transmit and receive additional data.

The DAC card's digital output feeds the reference voltage value calculated by the controller of the motor drivers. In order to drive the SEA units, Maxon's ESCON 70/10 4-Q Servocontroller model is used. These controllers can supply +/-10A current to the actuators. The sign of the supplied current determines the direction of rotation.

In order to drive the prismatic joint, BAMSI 4Q.DC.DRV.200S motor driver is used. This motor driver can only supply a positive current. Therefore, in order to determine the direction of rotation, additional digital inputs are needed to be fed into the driver. The truth table for the action that the motor will take can be seen in Table 8.

Table 8: *The truth table for BAMSI motor driver*

Forward	**Reverse**	**Stop**	**Output**
Low	High	High	Forward
High	Low	High	Reverse
High	High	Low	Stop

These digital inputs are fed through ADC's digital output terminals. In addition to this, the ADC module also receives analog inputs outputted by the intention estimating brace and relays them to the main computing unit to be interpreted as reference torques. The operational schematic of this system can be seen in Figure 45.

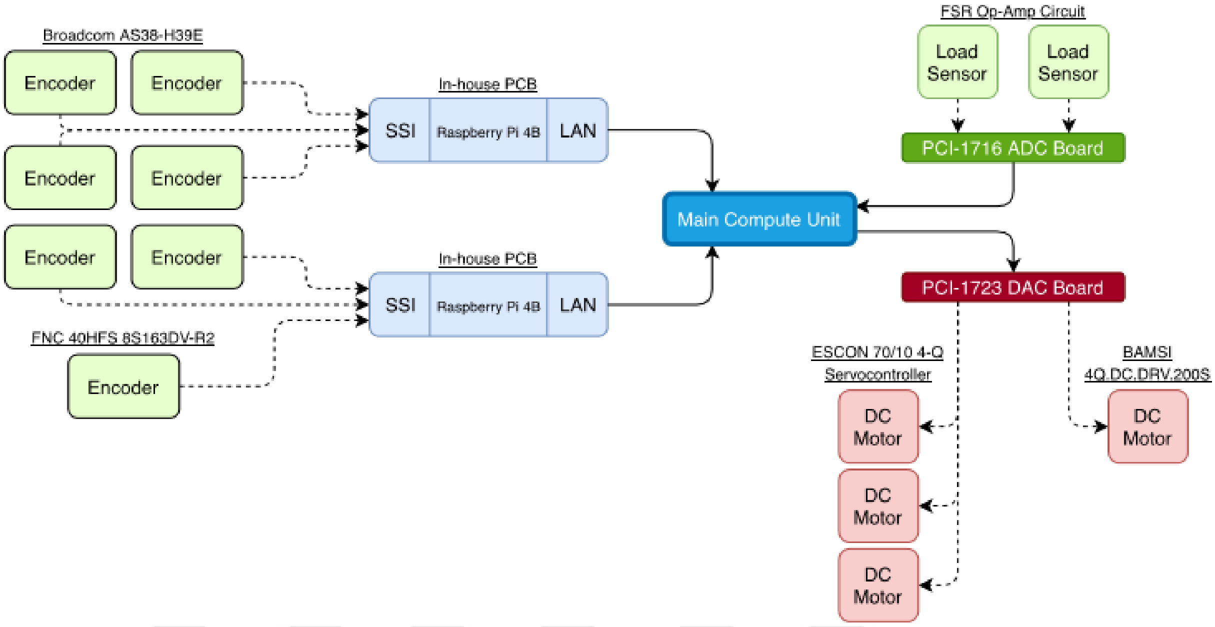

Figure 45: *Computational system layout*

3.6 Safety

In Chapter 1, the impact of the perceived safety of the exoskeletons and measures to render the system to be perceived as safe by the workers is explained. With that being said, in addition to the perceived safety of a system, the actual safety is also an equally crucial aspect. Safe utilization of robotic systems in factories are utilized through safety measures and standards. The requirements for the safe and reliable utilization of any kind of robotic system is explained in detail in Chapter 1. These requirements are divided into three phases of the robot's life cycle, namely the installation phase, operation phase and the maintenance phase. To ensure that these requirements are met, several definitions of existing components in a robotic system are derived and regulations are being implemented internationally through related ISO documentations. These standards can be application specific, such as the environment and the task that the robot will conduct.

They can also be type specific, such as the nature and the type of interaction that the robot is going to conduct with its environment.

In order for any system to be able to see commercial use a CE certification for the system is required. To obtain this certification, the relevant harmonized standards for the system is needed to be met. Followingly the remaining possible safety issues are needed to be identified, and finally a risk factor analysis is needed to be conducted on them [83].

Presently, there are a total of 98 different regulations and definitions including documents for different robotic systems. Additionally, with the inclusion of the same parameters for electrical machinery, which the robotic systems are a subset of, this number increases to 167. Given this multitude, following deductions were made to reach the set of regulations that would apply the proposed system:

- The proposed system is an exoskeleton, i.e. a personal assistance device used to augment physical capabilities of its users.
- The proposed system is an electrical machinery with a control algorithm.
- The proposed system is intended to be used in an industrial setting, i.e. a factory.
- The proposed system can be considered as a mobile robot.
- The proposed system targets the upper limb of its user.
- The proposed system assists its user in manual labor tasks.
- The proposed system is intended to be used by able-bodied individuals.
- During operation, the proposed system can be considered under the definition of a collaborative robot (co-bot), depending on the nature of the conducted task (i.e. two hand requiring tasks).

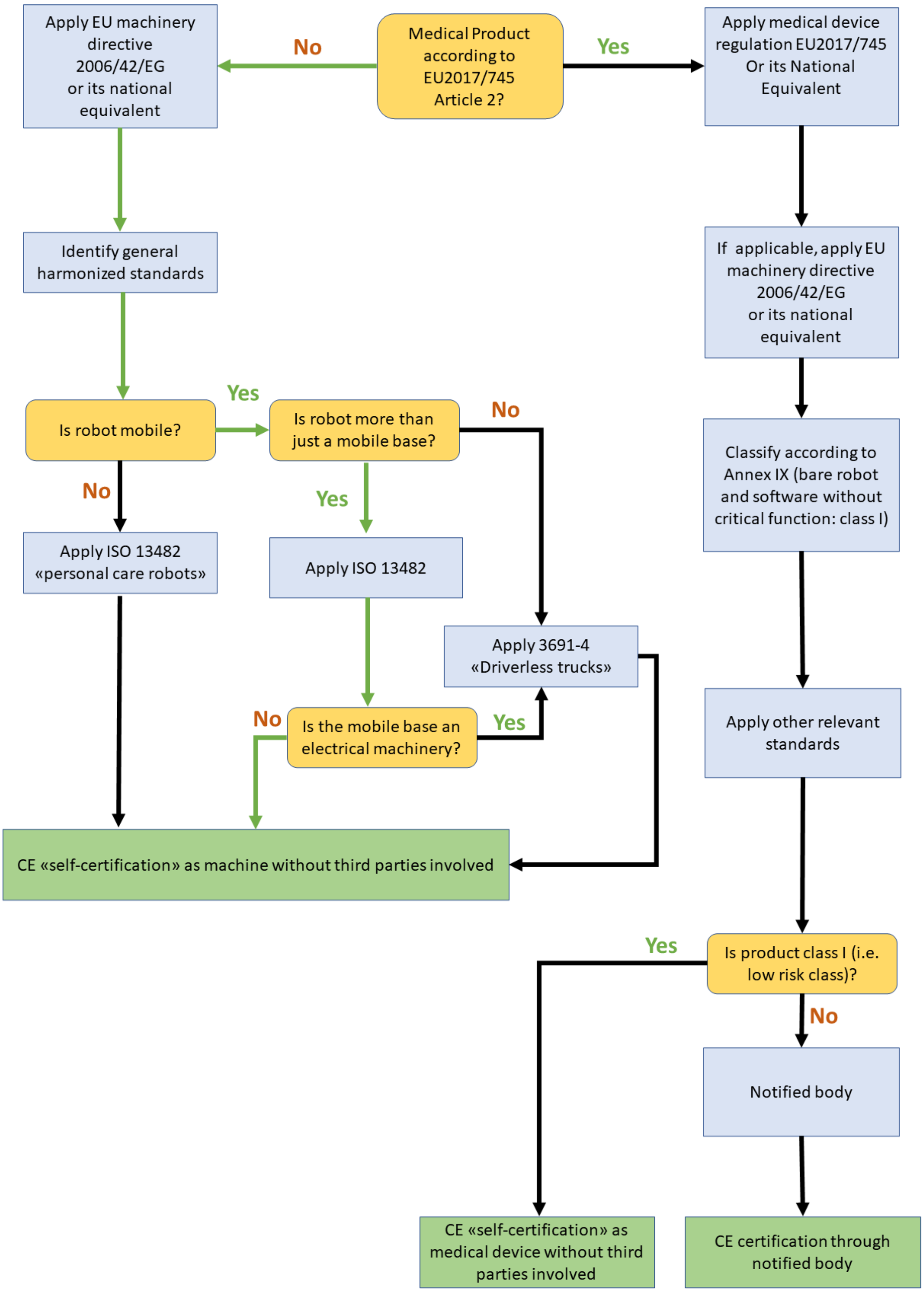

Figure 46: *Standard identification pathway for wearable robots (pathway for the upper limb exoskeleton is shown with green arrows) [83]*

The flow chart in which these assumptions were applied to the system at hand is given in Figure 46. Based on these definitions, the scope that is related to the exoskeleton at hand was narrowed down to 22. These are the design, implementation and utilization guidelines, performance testing methods, safety regulations and the definitions of electrical machinery, robotic systems in factories, co-bots, wheeled robots and wearable assistive systems. A comprehensive list of these documentations are given in Appendix C.

With that being said, these regulations govern more than the design aspect of the upper limb exoskeleton and include aspects such as field testing, robot placement and similar additional factors that differ from factory to factory. In order to make the system as compatible as possible to regulations related to the placement, the size of the system's frame was kept as small as possible while preserving its balance, as detailed in the previous section. For enabling on-site testing, the computational equipment was mounted on the back of the frame. This region lies outside of the robot's workspace and is separated from the robot by a robot by a plexiglass guard in addition to several sigma profiles. However, the remaining criteria was not able to be addressed due to the multitude. Thus, the regulatory aspects other than the safety requirements of the design of the robot are omitted from the scope of this thesis. This omission reduces the final guideline count to 14. These are:

- EU machinery directive 2006/42/EC [84]
- ISO 13482:2014 Robots and robotic devices — Safety requirements for personal care robots [85]
- ISO 10218-1:2011 Robots and robotic devices — Safety requirements for industrial robots — Part 1: Robots [86]

- ISO 12100:2010, Safety of machinery — General principles for design — Risk assessment and risk reduction [87]
- ISO 13849-1, Safety of machinery — Safety-related parts of control systems — Part 1: General principles for design [88]
- ISO 13850, Safety of machinery — Emergency stop — Principles for design [89]
- ISO 13854, Safety of machinery — Minimum gaps to avoid crushing of parts of the human body [90]
- ISO 14118, Safety of machinery — Prevention of unexpected start-up [91]
- ISO 14119, Safety of machinery — Interlocking devices associated with guards — Principles for design and selection [92]
- ISO 15534 (all parts), Ergonomic design for the safety of machinery-1 [93]
- IEC 60204-1:2009, Safety of machinery — Electrical equipment of machines — Part 1: General requirements [94]
- ISO/TS 15066:2016 ROBOTS AND ROBOTIC DEVICES — COLLABORATIVE ROBOTS [95]

To adhere these remaining standards and to increase the safety of the system, several design considerations were included in the system [83]. Given that the exoskeleton is a machinery that operates with a human user in it, the joint ranges of the system should be compatible with a human's anatomical joint ranges. If the system were to exceed these during operation, the user would incur serious injuries. To alleviate this risk, the exoskeleton's joint ranges were limited to the joint ranges of the human arm. This is accomplished by utilizing mechanical sliders that permits the system to operate within these ranges. The stopers are designed as 8 mm diameter shafts. While these stoppers are sufficient to stop the system's any erratic behavior on a case basis, fatigue that may be experienced on these over long-term usage may cause the stoppers to fail (even though it was never observed during trials). Thus, an arbitrary risk factor of 0.01% is determined for the failure of the stoppers. This factor can be eliminated by a yearly replacement of these stoppers.

Due to the contact between the user's arm and the inner curvature of the pads, the contacted region experiences friction. Based on the nature of the fabric and sweat that the user excretes during physical labor, symptoms like rash and blister may occur on the arm. In order to reduce these risks, a neoprene fabric layer was utilized due to its high ergonomic characteristics. As a result, the risk of precuring such systems are expected to be 1.59% during excessive usage (5 workdays) [96]. Additionally, this type of fabric may result in allergic reactions in a small percentage of the population. The system is not safe to be used by such individuals [97].

Undesired start up of the system may cause severe injuries to the user and may damage the exoskeleton and its surroundings. To avoid such a case, the system is equipped with a three-layered activation routine. These are, onboard pc start-up, power supply start-up and actuator start-up, respectively. While following this routine diminishes the risk to 0%, the system is prone to human error, such as mixing up the order. To eliminate this risk the operator needs to receive a training on how to operate the system; furthermore, a set of verbal affirmations on the routine during start-up between the operator and the user needs to be used.

In order to prevent the exoskeletal arm to damage the electronical components or the operator during erratic motion, these components placed in a way that lies outside of the arm's range of motion. Thus, this risk is identified at 0%.

In order to utilize an emergency shutdown quickly, the system is equipped with an emergency power shutdown (that is intended to be used by either the user or the operator) and an actuator shutdown (that is intended to be used by the operator). The risk of failure for the system to shutdown is infinitesimally low (except for human error) and is arbitrarily assigned as 0.01%.

To alleviate the undesired displacement from the wheels for specific use cases, they are equipped with brakes. While these brakes are sufficient to stop the system's any undesired movement on a case basis, fatigue that may be experienced on them over long-term usage may cause the brakes to fail (even though it was never observed during trials). Thus, an arbitrary risk factor of 0.01% is determined for the failure of the stoppers. This factor can be eliminated by a yearly maintenance of these stoppers.

The tipping over of the system during relocation or operation may cause injuries to the user and severe damage to the system. To remedy this risk the system is equipped with counterweights and redundant support beams. Nevertheless, the system is prone to tip over while traversing in inclined surfaces with high velocities. Thus, the system should not be operated in inclined or uneven surfaces over 20 degrees and velocities higher than 1.5 m/s.

Finally, the communication interruption of the system is a possible risk during operation. Throughout the test trials, two types of such interruptions were observed.

The initial and more frequent one is the accidental unplugging of the encoder cables during erratic motion of the robot. The electronics components of the system are placed on the frame. However, as the robot operates the prismatic and the revolute joints' location with respect to the electronics change. Due to this, stretching in cables occur that may cause the cable plugs to separate. As a result of any separation in the encoder cables, the transmitted data is interrupted, and the robot behaves erratically. In order to remedy this risk, the cable lengths are extended to accommodate the full range of the exoskeleton’s motion. While this solution decreased the occurrence frequency, it did not fully eliminate it, as cases of this type of failure occasionally observed while the exoskeleton operates near the boundaries of its range of motion. Throughout 215 trials with varying controllers, this failure was observed a total of 11 times. Thus, a risk factor of 5.12% is determined for this type of failure.

The second one is the processor failure that would result from the main compute unit’s crash. Throughout 215 trials with the system, this failure was observed only once. Thus, a risk factor of 0.4 % is determined for this type of failure.

CHAPTER IV

CONTROLLER SYNTHESIS AND SYSTEM VALIDATION

This chapter focuses on the kinematic and the dynamic performance validation of the upper limb exoskeleton and its controller synthesis. In Section 4.1 the derivation of the kinematic structure of the system is derived. In Section 4.2 kinematic and the dynamic simulations for selected AFS is presented. In Section 4.3 the controller structure of the system is given. In Section 4.4 joint level experiments with the synthesized controller are presented.

4.1 Kinematic and Dynamic Simulations

In order to verify the applicability of the kinematic and dynamic structure for the AFS a simulation environment is constructed. The study was conducted in MATLAB environment that was run with a computer having an Intel Core TM i7 8550 CPU 1.8 GHz processor and 16 GB RAM This simulation enabled me to verify the torque requirement of the selected tasks and whether the exoskeleton meets its design criteria. To this end a pick and place simulation was conducted, in which a dynamic model of the exoskeleton was used. This model was derived through Lagrangian mechanics. The inverse kinematic of the system was derived using a discretization with a rate of 0.01 seconds.

For this task, a payload of 20 kg was displaced 0.7 meters within the duration of 5.6 seconds; picking up is completed in 2 seconds and placing is completed in 3.6 seconds. The trajectory is generated using a quintic polynomial set. The torque requirement for the given task can be seen in Figure 47, in which the axes of Flexion and Abduction motions are indicated as positive direction [98].

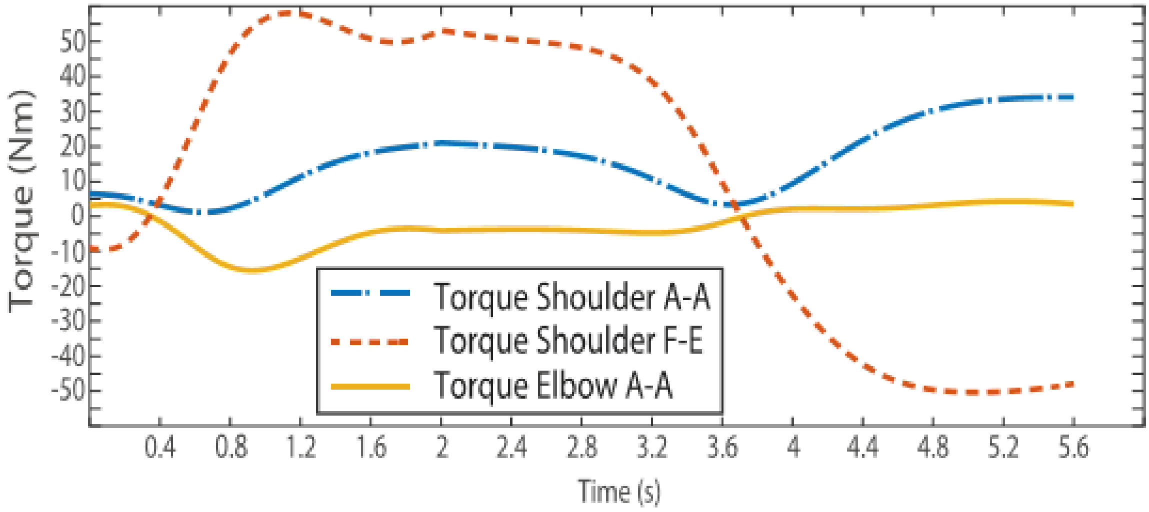

Figure 47: *Pick and place task simulation*

Following this simulation an overhead task simulation without a payload and picking up and positioning a power tool (of 15 kg) simulations were conducted to further verify the kinematic viability of the exoskeleton. The end effector position over time and the torque requirement during these tasks can be seen in Figures 48-51.

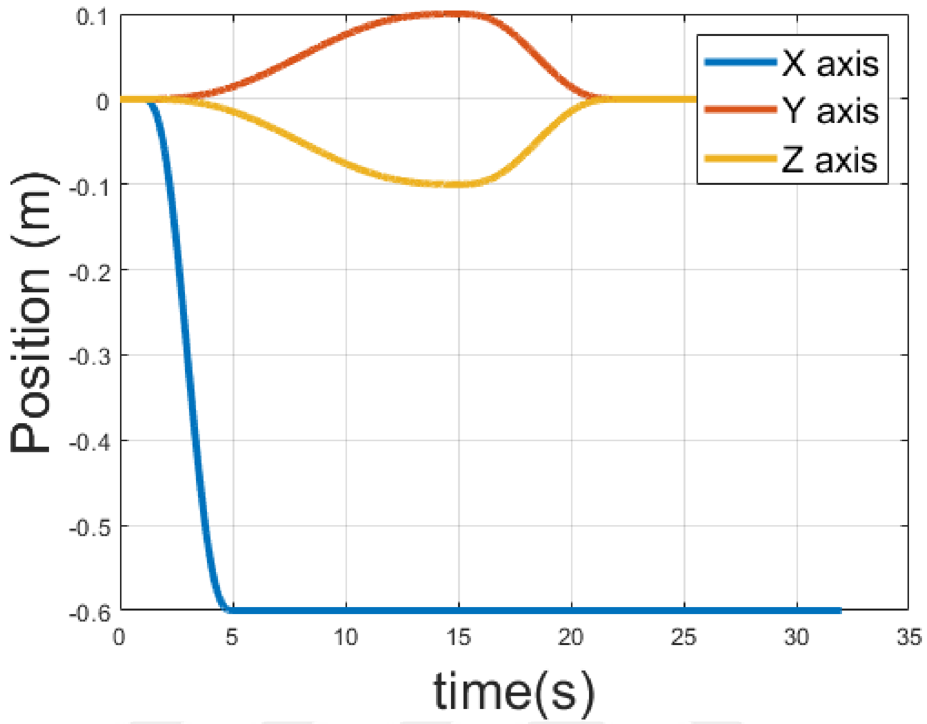

Figure 48: *Overhead arm manipulation task-end effector position over time*

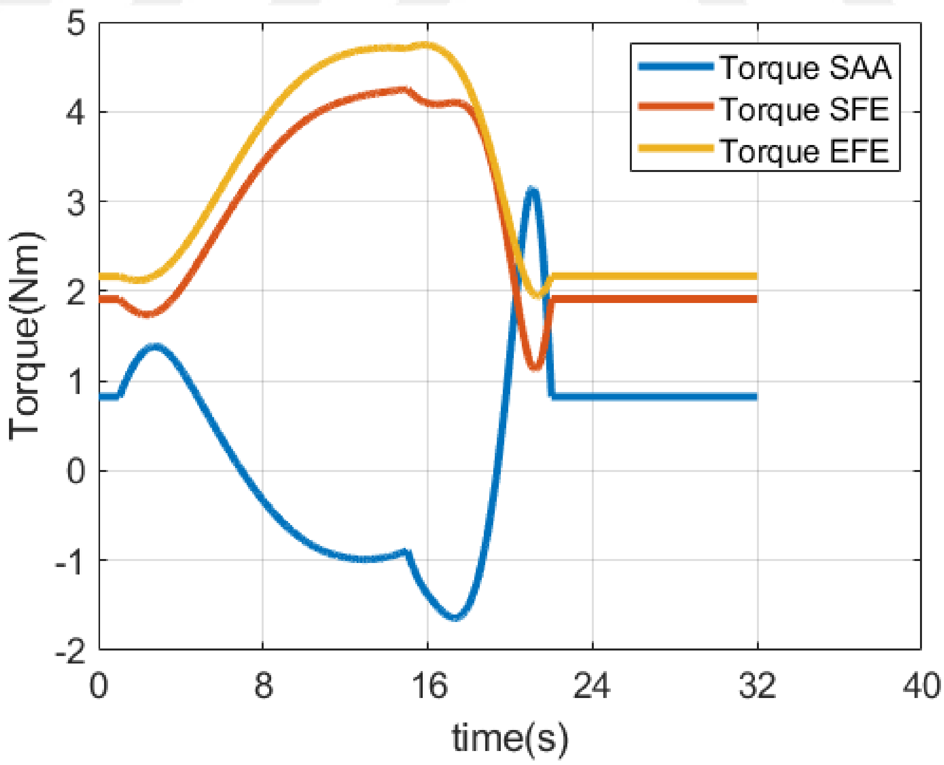

Figure 49: *Overhead arm manipulation task without payload-torque requirement over time*

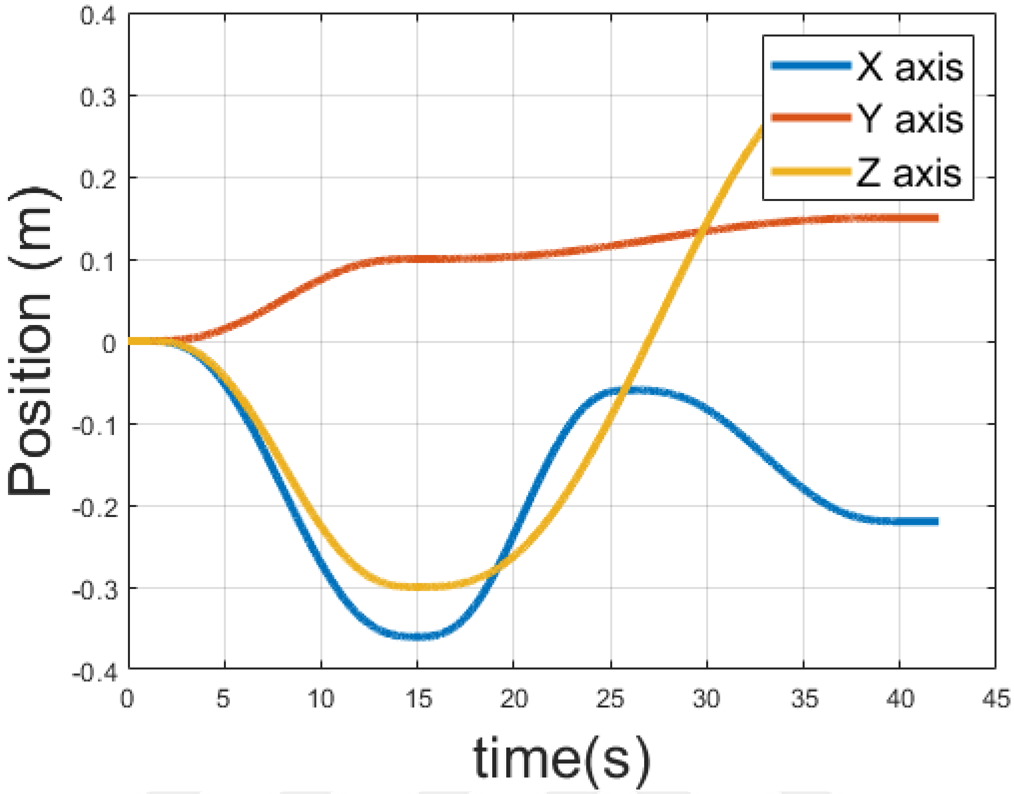

Figure 50: *Tool positioning task-end effector position over time*

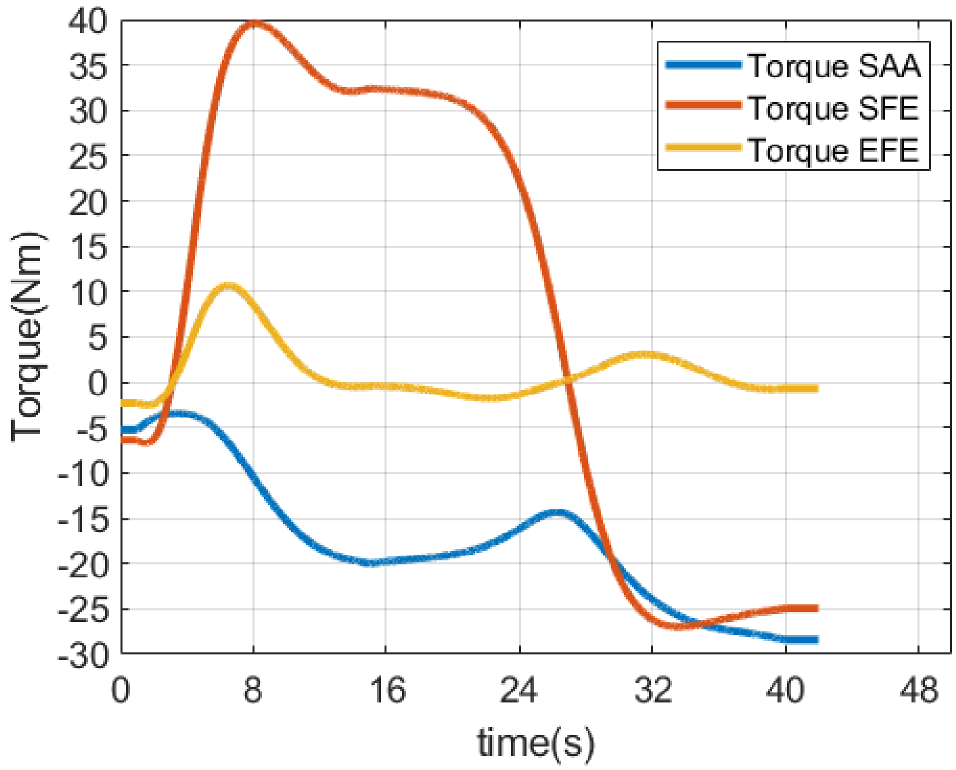

Figure 51: *Tool positioning task-torque requirement over time*

Finally in order to observe the full capacity of the actuators, thus the maximum load that the system can safely support under the longest arm configuration, additional loads for these tasks were applied. For the overhead task the maximum load that the system can carry was observed to be 39 kg whereas for the capacity for positioning a power tool was observed to be 45 kg. The torque requirement for these tasks can be seen in Figure 52 and Figure 53 respectively

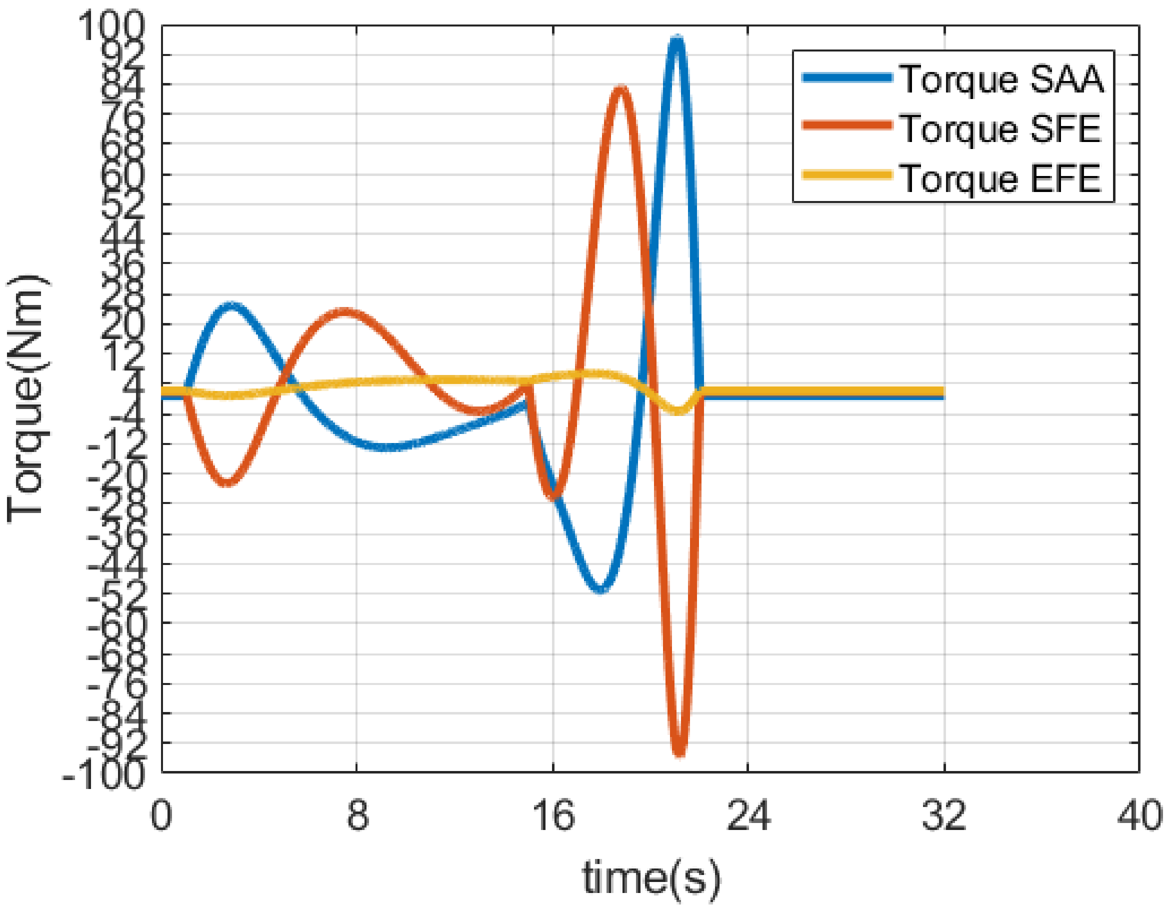

Figure 52: *Overhead arm manipulation task with 39 kg payload-torque requirement over time*

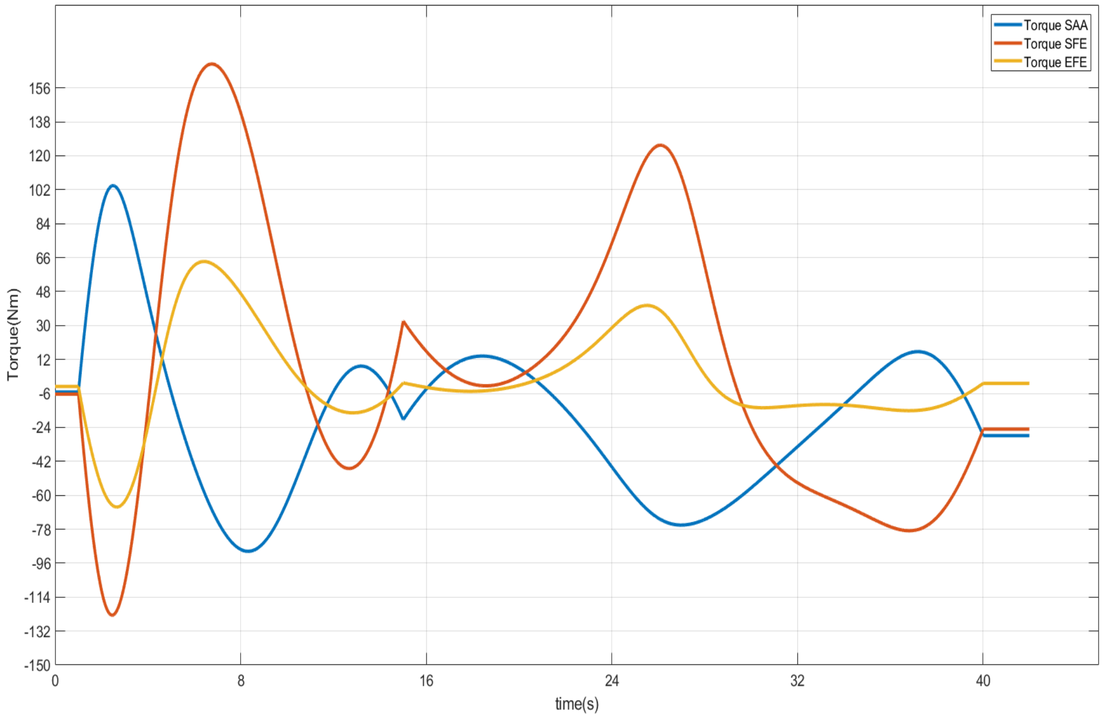

Figure 53: *Tool positioning task with a 44 kg tool-torque requirement over time*

4.2 Controller Synthesis

Torque control problem of the SEA can be converted into a position control problem due to a linear relationship between the deflection of the spring and the output torque of the actuator [99]. Even though straightforward control methodologies can be used in controlling such actuators, the torque control problem of the SEA is still an active research area due to its complicated dynamics. There are robust control techniques in the literature to improve the torque tracking performance of the SEA, even its subjected to various uncertainties. The cascaded control scheme for the SEA was proposed in [100] and [101], namely the Cascaded PD Controller with a Disturbance Observer (DOB) on the motor side to regulate the motor velocity, was adopted due its proven high bandwidth control performance [70].

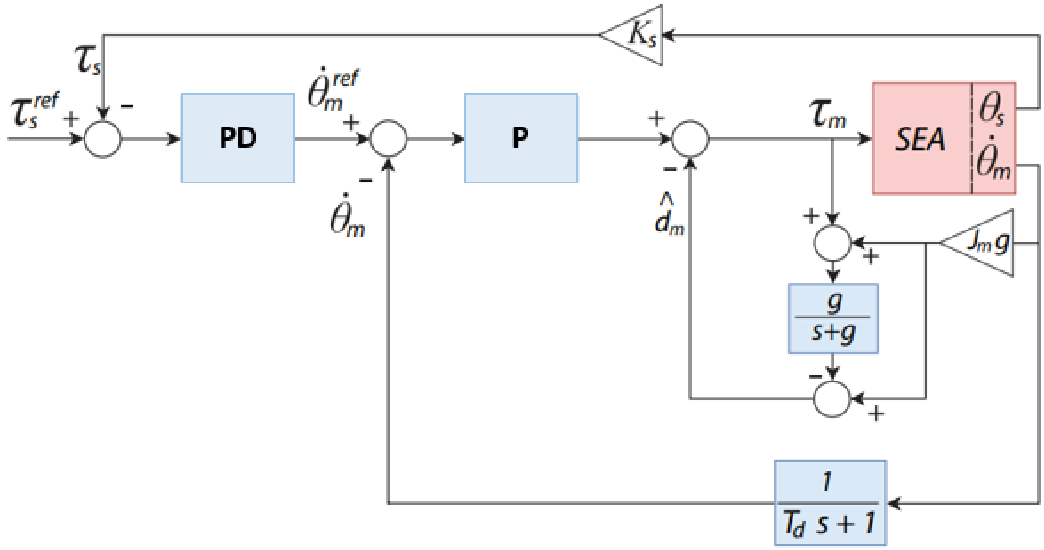

Figure 54: *The controller structure*

The block diagram of the controller can be seen in Figure 54. In the Figure where θ_d is deflection, θ_m is motor velocity, K is the spring constant, τ_d and τ_m are the output torque and the motor torque respectively. The inner velocity loop is controlled by a P controller. The outer loop has a PD controller in the outer loop. Motor velocity is derived from the motor position encoder data and the low pass filter with Td time constant is implemented to filter the noise. The motor velocity was then fed to a disturbance observer [70,101].

4.3 Joint Level Experiments

The synthesized controller was put to the test using the exoskeleton's EFE and SAA joints. A study on SFE joint was not able to be conducted due to a mechanical error that rendered the actuator inoperational.

In order to validate the performance of the implemented DOB and the torque controller an experimental setup with three phases was developed. In the first phase both the DOB and the torque control was active. In the second phase the DOB was turned off. In the last phase the torque was turned off. During the experiments two sets of data were recorded. In the initial set the required torque to move the limb and the supplied current for the three phases of the experiment was investigated to demonstrate the effectiveness of the torque control. The resulting plot can be seen in Figure 55.

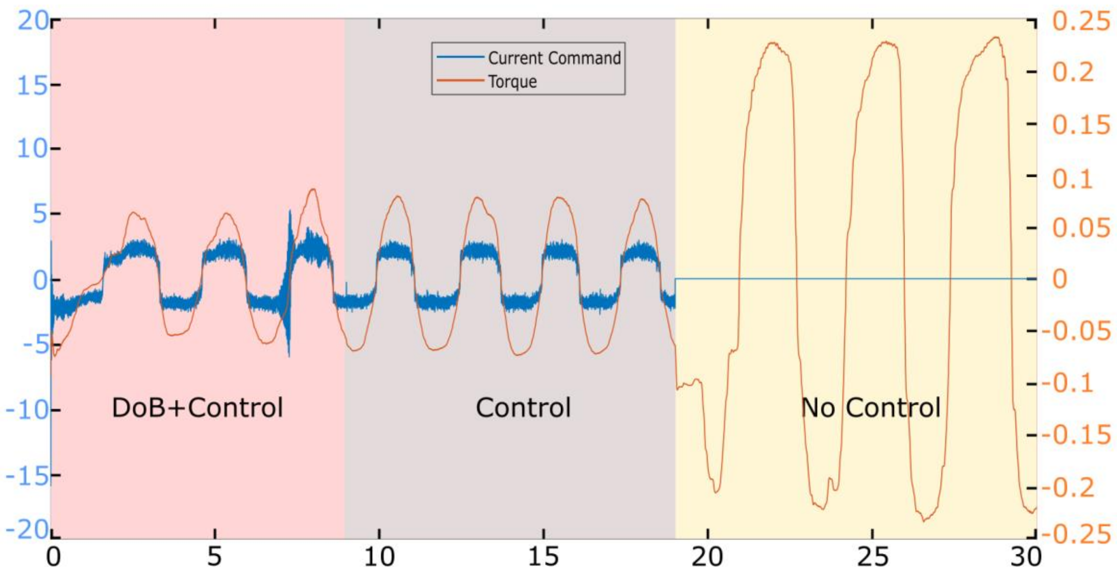

Figure 55: *Joint level experiment for the EFE joint-Torque response and demand current*

As can be seen from the graph, the torque required to move the limb when no current is supplied to the system is significantly higher than the phases where the controller was active.

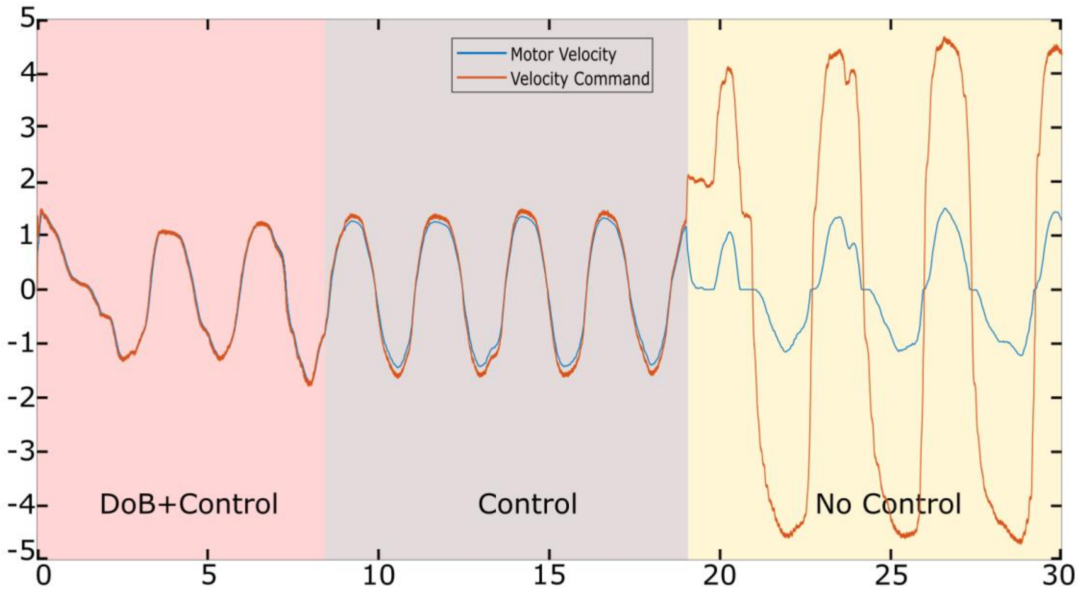

Figure 56: *Joint level experiment for the EFE joint-velocity response and velocity demand*

The second set of data was collected to examine and demonstrate the performance of the DOB on the motor velocity. These results were displayed in Figure 56. In the initial phase, the effect of the DOB can be seen from the tracking performance of the motor velocity, which can track the demand velocity curve with less steady state error in comparison to the second phase were the DOB is turned off.

CHAPTER V

CONCLUSION

In this study, design and mechatronic hardware development of an upper body exoskeleton is presented. Conclusions from this research are as follows:

- An integrated design approach for an intention estimating brace was proposed by focusing on its applicability in a factory setting. Several iterations of this brace were investigated and a final design for the system was reached in terms of cost, difficulty of assembly and functionality. These sensors calibrated using a combination of static and dynamic calibration methods in order to compensate for the inherent nonlinearity of these types of sensors. This calibration was conducted via a third order polynomial curve fitting. The system was tested on a healthy subject to demonstrate the force readings.
- Series elastic actuators that were previously developed by Yildirim et. al. were optimized and improved upon. During this process factors such as ease of assembly ease of maintenance were considered. To this end the actuators were converted into modular designs. The adaptability of the actuators was improved via this modular approach as they became attachable to a given surface via more than one configuration. A more compact version of the torsional spring that was developed by Yildirim was also shrunk down to increase the torque output to weight ratio of the actuator. This change was verified via finite element analysis and fatigue analysis. The torque reading performance of the encoders in the actuator were significantly improved by utilizing a new encoder cap design. This design prevented any slippage and tracking errors of the encoders. The performance of the design was verified in a comparative

experiment.

- A prismatic limb design was proposed to assist the user with shoulder's humeral head elevation.
- An upper limb exoskeleton design with four active degrees of freedom was that could assist workers in their routine activities in the factory. This exoskeleton was designed to be adjustable for the 99% of the world population's height, arm length and arm width measurements. This is enabled via size adjustable limb design. One of the goals of this exoskeleton is to assist the workers in high load manipulation. This assistance is required to prevent any occupational muscoskeletal disorders. A comprehensive finite element study was done on the limbs of the exoskeleton. For the analysis the limbs which were initially designed to be over safe were exposed to loads that would stall the actuators were applied to the limbs under longest configuration. Consequently, the parts experiencing slow stress were machined out to optimize the weight to safety ratio of the system.
- Several end effector module designs were proposed to assist these workers in various activities of factory setting. To this end most common AFS and their OMID inducing effects were identified and appropriate design solutions to remedy these were proposed.
- A mobile platform for the transportation of the system as well as transmitting the load to the ground was proposed.
- The exoskeletons performance was validated through simulation studies with various AFS.
- A controller for the real-time torque controller of the system was proposed. Experiments on the joint level for this controller were conducted.

APPENDIX A

INTENTION ESTIMATING BRACE STRUCTURE

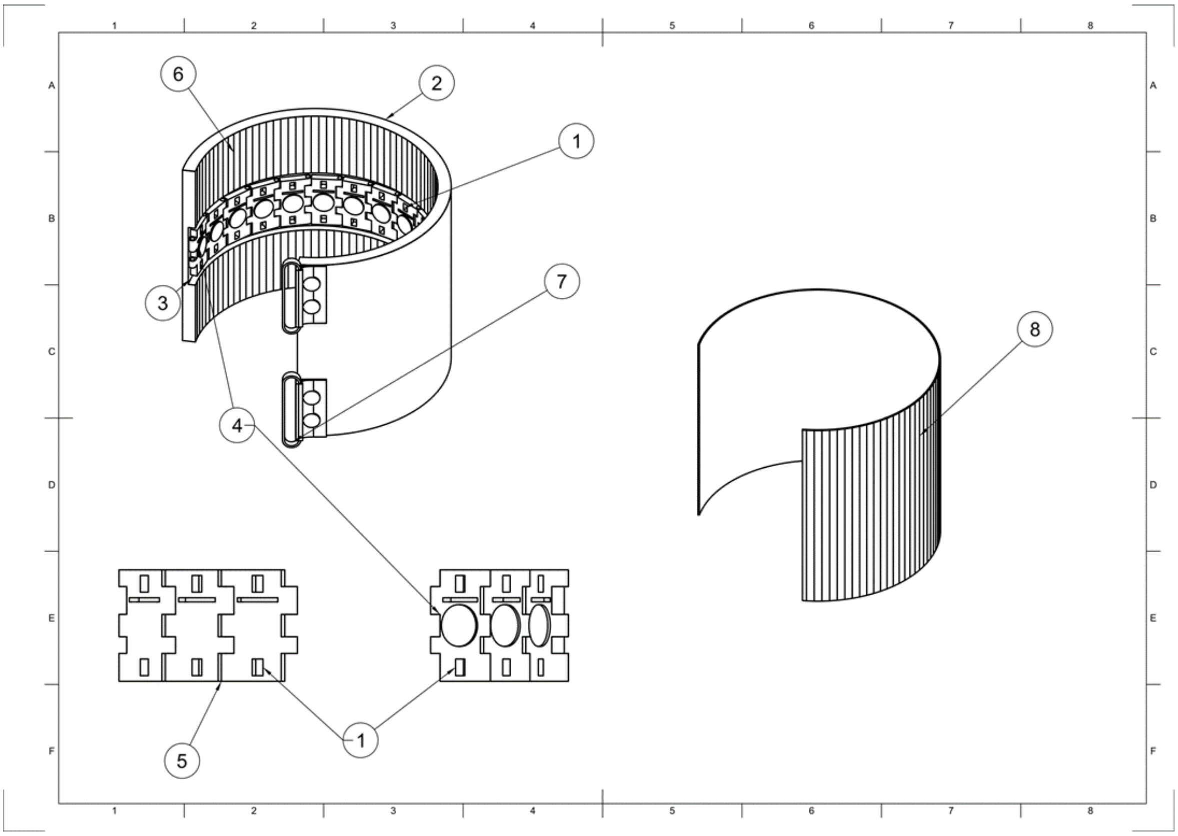

Element, No	Element Name
1.	Brace Pieces
2.	Pad
3.	Brace Housing
4.	Force Sensitive Resistors (FSR)
5.	Fastening shafts
6.	Strap on surface
7.	Buckle
8.	Strap on Neopren Fabric

APPENDIX B

CAD ASSEMBLY OF THE UPPER LIMB EXOSKELETON

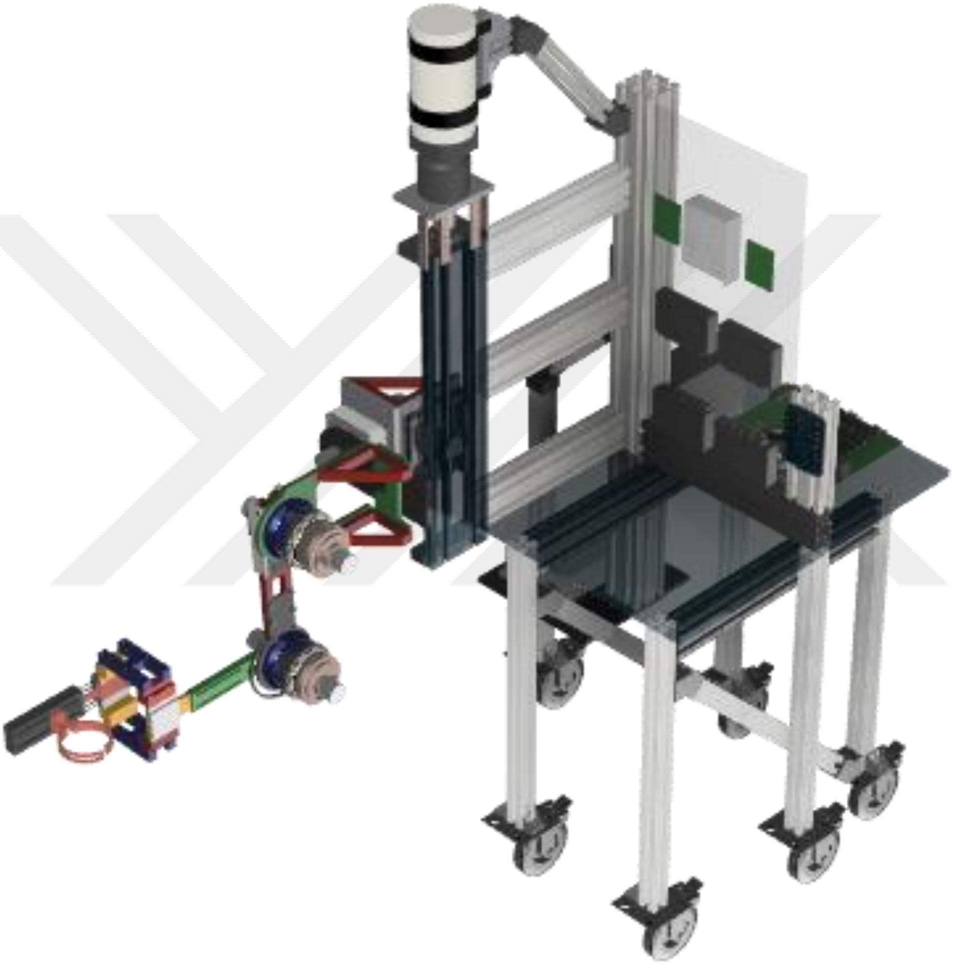

APPENDIX C

LIST OF STANDARDS FOR THE UPPER LIMB EXOSKELETON

ISO 11593:2022 Robots for industrial environments — Automatic end effector exchange systems — Vocabulary
ISO 10218-1:2011 Robots and robotic devices — Safety requirements for industrial robots — Part 1: Robots
ISO 10218-2:2011 Robots and robotic devices — Safety requirements for industrial robots — Part 2: Robot systems and integration
ISO 8373:2012, Robots and robotic devices — Vocabulary
ISO 12100:2010, Safety of machinery — General principles for design — Risk assessment and risk reduction
ISO 13849-1, Safety of machinery — Safety-related parts of control systems — Part 1: General principles for design
ISO 13850, Safety of machinery — Emergency stop — Principles for design
ISO 13854, Safety of machinery — Minimum gaps to avoid crushing of parts of the human body
ISO 138551, Safety of machinery — Positioning of safeguards with respect to the approach speeds of parts of the human body
ISO 13856 (all parts), Safety of machinery — Pressure-sensitive protective devices
ISO 13857, Safety of machinery — Safety distances to prevent hazard zones being reached by upper and lower limbs
ISO 14118, Safety of machinery — Prevention of unexpected start-up
ISO 14119, Safety of machinery — Interlocking devices associated with guards — Principles for design and selection

ISO 14120, Safety of machinery — Guards — General requirements for the design and construction of fixed and movable guards
ISO 15534 (all parts), Ergonomic design for the safety of machinery-1
ISO 19649:2017, Mobile robots — Vocabulary
IEC 60204-1:2009, Safety of machinery — Electrical equipment of machines — Part 1: General requirements
ISO 18646-1:2016 ROBOTICS — PERFORMANCE CRITERIA AND RELATED TEST METHODS FOR SERVICE ROBOTS — PART 1: LOCOMOTION FOR WHEELED ROBOTS
ISO 18646-3:2021 ROBOTICS — PERFORMANCE CRITERIA AND RELATED TEST METHODS FOR SERVICE ROBOTS — PART 3: MANIPULATION.
ISO/TS 15066:2016 ROBOTS AND ROBOTIC DEVICES — COLLABORATIVE ROBOTS

BIBLIOGRAPHY

[1] M. A. Ayoub, “Control of manual lifting hazards: I. Training in safe handling,” *JOEM: Journal of Occupational and Environmental Medicine*, vol. 24, issue 8, pp. 573-577, 1982.

[2] M. H. Cole, P. N. Grimshaw, “Low back pain and lifting: A review of epidemiology and aetiology,” *WORK: A Journal of Prevention, Assessment & Rehabilitation*, vol. 21, no. 2, pp. 173-184, 2003.

[3] D. M. Rempel, R. J. Harrison and S. Barnhart, "Work-related cumulative trauma disorders of the upper extremity," *JAMA: The Journal of the American Medical Association*, vol. 267, no. 6, 838-842, 1992.

[4] E. Innes and L. Straker, “Validity of work-related assessments,” *WORK: A Journal of Prevention, Assessment & Rehabilitation*, vol. 13, no. 2, pp. 125-152, 1999.

[5] J. de Kok, P. Vroonhof, J. Snijders, G. Roullis, M. Clarke, K. Peereboom et al., “Work-related musculoskeletal disorders: prevalence, costs and demographics in the EU,” *European Agency for Safety and Health at Work*, 2019.

[6] Eurofound, “6th European Working Conditions Survey: 2017 update,” 2017.

[7] G. Ferreira, J. Gaspar, C. Fujão, and I. L Nunes, “Piloting the use of an upper limb passive exoskeleton in automotive industry: Assessing user acceptance and intention of use,” in: Advances in Intelligent Systems and Computing, vol. 1207, I. L. Nunes (ed.), pp. 342–349, 2020.

[8] M. Hagberg, H. Morgenstern and M. Kelsh, “Impact of occupations and job tasks on the prevalence of carpal tunnel syndrome,” Scandinavian Journal of Work, Environment & Health, vol. 18, no. 6, pp. 337-345, 1992.

[9] G. Wieslander et al, “Carpal tunnel syndrome (CTS) and exposure to vibration, repetitive wrist movements, and heavy manual work: a case-referent study,” British Journal of Medicine, vol. 46, pp. 43-47, 1989.

[10] K. H. E. Kroemer, “Cumulative trauma disorders: Their recognition and ergonomics measures to avoid them”, Applied Ergonomics, vol. 20, no. 4, pp. 274-280, 1989.

[11] A. Nor Hazana et al., “Work-related musculoskeletal disorder (WRMD) among production operators: studies of differences in age and gender,” *Journal of Physics: Conference Series*, vol. 1049, no. 1, 2018.

[12] Government of Canada, “Work-related musculoskeletal disorders (WRMDs): Osh answers,” *Canadian Centre for Occupational Health and Safety*, 2021, https://www.ccohs.ca/oshanswers/diseases/rmirsi.html.

[13] K. S. Stadler, R. Altenurger, E. Schmidhauser et al., "Robo-mate an exoskeleton for industrial use - concept and mechanical design," in: *Advances in Cooperative Robotics: Proceedings of the 19th International Conference on CLAWAR 2016*, M. O. Tokhi (ed.), pp. 806-813, 2016.

[14] A. J. Young and D. P. Ferris, "State of the Art and Future Directions for Lower Limb Robotic Exoskeletons," in *IEEE Transactions on Neural Systems and Rehabilitation Engineering*, vol. 25, no. 2, pp. 171-182, 2017.

[15] J. Wesslén, "Exoskeleton Exploration: Research, development, and applicability of industrial exoskeletons in the automotive industry," Dissertation, Jönköping University School of Engineering, 2018.

[16] Toyota Motor Corporation, “Toyota Unveils Third Generation Humanoid Robot T-HR3”, 2017. Available From: https://global.toyota/en/newsroom/corporate/19841525.html

[17] A. Esquenazi, et al., "The ReWalk powered exoskeleton to restore ambulatory function to individuals with thoracic-level motor-complete spinal cord injury." *American Journal of Physical Medicine & Rehabilitation*, vol. 91, no.11, pp. 911-921, 2012.

[18] E. J. Rouse, L. M. Mooney et al., "Clutchable series-elastic actuator: Design of a robotic knee prosthesis for minimum energy consumption," *in 2013 IEEE 13th International Conference on Rehabilitation Robotics (ICORR)*, pp. 1-6, IEEE, 2013.

[19] T. Lenzi, S. M. M. De Rossi, N. Vitiello and M. C. Carrozza, "Intention-based EMG control for powered exoskeletons," in *IEEE Transactions on Biomedical Engineering*, vol. 59, no. 8, pp. 2180-2190, 2012.

[20] B. J. Martin and Y. Acosta-Sojo. "sEMG: A window into muscle work, but not easy to teach and delicate to practice - a perspective on the difficult path to a clinical tool," *Frontiers in Neurology*, vol. 11, article no. 588451, pp. 1573-1579, 2021.

[21] K. Langlois, J. Geeroms et al., "Improved motion classification with an integrated multimodal exoskeleton interface," *Frontiers in Neurorobotics*, vol. 15, article no. 693110, pp. 140-151, 2021.

[22] C. Lebosse, P. Renaud, B. Bayle, and M. de Mathelin, "Modelling and evaluation of low-cost force sensors", *in IEEE Trans. on Robotics*, vol. 27, no. 4, pp. 815-822, 2011.

[23] W. Wei, W. Wang, Z. Qu, J. Gu, X. Lin and C. Yue, "The effects of a passive exoskeleton on muscle activity and metabolic cost of energy," Advanced Robotics, vol. 34, no.1, pp. 19-27, 2020.

[24] J. Theurel, K. Desbrosses, "Occupational exoskeletons: overview of their benefits and limitations in preventing work-related musculoskeletal disorders," *IISE Transactions on Occupational Ergonomics and Human Factors*, vol. 7, no. 3-4, pp. 264-280, 2019.

[25] SuitX (n.d), "Products". Retrieved from: http://www.suitx.com/

[26] Ford and others are experimenting with wearable robotics. Retrieved from: https://www.theverge.com/2017/12/5/16726004/verge-next-level-season-two-indus-trial-exoskeletons-ford-ekso-suitx

[27] Levitate technologies (n.d), "AIRFRAME™ - FATIGUE HAS A NEW ENEMY". Extracted from: http://www.levitatetech.com/airframe/

[28] Laevo (n.d), "Laevo V2". Extracted from: http://en.laevo.nl/laevo-v2-product-infor-mation/

[29] Laevo Exoskeleton (n.d), "LAEVO EXOSKELTON A Complete Consumer Guide". Retrieved from: http://www.laevo-exoskeleton.com/

[30] M. M. Alemi, J. Geissinger, A. A. Simon, S. E. Chang and A. T. Asbeck, "A passive exoskeleton reduces peak and mean EMG during symmetric and asymmetric lifting," *Journal of Electromyography and Kinesiology*, vol. 47, pp. 25–34, 2019.

[31] D. J. Hyun et al., "A light-weight passive upper arm assistive exoskeleton based on multi-linkage spring-energy dissipation mechanism for overhead tasks," *Robotics and Autonomous Systems*, vol. 122, article no.103309, 2019.

[32] Ekso Bionics (n.d), "The EksoVest". Retrieved from: https://eksobionics.com/eksoworks/ford/

[33] M. J. Deng, Z. Wang, H. H. He and Y. Xue, "Design and weight lifting analysis of a strengthen upper limb exoskeleton robot," *Applied Mechanics and Materials*, vol. 437, pp. 695–699, 2013.

[34] R. B. Graham, M. J. Agnew, and J. M. Stevenson, "Effectiveness of an on-body lifting aid at reducing low back physical demands during an automotive assembly task: assessment of EMG response and user acceptability," *Applied Ergonomics*,

vol. 40, no. 5, pp. 936–942, 2009.

[35] A. Ebrahimi, "Stuttgart Exo-jacket: An exoskeleton for industrial upper body applications," *in 2017 IEEE 10th International Conference on Human System Interactions (HSI)*, IEEE, 2017.

[36] E. Beattie, et al., "Titan: A powered, upper-body exoskeleton," *ASTM International*, 2014.

[37] T. Noda et al., "Development of an upper limb exoskeleton powered via pneumatic electric hybrid actuators with bowden cable," *in 2014 IEEE/RSJ International conference on intelligent robots and systems*, IEEE, 2014.

[38] M. Mallwitz et al., "The capio active upper body exoskeleton and its application for teleoperation," *in proc. of the 13th ESA/Estec Symposium on Advanced Space Technologies in Robotics and Automation (ASTRA-2015)*, ESA. 2015.

[39] S. Elprama, B. Vanderborght and A. Jacobs, “An industrial exoskeleton user acceptance framework based on a literature review of empirical studies,*” in proc. of Journal of Applied Ergonomics*, vol. 100, article no. 103615, 2022.

[40] S. Kuz, J. Bützler, and C. M. Schlick, "Anthropomorphic design of robotic arm trajectories in assembly cells," *Journal of Occupational Ergonomics*, vol. 12, no. 3, pp. 73-82, 2015.

[41] B. S. Dhillon, "Robot reliability and safety,” in: *Robot reliability*, New York, NY, pp. 119-149, 1991.

[42] V. Venkatesh, J. Y. L. Thong and X. Xu, "Consumer acceptance and use of information technology: extending the unified theory of acceptance and use of technology," *MIS Quarterly*, vol. 36, no. 1, pp. 157-178, 2012.

[43] F. Cavallo et al., "Robotic services acceptance in smart environments with older adults: user satisfaction and acceptability study," *Journal of Medical Internet Research*, vol. 20, no. 9, 2018.

[44] S. Toxiri et al., "Back-support exoskeletons for occupational use: an overview of technological advances and trends." *IISE Transactions on Occupational Ergonomics and Human Factors*, vol. 7, no. 3-4, pp. 237-249, 2019.

[45] C. J. Walsh et al., "Development of a lightweight, underactuated exoskeleton for load-carrying augmentation," *in proc. of 2006 IEEE International Conference on Robotics and Automation (ICRA)*, IEEE, 2006.

[46] J. Rosen and J. C. Perry, "Upper limb powered exoskeleton," *International Journal of Humanoid Robotics*, vol. 4, no. 3, pp. 529-548, 2007.

[47] A. Otten et al., “LIMPACT: A hydraulically powered self-aligning upper limb exoskeleton," in IEEE/ASME Transactions on Mechatronics, vol. 20, no. 5, pp. 2285-2298, 2015.

[48] M. C. Yildirim et al., "An integrated design approach for a series elastic actuator: Stiffness formulation, fatigue analysis, thermal management," in 2017 IEEE-RAS 17th International Conference on Humanoid Robotics (Humanoids), IEEE, 2017.

[49] M, Mahdavian, et. al., “Design and fabrication of a 3DoF upper limb exoskeleton," in 2015 3rd IEEE/RSI International Conference on Robotics and Mechatronics (ICROM), pp. 342-346, IEEE, 2015.

[50] J. S. Schofield et al., “The effect of biomechanical variables on force sensitive resistor error: Implications for calibration and improved accuracy,” Journal of Biomechanics, vol. 49, no. 5, pp. 786-792, 2016.

[51] V. Varga, T. I. Erdei, and G. Husi, “Redesigning of the gripping system on KUKA KR5 by utilizing 3 dimension printing technologies and Arduino,” in MATEC Web of Conferences, vol. 184, EDP Sciences, 2018.

[52] M. H. Choi and W. W. Lee, “A force/moment sensor for intuitive robot teaching application,” in proc. of 2001 ICRA. IEEE International Conference on Robotics and Automation, vol. 4, pp. 4011-4016, IEEE, 2001.

[53] G. Barbadillo, K. Dautenhahn and L. Wood, “Using FSR sensors to provide tactile skin to the humanoid robot KASPAR”, Dissertation, University of Hertforshire, 2011.

[54] K. S. Krishnan and A. Saha, “Smart haptic technology for governing arm robot with 6 DOF,” Rochester Institute of Technology Dept. of Electrical Engineering, 2016.

[55] M. Anvaripour, M. Saif, “Controlling robot gripper force by transferring human forearm stiffness using force myography,” in 2018 IEEE 61st International Midwest Symposium on Circuits and Systems (MWSCAS), pp. 672-675, IEEE, 2018.

[56] Q. Wu, X. Wang et al., “Design and control of a powered hip exoskeleton for walking assistance,” International Journal of Advanced Robotic Systems, vol. 12, no. 18, 2015.

[57] A. Dementyev and J. A. Paradiso, “WristFlex: Low-power gesture input with wrist-worn pressure sensors,” in 27th ACM Symposium on User Interface Software and Technology, pp. 161-166, 2014.

[58] T. Stefanou et al., “Tactile signatures and hang motion intent recognition for wearable assistive devices,” Frontiers in Robotics and AI, vol. 6, no. 124, 2019.

[59] J. A. Szivek, G. C. Weatherly, R. M. Pilliar and H. U. Cameron, “A study of bone remodeling using metal-polymer laminates,” Journal of Biomedical Materials Research, vol. 15, pp. 853-865, 1981.

[60] S. Bistac, J. Guillemenet and J. Schultz, “Fracture of metal/polymer/metal assemblies: Viscoelastic effects,” Journal of Adhesion, vol. 78, no. 11, pp. 987-996, 2002.

[61] W. Huo et al., “Control of upper-limb power-assist exoskeleton based on motion intention recognition,” in 2011 IEEE International Conference on Robotics and Automation (ICRA), pp. 2243-2248, IEEE, 2011.

[62] N. Jaquier et al., “Combining electromyography and tactile myography to improve hand and wrist activity detention in prostheses,” Technologies, vol. 5, no. 64, 2017.

[63] A. K. Godiyal et al., “Analysis of force myography based on locomotion patterns,” Journal of the International Measurement Confederation (IMEKO), vol. 140, pp. 497-503, 2019.

[64] K. HT Chu et al., “Wearable step counting using a force myography-based ankle strap,” Journal of Rehabilitation and Assistive Technologies Engineering, vol. 4, pp.1-11, 2017.

[65] M. Hassan et al., “Exoskeleton robot control based on cane and body joint synergies,” in 2012 IEEE/RSJ International Conference on Intelligent Robots and Systems (IROS), IEEE, 2012.

[66] E. Andreozzi et al., “Forcecardiography: A Novel Technique to Measure Heart Mechanical Vibrations onto the Chest Wall,” Sensors, vol. 20, no. 14, p. 3885, Jul. 2020, doi: 10.3390/s20143885.

[67] Hans Robot, https://www.hansrobot.net/products/

[68] Franka Emika, https://www.franka.de/

[69] N. Kashiri, J. Malzahn, and N. G. Tsagarakis, “On the sensor design of torque controlled actuators: A comparison study of strain gauge and encoder-based principles," IEEE Robotics and Automation Letters, vol. 2, no. 2, pp. 1186-1194, 2017.

[70] M. C. Yildirim, “Development of a torque-controllable lower extremity exoskeleton for crutch-free 3D walking support,” Dissertation, Ozyegin University Dept. of Mechanical Engineering, 2018.

[71] S. Hamdan, E. Oztop, J. Furukawa, J. Morimoto, and B. Ugurlu, “Shoulder glenohumeral elevation can be estimated via gaussian regression with upper arm orientation,” in proc. of 2018 40th Annual Int. Conf. of IEEE Engineering in Medicine and Biology Society (EMBC), pp. 1481-1484, IEEE, 2018.

[72] S. A. Moussavi-Najarkola and R. Mirzaei, “Assessment of muscu- loskeletal loads of electric factory workers by rapid entire body assessment”, Health Scope, vol. 1, no. 2, pp. 71-79, 2012.

[73] M. Roser et al., “Human height,” OurWorldInData.org., retrieved from https://ourworldindata.org/human-height#citation

[74] S. Popovic, D. Bjelica et. al, “Body height and its estimation utilizing arm span measurements in Serbian adults,” International Journal of Morphol, vol. 31, no. 1, pp. 271-279, 2013.

[75] S. Popovic, D. Bjelica et. al, “Body height and its estimation utilizing arm span measurements in Bosnian and Herzegovinian adults,” Montenegrin Journal of Sports Science and Medicine (MJSSM), vol. 4, pp. 29-36, 2015.

[76] P. de Leva, “Adjustments to Zatsiorsky-Seluyanov’s segment inertia parameters,” Journal of Biomechanics, vol. 29, no. 9, pp. 1223-1230, 1996.

[77] R. G. Budynas, J. K. Nisbett, et al., “Shigley's mechanical engineering design”, vol. 8. McGraw-Hill New York, 2008.

[78] S. Tripathy, R. Panicker et. al, “Voice controlled upper body exoskeleton: A development for industrial application,” International Journal of Scientific & Technology Research, vol. 9, no. 06, 2020.

[79] A. Gupta, M. K. O’Malley et al., “Design, control and performance of RiceWrist: A force feedback wrist exoskeleton for rehabilitation and training,” International Journal of Robotics Research, vol. 27, pp. 233-250, 2008.

[80] N. Jarrasse and G. Morel, “Connecting a human limb to an exoskeleton”, in IEEE Trans. on Robotics, vol. 28, no. 3, pp. 697-709, IEEE, 2012.

[81] N. J. Seo and T. J. Armstrong. "Investigation of grip force, normal force, contact area, hand size, and handle size for cylindrical handles," Human Factors, vol. 50 no.5, pp. 734-744, 2008.

[82] M. Peters et al., “Finger length and distal finger extent patterns in humans,” American Journal of Physical Anthropology, vol. 117, no. 3, pp. 209-217, 2002 International Standard ISO 11593: Robots for industrial environments — Automatic end effector exchange systems — Vocabulary. (2022)

[83] Wecord Winter School Day 3 Jan Veneman, From research project to a (medical) product: the importance of standardization and testing methods, Feb. 10 2021, Available: https://www.youtube.com/watch?v=uniwd7P-SQs&list=PL-J1wJdPHovgzmQCJw8J5qrwVxKHKlMP5&index=11.

[84] DIRECTIVE 2006/42/EC OF THE EUROPEAN PARLIAMENT AND OF THE COUNCIL of 17 May 2006 on machinery, and amending Directive 95/16/EC (recast).

[85] International Standard ISO 13482:2014: Robots and robotic devices — Safety requirements for personal care robots.

[86] International Standard ISO 10218-1: Robots and robotic devices — Safety

requirements for industrial robots — Part 2: Robot systems and integration (2011)

[87] International Standard ISO 12100: Safety of machinery — General principles for design — Risk assessment and risk reduction (2010)

[88] International Standard ISO 13849-1: Safety of machinery — Safety-related parts of control systems — Part 1: General principles for design

[89] International Standard ISO 13850: Safety of machinery — Emergency stop — Principles for design

[90] International Standard ISO 13854: Safety of machinery — Minimum gaps to avoid crushing of parts of the human body

[91] International Standard ISO 14118: Safety of machinery — Prevention of unexpected start-up

[92] International Standard ISO 14119: Safety of machinery — Interlocking devices associated with guards — Principles for design and selection

[93] International Standard ISO 15534 (all parts): Ergonomic design for the safety of machinery-1

[94] International Standard IEC 60204-1: Safety of machinery — Electrical equipment of machines — Part 1: General requirements (2009)

[95] C. C. Lyon, J. Kulkarni, E. Zimersonc, E. Van Ross, and M. H. Beck, "Skin disorders in amputees," Journal of the American Academy of Dermatology, vol. 42, no. 3, pp. 501–507, Mar. 2000, doi: 10.1016/s0190-9622(00)90227-5.

[96] S. Hawkey and S. Ghaffar, "Neoprene Orthopaedic Supports: An Underrecognised Cause of Allergic Contact Dermatitis," Case Reports in Orthopedics, vol. 2015, p. 496790, 2015, doi: 10.1155/2015/496790.

[97] S. Coruk et al., "Design and development of a powered upper limb exoskeleton with high payload capacity for industrial operations," in 2020 IEEE International Conference on Human-Machine Systems (ICHMS), pp. 1-4, IEEE, 2020.

[98] G. A. Pratt, M. M. Williamson, P. Dillworth, J. Pratt, and A.Wright, "Stiffness isn't everything," in Experimental Robotics IV, pp. 253-262, Springer, 1997.

[99] D. W. Robinson, "Design and analysis of series elasticity in closed-loop actuator force control," PhD thesis, Massachusetts Institute of Technology, 2000.

[100] G. Wyeth, "Control issues for velocity sourced series elastic actuators," in in proc. of the Australasian Conference on Robotics and Automation 2006, Australian Robotics and Automation Association Inc, 2006.

[101] B. Ugurlu et al., "Benchmarking Torque Control Strategies for a Torsion-Based Series Elastic Actuator," in IEEE Robotics & Automation Magazine, 2021.

VITA

Sinan CORUK had taken his high school education in Uskudar American Academy. He had completed his B.Sc. in Mechanical Engineering at Ozyegin University in 2018. During his undergraduate studies, he had worked as an undergraduate research student at OzU Biomechatronics Laboratory for 2 years, under the supervision of Asst. Prof. Barkan Ugurlu. He is currently studying M.Sc. in Mechanical Engineering at Ozyegin University under the supervision of Asst. Prof. Barkan Ugurlu. During his graduate studies, he had continued to work as a research assistant at OzU Biomechatronics Laboratory. He is primarily focusing his studies on exoskeleton design, actuator development and wearable sensor development.